‘DNA Hybrid Materials Consisting of Oligonucleotides and Organic Molecules: Synthesis, Characterization and Applications’

Dissertation
zur Erlangung des Grades
“Doktor der Naturwissenchaften”

am Fachbereich
Chemie, Pharmazie und Geowissenschaften
der Johannes Gutenberg-Universität Mainz

Diana Milena Anaya
geb. in Bogotá, Kolumbien
Mainz 2010

Dekan:
1. Berichterstatter:
2. Berichterstatter:
Tag der mündlichen Prüfung:

Dedicated to my parents

“*Science knows no country, because knowledge belongs to humanity, and is the torch which illuminates the world.”*
(Louis Pasteur)

TABLE OF CONTENTS

LIST OF ABBREVIATIONS 13

Chapter 1

INTRODUCTION 17

1.1 DNA fundamentals 18
1.2 DNA as a construction material for nanoarchitectures 25
1.3 DNA-based hybrid materials 29
1.4 Summary 32
1.5 References 34

Chapter 2

MOTIVATION AND OBJECTIVES 39

Chapter 3

AGGREGATION OF DOUBLE STRANDED DNA INDUCED BY AROMATIC π-SYSTEMS 43

3.1 Introduction 43
3.2 Preparation of dsDNA-PDI hybrids 44
3.3 Analysis on surface by Atomic Force Microscopy (AFM) 46
3.4 Native polyacrylamide gel electrophoresis (PAGE) Analysis 48
3.5 Fluorescence correlation spectroscopy (FCS) study of DNA-PDI hybrids in solution 49
3.6 Photophysical study of DNA-PDI hybrids 52
3.7 Conclusions 55
3.8 Experimental Section 57
3.9 References 66

Chapter 4

INVESTIGATING THE DYNAMIC BEHAVIOR OF DNA POLYMER CHAINS BY TERMINALLY DYE-FUNCTIONALIZED POLYNUCLEIC ACIDS 69

4.1 Introduction 69

4.2 PCR technique as strategy to generate fluorescently labeled linear DNA ... 74

4.3 Preparation and characterization of linear unlabeled DNA on milligram scales by cell transformation 78

4.4 Single–molecule FRET and wide-field fluorescence microscopy measurements 81

4.5 Conclusions 86

4.6 Experimental Section 87

4.7 References 90

Chapter 5

TUNABLE HYDROPHOBICITY IN DNA MICELLES: DESIGN, SYNTHESIS AND CHARACTERIZATION OF A NEW FAMILY OF DNA AMPHIPHILES ... 93

5.1 Introduction 93

5.2 Solid phase DNA synthesis 95

5.3 Synthesis and micellization of lipid-DNAs 97

5.4 Morphological characterizations by AFM and DLS 100

5.5 Determination of critical micelle concentration 102

5.6 Hybridization with complementary DNA 104

5.7 Morphological characteristics of ss- and ds DNA-lipids 107

5.8 Conclusions 108

5.9 Experimental Section 110

5.10 References 120

Chapter 6

VIRUS PARTICLES TEMPLATED BY DNA MICELLES: A GENERAL METHOD FOR LOADING VIRUS NANOCARRIERS 125

6.1 Introduction 125

6.2 Loading of CCMV capsids using DNA amphiphiles 126

6.3 Conclusions 136

6.4 Experimental Section 138

6.5 References 143

Chapter 7

SINGLE-MOLECULE REDOX BLINKING OF PERYLENE DIIMIDE DERIVATIVES IN WATER 145

7.1 Introduction 145

7.2 Time-resolved single-molecule spectroscopy of DNA-perylene diimide conjugate (DNA-PDI) in aqueous buffer 146

7.3 Study of the photophysics of the water soluble DNA-PDI conjugate using a reducing and oxidizing system (ROXS) 151

7.4 Photophysics of PDI under non-aqueous conditions 153

7.5 Conclusions 155

7.6 Experimental section 157

7.7 References 163

Chapter 8

SUMMARY 167

LIST OF ABBREVIATIONS

A	Adenine
AIEX	Anion exchange
AFM	Atomic Force Microscopy
bp	base pair
C	Cytosine
CCD	Charge Coupled Device
CCMV	Cowpea Chlorotic Mottle Virus
CH_3CN	Acetonitril
CLSM	Confocal Laser Scanning Microscopy
CMC	Critical Micelle Concentration
CP	Coat protein
CPG	Controlled Porous Glass solid support
DBC	DNA block copolymer
DiI	1,1'-Dioctadecyl-3,3,3',3'-tetramethylindocarbocyanine perchlorate
DIPEA	Diisopropyl ethylamine
DLS	Dynamic light scattering
DM	Dichroic Mirror
DMF	*N,N*-dimethylformamide
DMSO	Dimethylsulfoxide
DMT-MM	4-(4,6-dimethoxy-1,3,5-triazin-2-yl)-4-methylmorpholinium chloride)
DNA	Deoxyribonucleic acid
dNTP	deoxynucleotide triphosphate
ds	double stranded
dTTP	deoxythymidine triphosphate
EDC	*N*-(3-dimethylaminopropyl)-*N*'-ethylcarbodiimide
EDTA	ethylenediaminetetraacetic acid
FCS	Fluorescence correlation spectroscopy

FPLC	Fast protein liquid chromatography
FRET	Fluorescence resonance energy transfer
G	guanine
HBTU	O-Benzotriazole-N,N,N',N'-tetramethyl-uronium-hexafluoro-phosphate
HOPG	Highly oriented pyrolytic graphite
HPLC	High pressure liquid chromatography
kpb	kilo base pair
LB	Luria Bertani medium
MALDI-TOF MS	Matrix Assisted Laser Desorption / ionization – time of flight mass spectrometry
MES	2-(*N*-morpholino)ethanesulfonic acid
M_n	Number average molecular weight
M_w	Weight average molecular weight
MWCO	Molecular Weight Cut-Off
MOPS	3-(*N*-morpholino)propanesulfonic acid
NHS	*N*-hydroxysuccinimide
NMR	Nuclear magnetic resonance
OD	Optical Density
ODN	Oligodeoxynucleotide
PAGE	Polyacrylamide gel electrophoresis
PBS	Phosphate buffered saline
PCR	Polymerase Chain Reaction
PDI	Perylene (di-)imide
$Pd(PPh_3)_4$	Tetrakis(triphenylphosphine)palladium(0)
PEG	poly(ethylene glycol)
PEI	polyethyleneimine
PEO	poly(ethylene oxide)
PLGA	poly(D,L-lactic-co-glycolic acid)
PLL	poly(L-lysine)
PNIPAM	poly(*N*-isopropylacrylamide)

PPO	poly(propylene oxide)
PS	polystyrene
RNA	Ribonucleic acid
SMFS	Single Molecule Fluorescence Spectroscopy
ss	single stranded
sulfo-NHS	sulfo-*N*-hydroxysuccinimide ester
T	Thymidine
TAE	Tris-acetate-EDTA Buffer
TBE	Tris-borate-EDTA Buffer
TEM	Transmission electron microscopy
TEMED	Tetramethylethylenediamine
T_m	Melting temperature
THF	Tetrahydrofuran
Tris	Tris(hydroxymethyl)aminomethane
U	Uracil
UV/Vis	Ultraviolet/visible spectroscopy
VC	Virus capsid

Chapter 1

INTRODUCTION

"One of the grand challenges is to design molecules that have nothing to do with biology but are inspired by biology"

Prof. Chad Mirkin
(Northwestern University, Evanston, Illinois)

The exploration of new techniques to fabricate structures in the nanometer scale has become of great interest in the last decades, in particular the production and characterization of novel structures in a molecular scale. This provides an opportunity for the development of all kinds of improved and miniaturized devices including biosensors, fluidic chips, optical devices and electronic circuits.[1-4] However, the miniaturization by means of top-down design is becoming difficult because of physical limitations.[5] For that reason, scientists and engineers have been looking for answers in nature, emerging a new stream of technology called "nanobiotechnology" that mainly focuses on bottom-up approaches.[6] The programmability and self-organizing properties of biological systems, such as

DNA (Deoxyribonucleic acid), allow the generation of nanostructures with more structural sections, having diverse and specific functions. The characteristics that qualify DNA as a particular constructing material are the following: well predictable and programmable molecular assembly, the possible introduction of organic and inorganic moieties in specific positions, facile chemical synthesis by the solid phase method[7] and easy manipulation by DNA modifying enzymes.[8, 9]
In the section below the structure as well as physical and chemical properties of DNA will be described.

1.1 DNA fundamentals

DNA has been studied in many areas within life sciences. In biology, DNA is the molecule for storing the information necessary for building and maintaining life.[10] From a physical point of view DNA appears as a polymer model of particular interest that can be studied according to its basic polymer properties (length and rigidity), and from a chemical perspective the structural composition of DNA is considered as a giant linear biopolymer.

DNA chemical structure and properties were gradually explained in the 1st half of the 20th century. In 1953, James Watson and Francis Crick reported a model of the DNA structure, revealing the molecule as an antiparallel double helix.[11]
One strand of DNA has a backbone consisting of deoxyribonucleic units and the repeating units are called nucleotides.[12] A nucleotide is composed of three parts: pentose, base and phosphate group. In aqueous solution, the phosphate groups are mostly deprotonated (pKa ≈ 2), therefore DNA molecules have usually a negative charge per base. One deoxyribose and one base form together a nucleoside. There are two kinds of nitrogen-containing heterocyclic bases, pyrimidines (cytosine (C) and thymine (T)) and purines (adenosine (A) and Guanine (G)). Purines consist of a six-membered and a five-membered ring, fused together. Pyridmidines have only a six-membered nitrogen-containing aromatic unit (Figure 1.1). [13, 14]

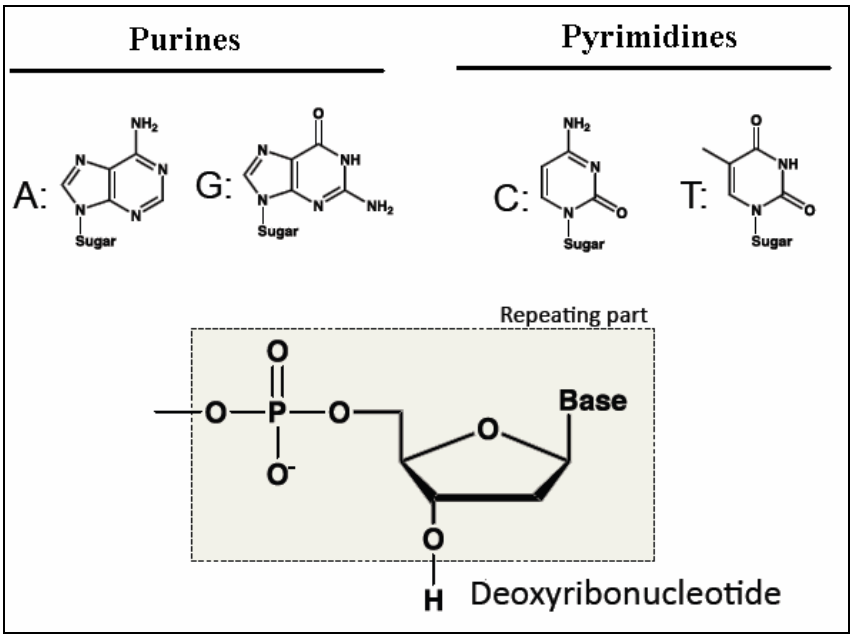

Figure 1.1 Chemical structure of nucleotides.

The purine and pyrimidine bases are directed to the center of the helix, while the phosphate and deoxyribose rests are found on the periphery. This conformation allows the formation of hydrogen bonds between the bases of the two strands for the cohesion of the double helix, where only the so-called Watson-Crick base pairs between A and T (2 hydrogen bonds) and between G and C (3 hydrogen bonds) are present (Figure 1.2).[14]

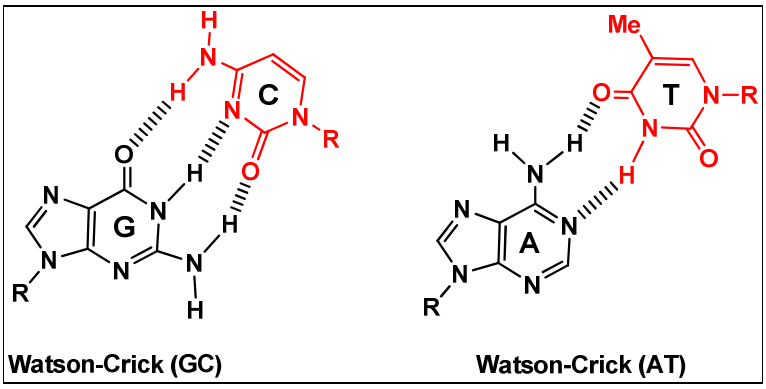

Figure 1.2 Canonical Watson-Crick base-pairing.

By convention, the base sequence is listed starting from the 5' end of the polymer and ending at the 3' end (these abbreviations refer to particular carbon atoms in the deoxyribose sugar units of the sugar-phosphate backbone).

The hydrogen bond formation determines the structure of DNA, showing a periodicity of 10-10.6 base pairs (bp) or 3.4 nm along the helix axis, so that the characteristic length per base pair is 0.34 nm and the diameter of the helix is 2 nm (Figure 1.3).[11]

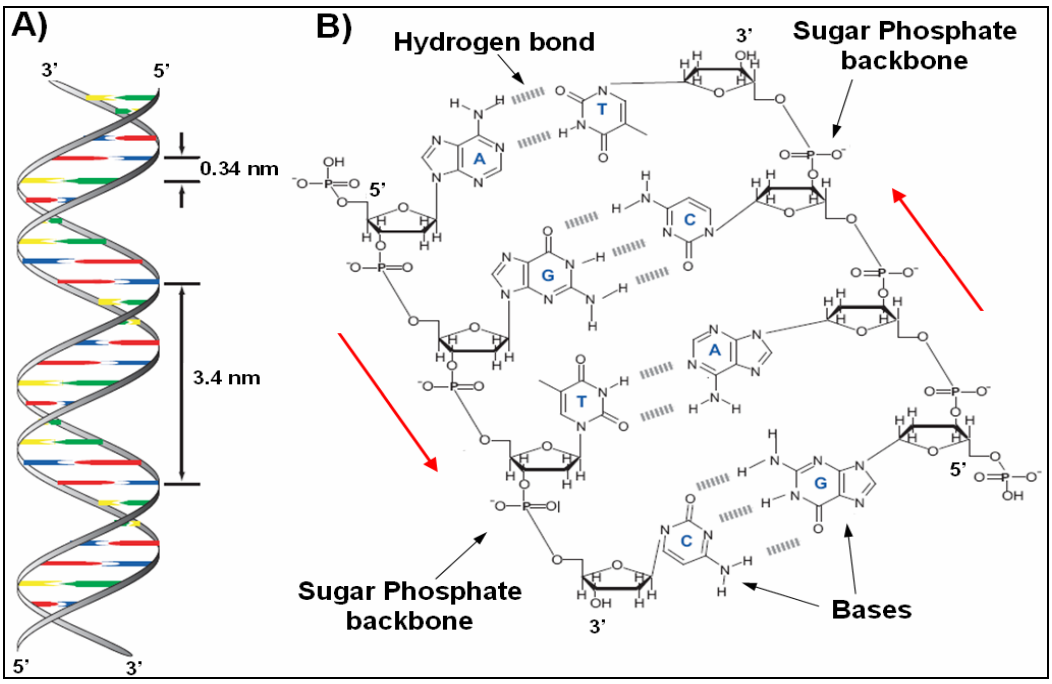

Figure 1.3 Structural features of DNA **(A)** Schematic representation of the double helical DNA **(B)** In single stranded DNA nucleoside units are linked by phosphodiester bonds and hydrogen bonds are formed between DNA bases.

1.1.1 Base pairing

The self-assembly of two single-stranded DNA sequences into a double stranded helix is driven by many intermolecular forces. These include aromatic π-stacking interactions, hydrophobic forces, van der Waals forces, and hydrogen bonding interactions.[15] Of these forces, the self-complementary Watson–Crick hydrogen-bonding interactions[11] that dictate specific base-pairing are crucial for

establishing the fidelity required for efficient storage, replication, and transcription of genetic information.

Despite the prevalence of Watson–Crick base-pairing within a DNA duplex, many alternative pairing patterns are possible (Figure 1.4).[16-18]

The Hoogsteen binding mode utilizes the C6–N7 face of purine nucleosides[19, 20] and is prevalent in DNA and RNA suprastructures and is also found in many protein–DNA and drug–DNA interactions. The other kind of non Watson–Crick base-pairing motifs include wobble base-pairs. These base pair motifs can occur between two nucleotides of RNA (secondary structure) and play an important role in the translation of the genetic code.[21] The four wobble base pairs are: Guanine-Uracil (G-U), Inosine-Uracil (I-U), Inosine-Adenine (I-A) and Inosine-Cytosine (I-C). The 'reverse' base-pairing mode is defined by a *trans* conformation of the two sugar moieties. Such a conformation can lead to reverse Watson–Crick and reverse Hoogsteen base-pairing modes (see Figure 1.4).

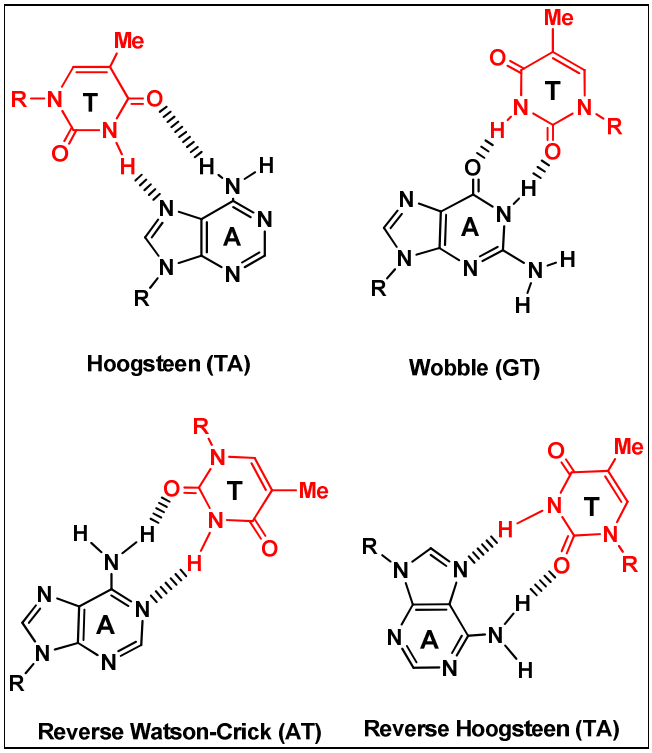

Figure 1.4 Some common non Watson–Crick base-pairing modes.[22]

1.1.2 Hybridization

DNA *hybridization* is defined as the process in which two or more complementary strands of nucleic acids join (Oligonucleotides, RNA or DNA) to form a single hybrid.[15]

The technique of DNA hybridization is based on two principles: double strands of DNA are held together by hydrogen bonds between complementary base pairs (A-T and G-C), and the more closely related two species are, the greater will be the number of complementary base pairs in the hybrid DNA.

Hybridization of DNA occurs in a buffer solution with appropriate pH, salinity and temperature.[23] Heating the DNA solution above a characteristic temperature causes the separation of the two strands of a double helix, breaking the hydrogen bonds between all the complementary base pairs.
In recent years the hybridization technique has been considered of interest for applications in materials chemistry and nanotechnology.[24-27] The concept is quite simple but very significant. For example, the hybridization process permits the facile functionalization of the DNA with different reactants and also DNA self-assembly, rendering then DNA an attractive candidate as an interface for electronic control, as carrier for drug delivery and in computation based on DNA.[28-30]

1.1.3 DNA stability

1.1.3.1 Effects of temperature

As it was already mentioned, double strands can be separated by increasing the temperature, until all the hydrogen bonds are broken. This temperature is called DNA melting or denaturation, abbreviated T_m. At T_m, 50% of the double helix is separated into single strands. For a natural DNA, the T_m depends primarily on its GC content.[31]

The thermodynamic properties of a DNA can be monitored by UV-spectroscopy. As the ordered regions of stacked base pairs in the DNA duplex are disrupted, the UV absorbance at 260 nm increases.[32] This difference in absorbance between the duplex and single strand states is due to an effect called hypochromicity, which is the result of nearest neighbor base pair interactions. When the DNA is in the duplex state, interactions between base pairs decrease the UV absorbance relative to single strands. When the DNA is in the single strand state the interactions are much weaker, due to the decreased proximity, and the UV absorbance is higher than the duplex.[33] The profile of UV absorbance versus temperature is called a melting curve; the midpoint of the transition is defined as the melting temperature (Figure 1.5). The T_m of DNA (in absence of salt) can be calculated using the following equation:

$$T_m = 64.9\,℃ + 41\,℃ \times (\text{number of G's and C's} - 16.4)\ /N \quad \text{(Equation. 1)}$$

where N is the length of the DNA sequence.

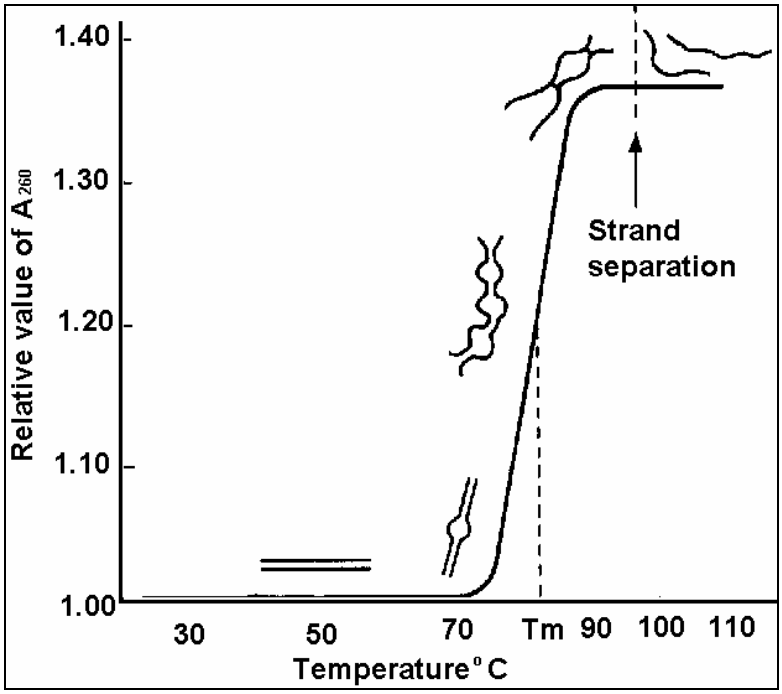

Figure 1.5 Melting curve of DNA: theoretical hyperchromic shift associated with DNA strand separation (denaturation) as a function of temperature.

1.1.3.2 Effects of Stringency

The annealing of single stranded DNA hybrids not only depends on the temperature, but also on the salt concentration and pH.

Stringency is a term used to describe the conditions of hybridization. By varying the conditions (especially salt concentration and temperature) a given probe sequence may be allowed to hybridize only with its exact complement (high stringency), or with any somewhat related sequence (relaxed or low stringency). Increasing the temperature or decreasing the salt concentration (ionic strength) will tend to increase the DNA stability. The phosphates of the backbone, having a negative charge, tend to repel each other. This repulsion destabilizes the DNA double helix. High ionic strength (high salt concentration) shields the negatively charged phosphates from each other. This decreases the repulsion and stabilizes the double helix.[34, 35]

The stability of the double helix is affected also by the GC content. The three hydrogen bonds from a GC base pair, form more stable structures than AT-rich regions.

1.1.4 DNA conformations and grooves

DNA can exist in different conformations (A, B and Z) and these are important for a range of DNA mechanisms (Figure 1.6). These conformations can be formed by rotating various bonds that connect the structure and depend on the temperature and salt concentration as well as the base composition of DNA. Most common conformation *in vivo* is B-DNA, found at low salt concentrations.[36]

The A and B conformations are both right-handed helices that differ in pitch (how much the helix rises per turn) and Z-DNA is a left-handed helical form of DNA in which phosphate backbones of the two antiparallel DNA strands are still arranged in a helix but with more irregular appearance.[37]

A)

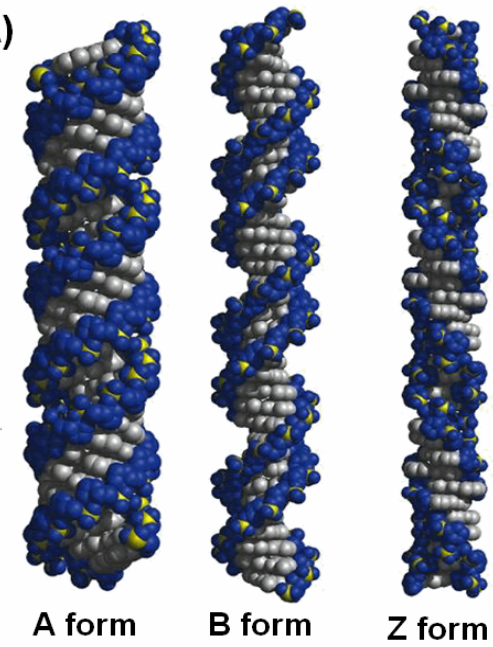

B)

	A	B	Z
Helix Sense	Right-handed	Right-handed	Left-Handed
Repeating unit	1 bp	1 bp	1 bp
Rotation / bp	33.6º	35.9º	60º
Mean bp / turn	10.7	10	12
Rise/bp along axis	2.3 Å	3.2 Å	3.8 Å
Pitch	26.6 Å	33.2 Å	45.6 Å
Diameter	26 Å	20 Å	18 Å

Figure 1.6 A, B and Z conformations of double stranded DNA. **(A)** Schematic representation of the DNA forms **(B)** Geometry differences between the DNA forms.[37]

Another important concept in the DNA conformations is the tracing of spaces, or grooves in the double helix. These grooves play important roles in DNA functioning and allow different processes in cells, for example grooves make possible the contact of proteins with bases. The major groove occurs where the backbones are far apart, the minor groove occurs where they are close together. The grooves twist around the molecule on opposite sides. The major groove is 22 Å wide and the other, the minor groove, is 12 Å wide.[38]

1.2 DNA as a construction material for nanoarchitectures

The fundamental goal of DNA nanotechnology is to construct periodic matter, nanomechanical devices at nanometer scale and extending these structures to macroscopic scale using structural, functional and intermolecular interaction properties of DNA.

The advance in different methods for chemical DNA synthesis[7, 39-43] and its analogs[44, 45] has allowed the fabrication of DNA molecules with specific sequence and length. By using synthesized DNA as building units, various nanostructured materials for computation, engineering and medical applications have been prepared.[9, 46-49]

The study of artificial DNA structures for applications in nanotechnology began during the early 1980s when Ned Seeman and coworkers designed and constructed periodic and discrete objects assembled from synthetic DNA oligonucleotides.[50] He noted that simple double helical DNA could be used for construction of linear assemblies and that more complex building blocks would be required for 2D or 3D architectures. In 1991, Seeman published the synthesis of a 3D cube made of DNA, followed by a DNA truncated octahedron (Figure 1.7) and the assembly of Borromean rings and knots using DNA.[51]

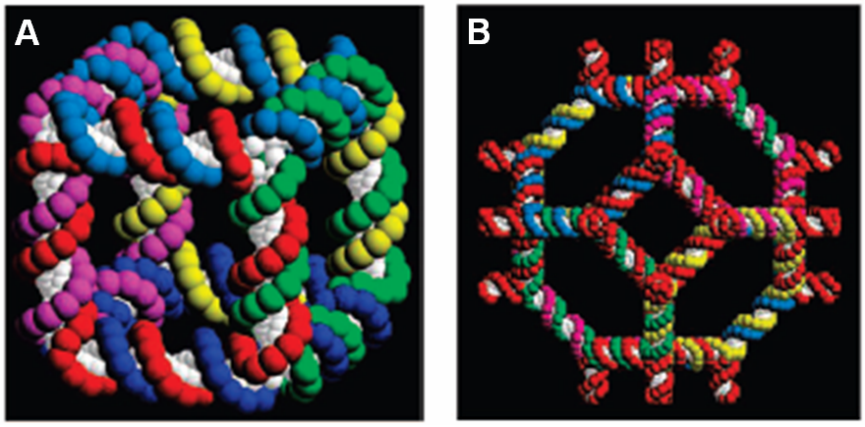

Figure 1.7 Topologies of **(A)** DNA cube and **(B)** DNA truncated octahedron.[52]

Later, Seeman developed in collaboration with Erik Winfree, branched DNA motifs like Holliday junctions (two adjacent DNA helices form a junction with one strand of each DNA helix crossing over to the other DNA helix) or related structures, such as double-crossover (DX), triple crossover (TX), paranemic crossover (PX) and parallelogram motif molecules[53, 54] and provided details on

design and construction methods for generation of complex molecular building blocks (called DNA tiles). The generation of these tiles is based on the combination of the branched structures, the sticky-end cohesion ability and other properties of DNA structures.

DX refers to two parallel helices that are connected twice by crossovers (branched junctions); the crossovers can be between strands of the same polarity or the opposite polarity. The triple crossover tiles contain three coplanar double helices linked at each of four crossover points.

The “PX” motif consists of having a crossover at every possible position where two double helices would juxtapose and the strands are of the same polarity (those are stable).[50] Winfree and Paul Rothemund, demonstrated that these tiles formed large lattices useful in DNA computing (Figure 1.8).[55]

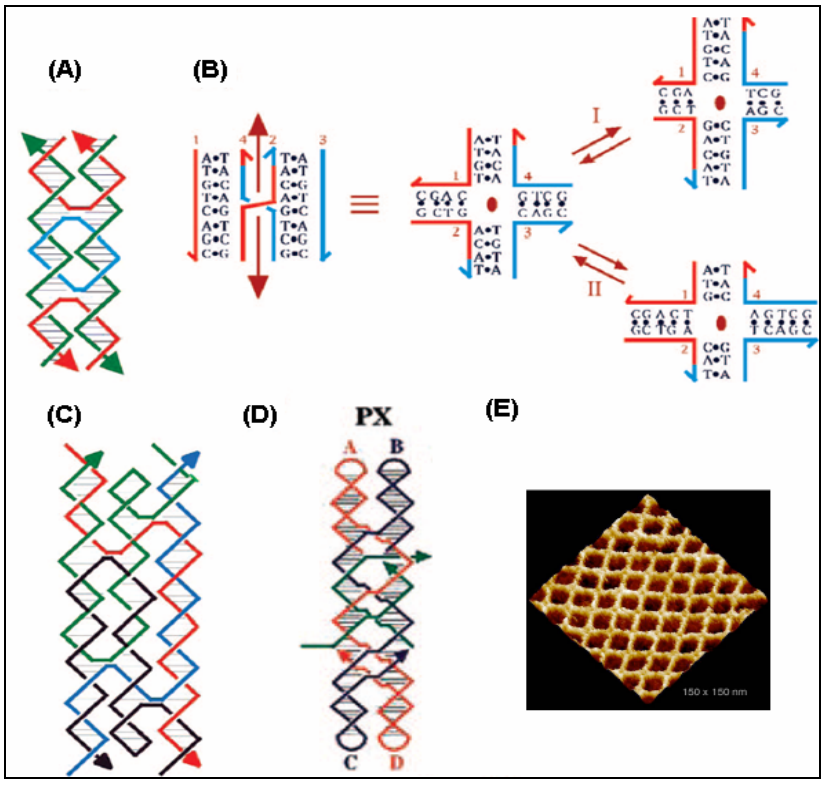

Figure 1.8 Topology of DNA junctions. **(A)** double-crossover (DX), **(B)** Holliday, **(C)** triple-crossover (TX), and **(D)** paranemic crossover (PX)[52] **(E)** AFM image of 2D Lattice of Cross tiles.[55]

The use of DNA to fabricate periodic frameworks and self-assembled nanostructures, consisting of inorganic and bioorganic compounds has been also reported.[56]

In recent years, the base sequence design for nanostructures has been explored by introducing different approaches and new strategies. In the field of DNA nanotechnology, Paul Rothemund developed a new technique called "DNA origami",[57, 58] consisting of the self-assembly of DNA to create arbitrary 2D and 3D shapes and patterns at small scales (Figure 1.9).

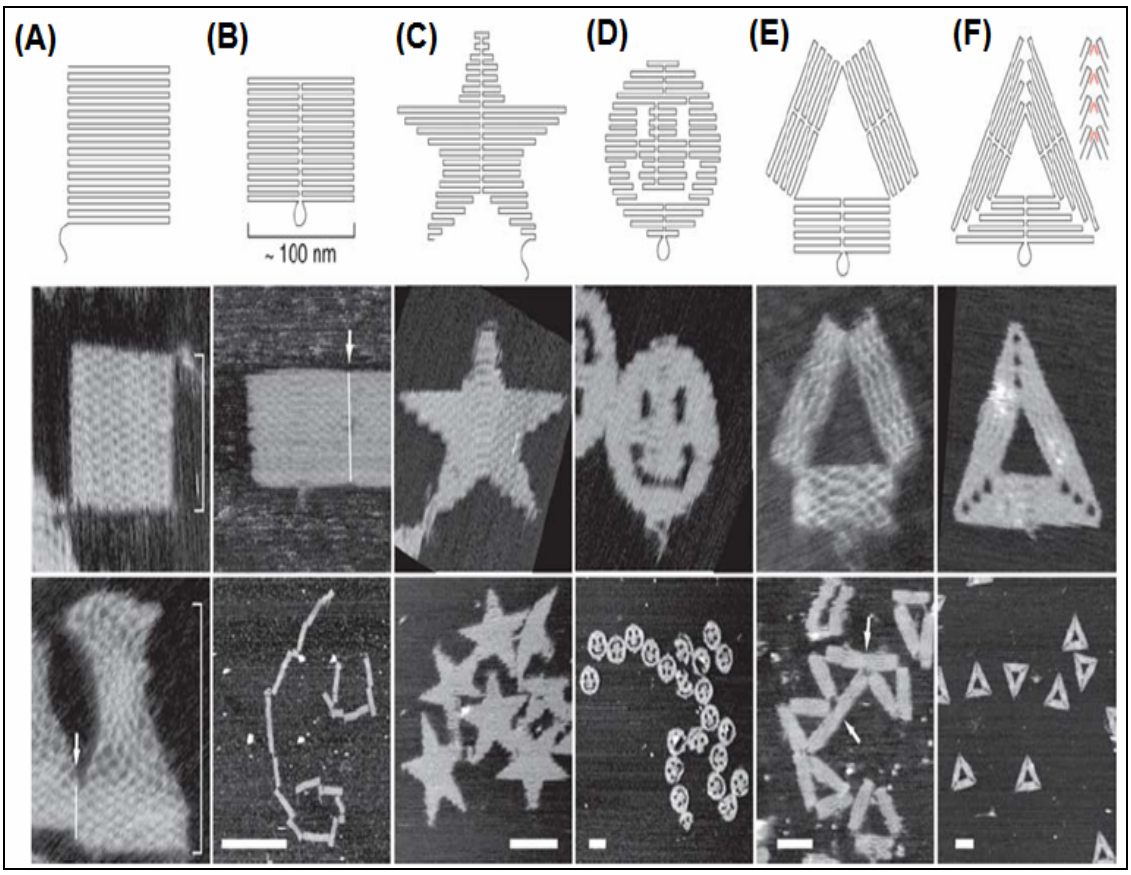

Figure 1.9 DNA origami shapes. Top row, folding paths of : **(A)** square; **(B)** rectangle; **(C)** star; **(D)** disk with three holes; **(E)** triangle with rectangular domains; **(F)** sharp triangle with trapezoidal domains. Bottom row: AFM images. All images and panels without scale bars are the same size, 165 nm x 165 nm^2. Scale bars for lower AFM images: (B) 1 mm and (C–F) 100 nm.

1.3 DNA-based hybrid materials

In addition to the use of DNA as a scaffold for the generation of nanostructured materials, scientists have been also taking advantage of the physicochemical stability, mechanical rigidity, and high precision programmability of DNA to generate novel DNA-hybrid materials.
In this field, the automated DNA synthesis on solid phase has provided not only the possibility to generate DNA in large scale, but has also allowed the conjugation of oligonucleotides with radioactive markers[59] (^{32}P and ^{33}P), different organic polymers[60-66] or fluorescent dyes,[67-69] just to name a few.

1.3.1 DNA-dye conjugates

DNA labeling plays an important role in many molecular biology procedures, including DNA sequencing and *in situ* DNA hybridization. DNA labeling enables the visualization of particular DNA molecules in a variety of analytical systems, such as nylon membranes, agarose or acrylamide gels, or at the cellular level in histological preparates. Furthermore, the interest in DNA-dye conjugates has been growing in the last years, due to their potential as components for molecular electronic devices.[70, 71]

Based on such an approach, Abdalla *et al* exploited the assembly properties of DNA and functionalized with a perylenediimide chromophore (Figure 1.10).[72]
These bioorganic conjugates were water soluble and capable of hybridization with complementary oligonucleotide sequences. The hybridization of this conjugate induced the formation of linear structures including dimers, trimers, tetramers and pentamers. Besides the supramolecular assembly, these chromophore-DNA-hybrids were used as fluorescent probes. The physicochemical properties of the dye–DNA polymers were characterized by fluorescence correlation spectroscopy (FCS), UV/Vis spectroscopy, and gel

electrophoresis. This system showed favorable and adaptable chromophoric properties, qualifying it as a promising material for electronic and photonic applications.

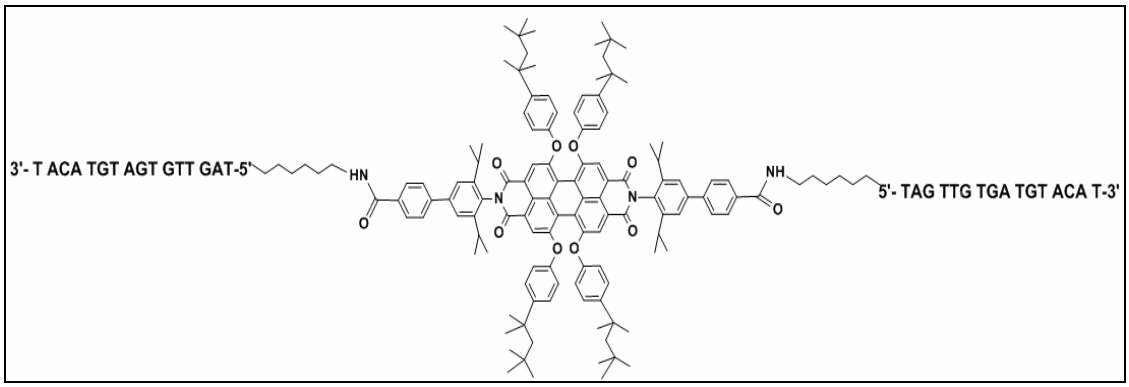

Figure 1.10 Structure of perylenediimide-oligonucletide conjugates.

In other approach, Kashida *et al* reported the preparation of hetero H aggregates, in which two dyes (Methyl red and naphthyl red) are stacked alternately. The dyes were introduced into the DNA, employing automated DNA synthesis by using the corresponding phosphoroamidite monomer. The system was prepared by interstrand stacking from two DNA–dye conjugates.[73] The control of dye aggregation is of great importance,[74] especially for processes of photoinduced electron transfer[75] and enhancement of nonlinear optical properties.[76]
In conclusion, DNA has played and will play an important role in the spatial organization of chromophores.

1.3.2 DNA block copolymers (DBCs)

Besides functionalizing DNA with dye molecules, DNA was combined with synthetic macromolecules.[61 ,62, 65] The coupling of oligonucleotides to organic polymers has emerged as a promising research area where the combination of properties related to the polymer backbone and the DNA can be simultaneously addressed, manipulated, and optimized for a specific purpose. The combination

of oligonucleotides with organic polymers allows the formation of DNA block copolymers (DBCs) (i.e., polymers containing two different polymer chains that are covalently linked together). Different coupling strategies have been employed to generate DBCs, including the preparation of the conjugates in solution and on solid phase.

Conjugates based on oligonucleotide segments and organic polymers such polybutadiene,[66] polystyrene (PS)[65] or poly(D,L-lactic-*co*-glycolic acid) (PLGA)[61] have been developed successfully and have proven promising.

For example, Mirkin and coworkers generated linear DNA block copolymers based on ODN and polystyrene (PS) segments.[65] The PS block was coupled to the ODN employing standard phosphoramidite chemistry on solid support. The amphipilic characteristics of this kind of molecules allowed the formation of micelles by self-assembly in aqueous medium. The amphiphiles were functionalized with gold nanoparticles through DNA hybridization. Additionally it was shown that aggregation of the micelles can be controlled by reversible thermal denaturation and rehybridization. Further studies revealed that this principle is equally applicable to nanoparticles of different size.[77]

More recently, Alemdaroglu *et al* reported the synthesis of a new class of amphipilic hybrids based on polypropylene oxide (PPO) as hydrophobic block and DNA as hydrophilic part.[62, 63, 78] These DNA-PPO block copolymers self-assembled into micelles and were demonstrated to be a highly modular platform for drug delivery, being able to accommodate lipophilic drugs in the core of the micelles. In addition, the same author investigated the alternation of the micelles shape by hybridization converting the single stranded micelles into double stranded DNA by employing Watson-Crick base pairing. Moreover, the hybridization of the nanoobjects allowed their functionalization with different reactants. The subsequent chemical reactions at the surface of the micelles within the interior were also reported (Figure 1.11).[78]

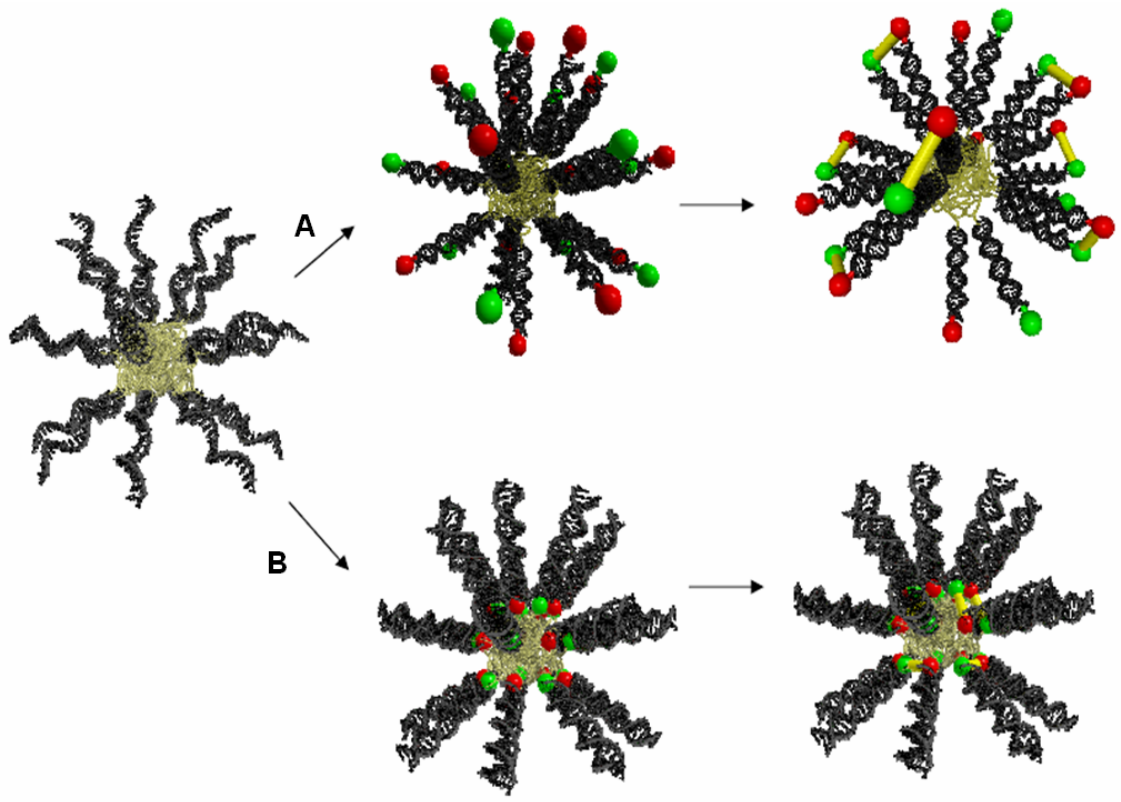

Figure 1.11 Schematic illustration of DNA-templated synthesis in DBC micelles. The micelles consist of a hydrophobic core and a shell of DNA. Single stranded micelles can be hybridized with ODNs that are equipped with reactants (green and red balls). **(A)** The subsequent chemical reaction proceeds at the surface of the micelle or **(B)** within the core.[78]

1.4 Summary

Undoubtedly, DNA's unique recognition capabilities, its physicochemical stability and its mechanical properties qualify this macromolecule as a promising material for the generation of novel materials to be used in different applications.

Despite the significant progress and investigations made in the last years, the study of DNA-based nanostructures and hybrids is still at its early stage. Advanced studies in this field will not only provide valuable fundamental information about the collective physical and chemical properties of the

nanostructured DNA hybrid materials, but may also provide access to novel and useful structures applicable to medicine, biology and the industry.

In this regard, in the following chapters of this thesis it will be described how DNA's physical and chemical properties were used as a tool for the generation of promising macromolecular architectures by combining different synthetic strategies from classical polymer chemistry and molecular biology.

1.5 References

[1] W. Mok, Y. F. Li, *Sensors* **2008**, *8*, 7050.

[2] C. M. Niemeyer, C. A. Mirkin, *Nanobiotechnology, Concepts, Applications and Perspectives*, VCH, Weinheim, **2004**.

[3] D. E. Diggs, J. G. Grote, F. K. Hopkins, J. Hagen, *Proc. SPIE-Int. Soc. Opt. Eng*. **2006**, *6331*, O3310.

[4] C. Dekker, M. A. Ratner, *Phys. World.* **2001**, *14*, 29.

[5] R. Bashir, *Superlattice. Microst.* **2001**, *29*, 1.

[6] M. C. Roco, *Curr. Opin. Biotechnol.* **2003**, *14*, 337.

[7] S. L. Beaucage, M. H. Caruthers, *Tetrahedron Lett.* **1981**, *22*, 1859.

[8] C. X. Lin, Y. Liu, S. Rinker, H. Yan, *ChemPhysChem* **2006**, *7*, 1641.

[9] Y.Sun, C. H. Kiang, in *Handbook of Nanostructured Biomaterials and Their Applications in Nanobiotechnology Vol. 1*, Nalwa American Scientific Publishers **2005**.

[10] J. D. Watson, F. H. C. Crick, *JAMA-J. Am. Med. Assoc.* **1993**, *269*, 1967.

[11] J. D. Watson, F. H. C. Crick, *Nature* **1953**, *171*, 737.

[12] W. Sanger, *Principles of Nucleic Acid Structure*, Springer, New York, **1984**.

[13] C. R. Cantor, P. Schimmel, *Biophysical Chemistry Part I: The Conformation of Biological Macromolecules*, W. H. Freeman, San Francisco, **1980**.

[14] V. A. Bloomfield, D. M. Crothers, I. Tinoco, *Nucleic Acids: Structures, Properties and Functions*, University Science Books, Sausalito, **2000**.

[15] R. R. Sinden, *DNA Structure and Function*, Academic Press, Inc, New York, **1994**.

[16] G. A. Jeffrey, W. Saenger, *Hydrogen Bonding in Biological Structures*, Springer, Berlin, **1991**.

[17] N. B. Leontis, J. Stombaugh, E. Westhof, *Nucleic Acids Res.* **2002**, *30*, 3497.

[18] M. G. M. Purwanto, K. Weisz, *Curr. Org. Chem.* **2003**, *7*, 427.

[19] K. Hoogsteen, *Acta Crystallogr.* **1959**, *12*, 822.

[20] K. Hoogsteen, *Acta Crystallogr.* **1963**, *16*, 907.

[21] G. Varani, W. H. McClain, *EMBO Reports* **2000**, *1*, 18.

[22] J. L. Sessler, J. Jayawickramarajah, *Chem. Commun.* **2005**, 1939.

[23] J. H. Reif, T. H. LaBean, in *Bio-inspired and Nano-scale Integrated Computing* (Ed: M. Eshaghian), Wiley, USA, **2007**

[24] N. C. Seeman, *Curr. Opin. Struct. Biol.* **1996**, *6*, 519.

[25] N. C. Seeman, *Acc. Chem. Res.* **1997**, *30*, 357.

[26] J. L. Seifert, R. E. Connor, S. A. Kushon, M. Wang, B. A. Armitage, *J. Am. Chem. Soc.* **1999**, *121*, 2987.

[27] Z. Deng, Y. Chen, Y. Tian, C. Mao, *A fresh look at DNA nanotechnology, chapter in Nanotechnology: Science and Computation*, Springer, **2006**.

[28] K. V. Gothelf, T. H. LaBean, *Org. Biomol. Chem.* **2005**, *3*, 4023.

[29] K. Hamad-Schifferli, in *Dekker Encyclopedia of Nanoscience and Nanotechnology*, Taylor & Francis, **2004**.

[30] K. Hamad-Schifferli, J. J. Schwartz, A. T. Santos, S. G. Zhang, J. M. Jacobson, *Nature* **2002**, *415*, 152.

[31] K. L. Lerner, B. W. Lerner, in *World of Microbiology and Immunology* Gale Cengag, **2003**.

[32] J. Marmur, P. Doty, *J. Mol. Biol.* **1962**, *5*, 109.

[33] K. Sauer, *Biochemical Spectroscopy, Vol. 246*, Academic Press, **1995**.

[34] Gruenwed.Dw, C. H. Hsu, *Biopolymers* **1969**, *7*, 557.

[35] Gruenwed.Dw, C. H. Hsu, D. C. Lu, *Biophys. J.* **1969**, *9*, A53.

[36] L. Stryer, *Biochemistry*, 4th ed., W.H. Freeman & Company, New York, **1995**.

[37] R. E. Dickerson, H. R. Drew, B. N. Conner, R. M. Wing, A. V. Fratini, M. L. Kopka, *Science* **1982**, *216*, 475.

[38] R. Wing, H. Drew, T. Takano, C. Broka, S. Tanaka, K. Itakura, R. E. Dickerson, *Nature* **1980**, *287*, 755.

[39] H. G. Khorana, G. M. Tener, J. G. Moffatt, E. H. Pol, *Chem. Ind.* **1956**, 1523.

[40] Letsinge.Rl, K. K. Ogilvie, P. S. Miller, *J. Am. Chem. Soc.* **1969**, *91*, 3360.

[41] B. Yuodka, W. B. Lunsford, R. L. Letsinger, *Bioorg. Khim.* **1976**, *2*, 1318.

[42] R. L. Letsinger, W. B. Lunsford, *J. Am. Chem. Soc.* **1976**, *98*, 3655.

[43] L. J. Mcbride, M. H. Caruthers, *Tetrahedron Lett.* **1983**, *24*, 245.

[44] F. Eckstein, *Oligonucleotides and Analogues*, IRL Press, New York, **1991**.

[45] R. L. Letsinger, M. J. Kornet, *J. Am. Chem. Soc.* **1963**, *85*, 3045.

[46] T. H. LaBean, in *Introduction to Self-Assembling DNA Nanostructures for Computation and Nanofabrication* (Ed: J. T. L. Wang, Wu, C. H. & Wang, P. P), World Scientific Publishing, **2003**.

[47] A. Condon, *Nat. Rev. Genet.* **2006**, *7*, 565.

[48] T.Kubik, K.Kubik, M.Sugisaka, *Nanotecnology on Duty in Medical Applications, Vol. 6*, Bentham Science Publishers Ltd, **2005**.

[49] Y. Benenson, B. Gil, U. Ben-Dor, R. Adar, E. Shapiro, *Nature* **2004**, *429*, 423.

[50] N. C. Seeman, *J. Theor. Biol.* **1982**, *99*, 237.

[51] N. C. Seeman, C. D. Mao, W. Q. Sun, *Math. Intelligencer.* **1998**, *20*, 3.

[52] N. C. Seeman, *Biochemistry* **2003**, *42*, 7259.

[53] N. C. Seeman, *Annu. Rev. Biophys. Biomol. Struct.* **1998**, *27*, 225.

[54] E. Winfree, F. R. Liu, L. A. Wenzler, N. C. Seeman, *Nature* **1998**, *394*, 539.

[55] M. Cook, P. W. K. Rothemund, E. Winfree, *LNCS* **2004**, *2943*, 91.

[56] C. M. Niemeyer, *Curr. Opin. Chem. Biol.* **2000**, *4*, 609.

[57] P. W. K. Rothemund, *IEEE. IC.CAD* **2005**, 471.

[58] P. W. K. Rothemund, *Abstr. Papers Am.Chem.Soc.* **2006**, *231*.

[59] D. Schuler, M. Otteneder, P. Sagelsdorff, E. Eder, R. C.Gupta, W. K.Lutz, *Carcinogenesis* **1997**, *18* 2367.

[60] K. Ding, F. E. Alemdaroglu, M. Börsch, R. Berger, A. Herrmann, *Angew. Chem., Int. Ed.* **2007**, *46*, 1172.

[61] J. H. Jeong, T. G. Park, *Bioconjugate Chem.* **2001**, *12*, 917.

[62] F. E. Alemdaroglu, N. C. Alemdaroglu, P. Langguth, A. Herrmann, *Adv. Mater.* **2008**, *20*, 899.

[63] F. E. Alemdaroglu, A. Herrmann, *Org. Biomol. Chem.* **2007**, *5*, 1311.

[64] F. E. Alemdaroglu, M. Safak, J. Wang, R. Berger, A. Herrmann, *Chem. Commun.* **2007**, 1358.

[65] Z. Li, Y. Zhang, P. Fullhart, C. A. Mirkin, *Nano Lett.* **2004**, *4*, 1055.

[66] F. Teixeira, P. Rigler, C. Vebert-Nardin, *Chem. Commun.* **2007**, 1130.

[67] J. White, K. Truesdell, L. B. Williams, M. S. AtKisson, J. S. Kauer, *PLoS Biology* **2008**, *6*, 30.

[68] H. Asanuma, K. Shirasuka, T. Takarada, M. Komiyama, *Nucleic Acids Res.* **2001**, *1*, 193.

[69] J. White, K. Truesdell, L. B. Williams, M. S. AtKisson, J. S. Kauer, *PLoS Biology* **2008**, *6* 30.

[70] M. A. Fox, *Acc. Chem. Res.* **1999**, *32*, 201.

[71] C. M. Niemeyer, M. Adler, *Angew. Chem. Int. Ed.* **2002**, *41*, 3779.

[72] M. A. Abdalla, J. Bayer, J. O. Radler, K. Müllen, *Angew. Chem., Int. Ed.* **2004**, *43*, 3967.

[73] H. Kashida, H. Asanuma, M. Komiyama, *Supramol. Chem.* **2004**, *16*, 459.

[74] T. Kobayashi, *J-aggregates*, World Scientific Publishing Co., Singapore, **1996**.

[75] H. Asanuma, T. Tani, *J. Phys. Chem. B* **1997**, *101*, 2149.

[76] F. Wurthner, C. Thalacker, S. Diele, C. Tschierske, *Chem. Eur. J.* **2001**, *7*, 2245.

[77] R. C. Mucic, J. J. Storhoff, C. A. Mirkin, R. L. Letsinger, *J. Am. Chem. Soc.* **1998**, *120*, 12674.

[78] F. E. Alemdaroglu, K. Ding, R. Berger, A. Herrmann, *Angew. Chem., Int. Ed.* **2006**, *45*, 4206.

Chapter 2

MOTIVATION AND OBJECTIVES

In addition to being the natural biological information carrier, DNA structure and properties, already described in *Chapter 1*, make it a promising molecular building block for the construction of nanoscale objects that can be used for many potential applications including the fabrication of nanoparticles and protein arrays, nanomechanical switches and biomedical nanodevices.

DNA's intermolecular interactions, especially base-pair affinities allow defined strand association and provide precise spatial control, serving as an ideal tool for structural design. DNA is a stable molecule and its structure permits the attachment of diverse materials at defined positions. In addition, DNA can be obtained from a variety of sources including live cells, enzymatic reactions and chemical synthesis. The easy access of DNA from short oligonucleotides to high molecular weight polynucleic acids represents another attractive feature of this material.

The aim of this work was to take advantage of the exceptional physicochemical properties of DNA to design novel hybrid materials, consisting of DNA and different organic molecules, especially highly fluorescent dyes.

The properties of the emissive DNA-hybrid materials were analyzed by different methods such as Fluorescence Correlation Spectroscopy (FCS), Atomic Force Microscopy (AFM), Dynamic Light Scattering (DLS), and single molecule Fluorescence Resonance Energy Transfer (FRET).
The preparation of the structures was achieved by a multidisciplinary approach combining techniques from organic chemistry and molecular biology. The biological methods include gel electrophoresis, polymerase chain reaction (PCR), transformation of cells and restriction enzyme digests.

In the first part of this thesis (*Chapter 3*), the formation of DNA aggregates induced by a perylenediimide (PDI) dye exhibiting an extended aromatic core was investigated. Short PDI labeled nucleic acid segments were hybridized with a long DNA template, forming a double helix onto which four PDI units were annealed. The resulting double stranded helices self-assembled into structures of higher order, induced by π-π stacking. The behavior of this system was studied on a surface employing Atomic Force Microscopy (AFM) and in solution by Fluorescence correlation spectroscopy (FCS) and by photoluminiscence (PL) spectroscopy.

In the second part of the thesis (*Chapter 4*), the reptation of linear DNA chains was investigated. Of special interest was the analysis of end-to-end contacts of DNA macromolecules in semidilute and concentrated solutions. The PCR technique was used to amplify a DNA chain of 7 kbp (2.38 µm in length) and to incorporate ATTO dyes at the termini of the double helix. Additionally, unlabelled DNA was prepared in milligram scale by transforming *E.coli* cells with the plasmid pET44a+. Single–molecule FRET and wide field fluorescence microscopy were employed to provide information about the Brownian end-to-end motion and about the segmental motion of the labeled DNA chain at the molecular level.

In *Chapter 5* the design and characterization of a family of DNA amphiphiles containing modified uracil nucleobases was introduced. The uracil nucleobases were functionalized at the 5-position with dodec-1-yne ($-C_{12}H_{22}$), imparting hydrophobicity to the material. Three lipid-DNA sequences were efficiently synthesized employing solid-phase DNA synthesis. The sequences differ in the positions and number of modified bases along a fixed 12mer sequence length and all self-assembled into micelles at room temperature, containing a hydrophobic core and a hydrophilic DNA corona. The influence of the structure of the ODNs on the morphology, size and stability of the micelles was investigated. Furthermore, the ability of hybridization of the DNA amphiphiles was studied employing polyacrylamide gel electrophoresis (PAGE) and SYBR Green I fluorescence analysis.

In *Chapter 6* a new strategy for facile self-assembly and loading of Cowpea Chlorotic Mottle Virus (CCMV) capsids using DNA micelles that were introduced in the previous chapter was described. The DNA amphiphile aggregates with their negatively charged corona template the virus capsid (VC) formation from protein dimers in solution. The preloading of the micelles with hydrophobic or hydrophilic entities enabled the encapsulation of various small molecules inside VCs. The VC formation as well as the loading was analyzed by various techniques including high resolution transmission electron microscopy, size exclusion chromatography, UV/Vis absorption and fluorescence spectroscopy. For the latter characterization method, again dye functionalized oligonucleotides were of major importance.

While loading of virus particles was confirmed with fluorescence measurements in the bulk, in the last chapter of this thesis (*Chapter 7*), oligonucleotide-dye conjugates were investigated on the single molecule level. Single-molecule spectroscopy was used to study water-soluble perylene dicarboximide fluorophores (PDI), which were immobilized in aqueous buffer by hybridization with a DNA-functionalized surface. The fluorescence of the PDI was controlled

through photoinduced electron-transfer reactions. In order to test whether the photophysics of PDI could be manipulated similarly in nonaqueous conditions, the fluorophore was immobilized on a streptavidin coated surface via a biotin-modified poly(ethylene glycol) (PEG) linker and was analyzed in acetonitrile.

In summary, a variety of synthetic strategies were applied to generate bioorganic hybrid polymers employing molecular biology and organic chemistry techniques. Moreover, these structures were investigated regarding their physical properties like optical behavior or self-assembly into superstructures. Finally, novel functionalities were successfully realized with DNA conjugates such as the loading of virus-like particles. In the following it will be outlined how the fascinating field of DNA hybrids materials is advanced especially by the combination of nucleic acids and dyes as well as amphiphiles.

Chapter 3

AGGREGATION OF DOUBLE STRANDED DNA INDUCED BY AROMATIC π-SYSTEMS

3.1 Introduction

In recent years, the number of studies dealing with dye aggregates has been rapidly growing. Such kind of systems exhibit photophysical properties sometimes different from that of single chromophores which results in numerous possible technological applications.[1] It is still a big aim in the field to find synthetic strategies how stable and precisely defined dye superstrucures like J- and H-aggregates are achieved. Different designs based on amphiphiles,[2] polyelectrolytes,[3] inorganic salts[4] and biopolymers[5] were utilized to control the supramolecular arrangements of various dyes. Among biomacromolecules nucleic acids with their programmable self-recognition properties and their mechanical rigidity[6] are an appealing scaffold for the defined spatial organization of chromophores. Multiple adjacent pyrene units in a π-stacked configuration were incorporated into synthetic RNA by functionalizing the 2'-position of the ribose unit.[7, 8]
By coupling the same dye to the nucleobase similar helical stacks were achieved.[9] Likewise, porphyrin arrays were generated by DNA as a supramolecular scaffold.[10] While in the above mentioned examples the dyes

are attached as side chains into the polynucleic acid scaffolds, chromophores can also be incorporated as constituent components of the main chain. In this way dye aggregates with pyrene[11] and perylenediimide (PDI) were fabricated.[12] In the latter case the integration of synthetic and natural oligomeric sequences within a single macromolecule resulted in folded nanostrucures with unusual temperature dependent aggregation behavior.[12] While an increase in the temperature resulted in stronger π-π interactions of the perylene derivatives the dye aggregates could be unzipped by DNA hybridization. In subsequent AFM experiments the attractive forces between the large aromatic units could be even quantified to the pico-Newton regime by mechanical stretching.[13]

In this study those π-π interactions were not only employed to fabricate dye aggregates but also well defined DNA nanostrucures. While the Watson-Crick base-paring of DNA was used to precisely position perylene dyes on a DNA scaffold their π-π stacking ability was utilized to arrange different DNA strands into structures of higher complexity resulting in parallely aligned double helices.

3.2 Preparation of dsDNA-PDI hybrids

Dyes such as perylene, perylenediimide and other higher members of the rylene series, reveal exceptional chemical, thermal and photochemical stabilities paired with high fluorescence quantum yields in organic solvents[14, 15] but poor emission properties in aqueous medium. The water soluble perylenediimide dye employed in this study does not reveal this shortcoming.[16] This rylene derivate contains four aryl substituents bearing sulfonic acid groups that introduce water solubility (Figure 3.1).[17]

On the other hand, the large π-electron system of the rigid core still enables stacking between the molecules.[18] Previous studies already elucidated the

photophysical properties of this water soluble rylene dye at the ensemble and single molecule level, revealing a high fluorescence quantum yield, high photostablity and appropriate characteristics to be used in biological studies.[19]

Here, as the first step, the water soluble PDI was coupled to single stranded (ss) DNA (22mer; 5'-CCTCGCTCTGCTAATCCTGTTA-3'; M_w=6612 g/mol) to form ssDNA-PDI. The water-souble perylenediimide (PDI) dye mentioned in this chapter and in *chapter 7* was synthesized by *Dr. Carla Spagnuolo*.

The ssDNA-PDI conjugate was synthesized employing the so called "syringe synthesis technique",[20, 21] enabling the direct labeling of the 5' amino hexyl group of the oligonucleotide with the carboxyl-functionalized PDI (M_w=1311 g/mol) on the solid-support (Figure 3.1). A yield of 71 % was achieved for the amide bond formation (Synthesis details in experimental section).

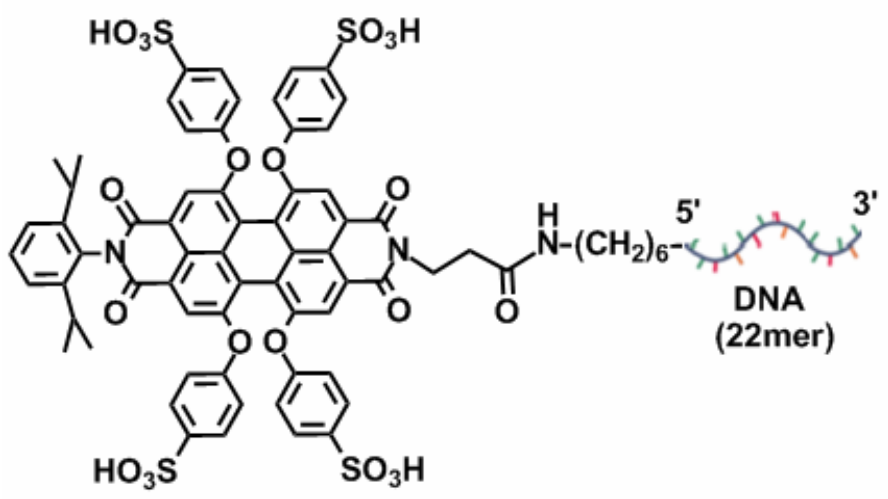

Figure 3.1 ssDNA-PDI conjugate (22mer) synthesized on a solid support by amide bond formation.

The conjugate was hybridized with a 88mer template (T88) (5'-$(TAACAGGATTAGCAGAGCGAG)_4$-3') that encoded four times the complement of ssDNA-PDI. The ratio of the ssDNA-PDI and 88 bp DNA was adjusted four to one (Figure 3.2) allowing full hybridization of the template.

The double stranded DNA helix twists 360° per 10.6 base pairs,[22, 23] meaning that the 22 bp sequence completes 2 turns and the four PDIs should be orientated to the same side every 2 helical twists within the 88 bp dsDNA. The supramolecular aggregates that result from individual dsDNA-PDI(4) (88 bp) are investigated in the following.

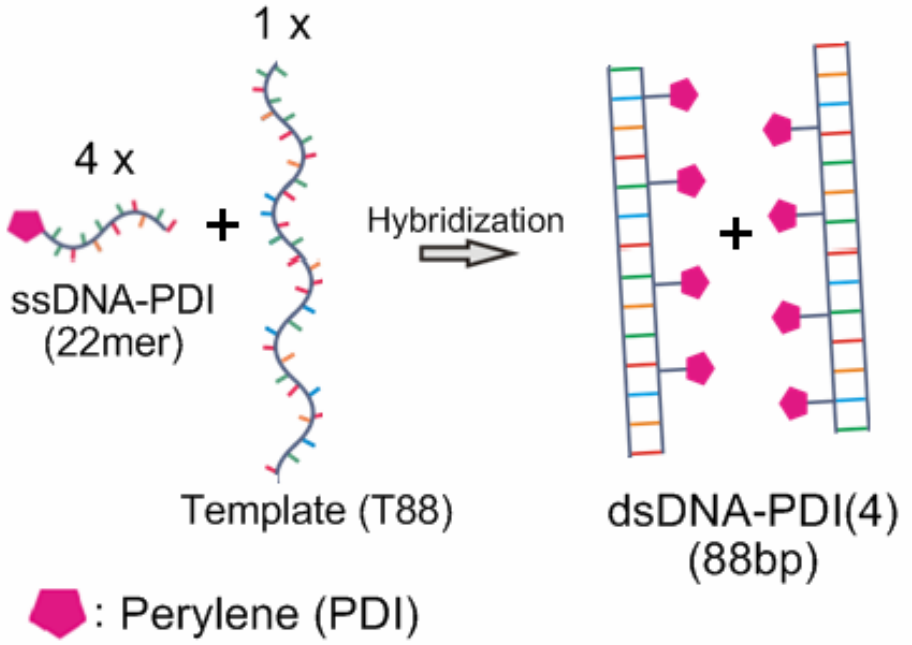

Figure 3.2 Schematic representation of hybridization of ssDNA-PDI with a long DNA template (88 mer).

3.3 Analysis on a surface by Atomic Force Microscopy (AFM)

In order to directly visualize the superstructures on a surface, AFM was performed in buffer (10 mM Tris pH = 7.4, 1 mM $NiCl_2$) using a mica substrate. AFM measurments were carried out by *J.Wang* in the group of *Dr. R. Berger* at the Max-Planck Institute for Polymer Research.

Clearly several dimeric structures were observed (see black circled areas in

Figure 3.3) suggesting that two helices were aligned parallel to each other. A detailed analysis of 13 objects revealed an average length of the rod structures of 33 ± 5.3 nm. The length of the rod-like aggregates corresponds very well with the length of dsDNA exhibiting the same number of nucleotides as present in the template T88 (~29.9 nm) when assuming a contribution of 0.34 nm per base pair. The distance of the dimeric structure from the center of the dsDNA to the center of the adjacent dsDNA was estimated to be 4.1 ± 0.4 nm. The measured value is in agreement with the theoretical value given by the radius of dsDNA (1.1 to 1.3 nm)[24] and the diameter of PDI (1.0 - 1.8 nm) resulting in a distance of DNA aggregates in the range of 3.2 to 4.4 nm.

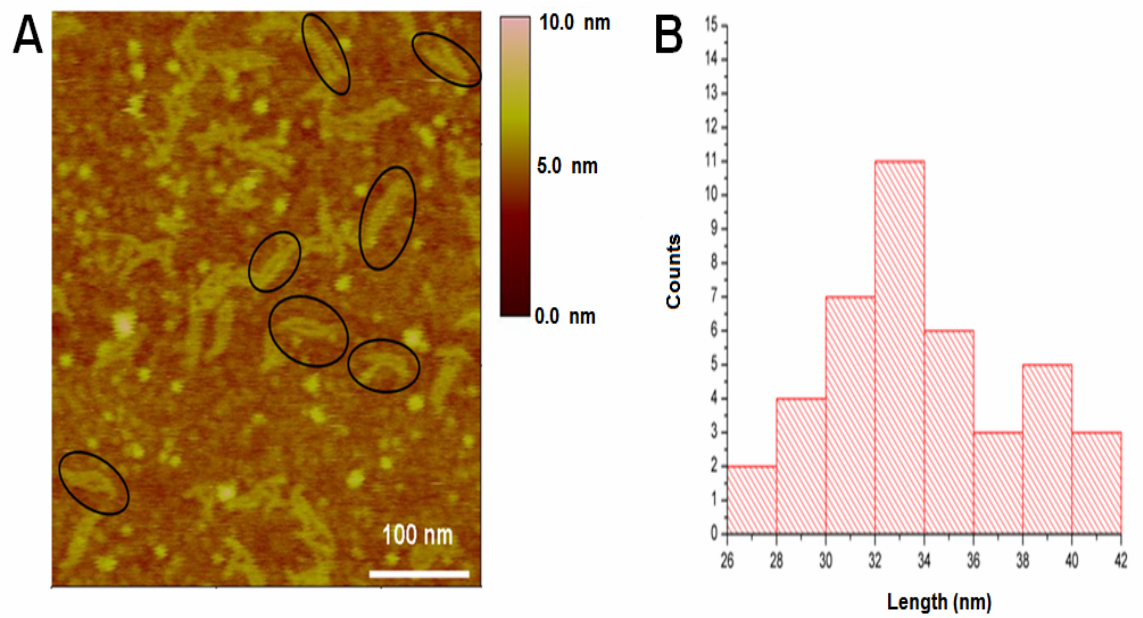

Figure 3.3 (A) AFM image of the hybridization product of ssDNA-PDI and T88. **(B)** Histogram showing the length distribution of the structures.

With the purpose of proving that the π-π interactions between PDIs are the reason for aggregation, a control experiment was carried out. A 22mer ssDNA without PDI was hybridized with the 88mer template.

The resulting AFM image does not show any dimer structures, proving that the presence of perylenes is necessary for the pair formation (Figure 3.4).

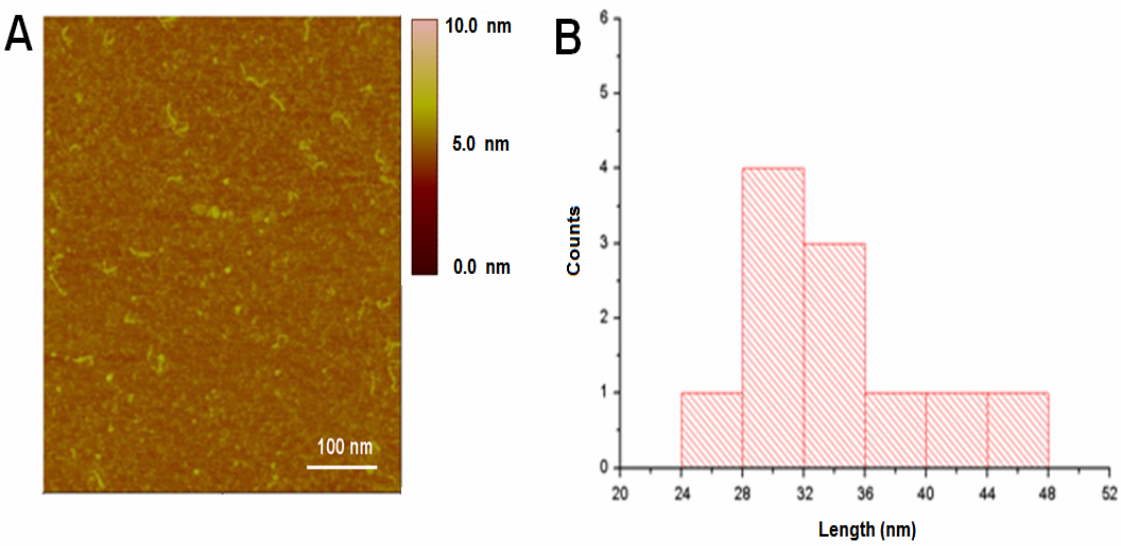

Figure 3.4 (A) AFM image of the hybridization products of ssDNA and T88 (control). **(B)** Histogram showing the length distribution of the structures.

3.4 Native polyacrylamide gel electrophoresis (PAGE) Analysis

After direct visualization, the product of the hybridization reaction was analyzed by 20% non-denaturing polyacrylamide gel electrophoresis (PAGE) without ethidum bromide staining (Figure 3.5). Several controls were prepared for the PAGE experiments. The 88mer template and ssDNA-PDI conjugate were hybridized in a 1:1 molar ratio so that on average 3/4 of the T88 sequence remained single stranded (Figure 3.5, lane 2, Abbreviation: ds/ssDNA-PDI1). Similarly, a hybridization product of T88 with one ssDNA-PDI and an unlabeled 66mer of ssDNA was prepared. The sequence composition of the 66mer was the same as that of ssDNA-PDI conjugate, but sequentially repeated three times. In this way ds 88mers were generated including only one PDI molecule (Figure 3.5, lane 3, Abbreviation: dsDNA-PDI1).

From the PAGE analysis it can be concluded that the negatively charged PDI chromophore does not hinder hybridization. The electrophoretic mobility of four ssDNA-PDI hybridized with T88 (Figure 3.5, lane 4, Abbreviation: dsDNA-PDI4) was much lower than the double stranded controls. This result strongly suggests that aggregation of PDIs takes place to form larger aggregates.

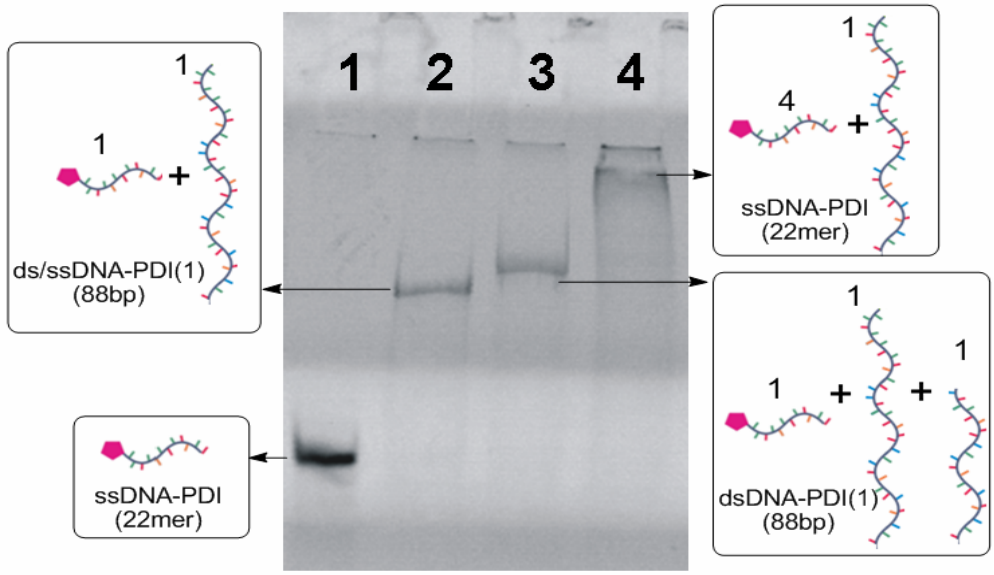

Figure 3.5 20% non-denaturing PAGE without ethidium bromide staining: *Lane 1*: ssDNA-PDI conjugate (22mer). *Lane 2-4*: Hybridization products of: T88 with ssDNA-PDI (1:1); T88 with ssDNA-PDI and ssDNA(66mer) (1:1:1) and T88 with ssDNA-PDI (1:4), respectively.

3.5 Fluorescence correlation spectroscopy (FCS) study of DNA-PDI hybrids in solution

AFM imaging has clearly shown the presence of dsDNA-PDI4 aggregates in the form of two parallelly alligned helices on a mica surface.

Fluorescence Correlation Spectroscopy (FCS) studies of dsDNA-PDI4 solutions were performed at different concentrations in order to verify if the

parallel alignment is guided by the restricted DNA mobility on the surface or takes place already in solution. The FCS measurements were performed by *Ting Liu* in the group of *Dr. R. Berger*.

The FCS technique is based on detecting the fluctuations of the fluorescent light intensity caused by the diffusion of chromophores through a small observation volume, usually formed by the focus of a confocal microscope. The analysis gives the average number of the fluorescent particle and average diffusion time, when the particle is passing through space. Eventually, both the concentration and size of the particle (molecule) can be determined.

The fluctuation of the fluorescence intensity is observed due to the in-out motion at the observation volume. This random fluctuation is generally analyzed by the autocorrelation function of the fluctuation signal, characterized by two parameters, the correlation time and the correlation amplitude.[25] The autocorrelation function G(τ) can be calculated analytically as:

$$G(\tau)=\frac{\langle I(t)I(t+\tau)\rangle}{\langle I(t)\rangle^2}=g(\tau)+1=1+\frac{1}{N}\frac{1}{\left(1+\frac{\tau}{\tau_c}\right)\sqrt{1+\frac{\tau}{q^2\tau_c}}} \qquad \text{(Equation.1)}$$

where N and τ_c is the average number of fluorescent particles in the volume element and the diffusion time, respectively. q is the ratio of the $1/e^2$ distance in z-axis and radius in the x-y plane in the confocal space. τ_c is determined by $w_{xy}^2/4D$ where D and w_{xy} are the diffusion coefficient and the $1/e^2$ radius.

Due to its very high sensitivity and selectivity, FCS is particularly suitable for studies of DNA hybridization and molecular aggregation.[25-27]

As the dsDNA-PDI4 molecules carry a PDI chromophore it appears natural to use the PDI fluorescence for the FCS studies. However, the method is most sensitive at nanomolar chromophore concentrations and can not be directly applied to study the 1.5 μM dsDNA-PDI4 solutions as used for AFM.

To overcome this problem an additional independent dye (Alexa488) was used to label the 88mer single stranded template (T88-Alexa) at the 5' end and serve as a source of fluorescence signal for the FCS experiments. The ratio between the labeled and unlabeled T88 was carefully adjusted to result in typically nano molar overall concentration of the Alexa488 in all studied solutions. A typical autocorrelation curve measured for 15 nM solution of T88-Alexa (M_w=28315 g/mol) is shown in Figure 3.6 (green squares).

The curve can be fitted with the corresponding analytical expression for one type of freely diffusing identical species yielding a diffusion coefficient of the T88-Alexa D = 63±5 $\mu m^2/s$. The autocorrelation curve for 15 nM solution of dsDNA-PDI4 (blue circles in Figure 3.6) indicates significantly slower diffusion than that of the T88-Alexa and yields a diffusion coefficient of 41±4 $\mu m^2/s$. This value should be compared with the expected diffusion coefficients for a single dsDNA-PDI4 helix and for an aggregate of two parallelly alligned helices. Using the dimensions obtained from the AFM studies, the diffusion coefficients of these rod-like structures can be calculated through:[28]

$$D_{rod} = \frac{k_B T}{3\pi\eta L}\ln(x + 0.312 + \frac{0.565}{x} + \frac{0.1}{x^2}) \qquad \text{(Equation. 2)}$$

Here *k* is Boltzmann constant, *T* the temperature (298 K), η the viscosity of the solution ($1.0 \cdot 10^{-3}$ $kg \cdot m^{-1} \cdot s^{-1}$) and *x* is the ratio of the molecular length (32 nm for both 88 bp dsDNA) to its diameter (2.4 nm for 88 bp dsDNA-PDI4, 5.4–7.0 nm for rod-like aggregates with two 88 bp dsDNA-PDI4). With these parameters D_{rod} should be 38 $\mu m^2/s$ for dsDNA-PDI4 and 22-26 $\mu m^2/s$ for aggregates with dimeric structure.

Clearly the diffusion coefficient of 41±4 $\mu m^2/s$ measured with FCS for 15 nM solution of dsDNA-PDI4 (blue circles in Figure 3.6), corresponds to single molecules and indicates that aggregates do not form.

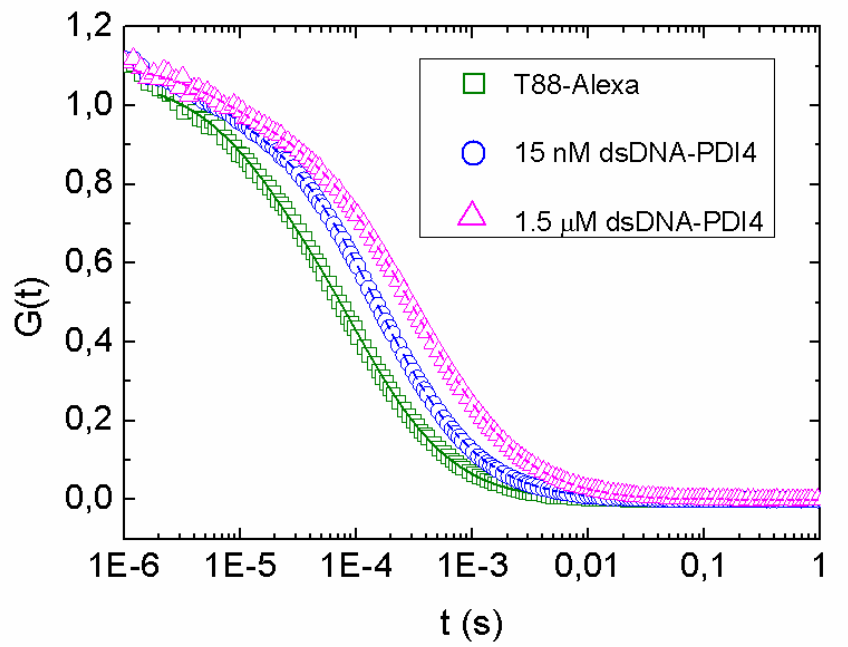

Figure 3.6 Normalized autocorrelation curves for T88-Alexa (ssDNA) at concentration of 15 nM (green squares) and dsDNA-PDI4 at concentrations of 15 nM (blue circles) and 1.5 µM (pink triangles), respectively. The solid lines represent the corresponding fits.

The autocorrelation curve measured for 1.5 µM dsDNA-PDI4 solutions, i.e. at a concentration similar to that used in AFM studies is shown with pink triangles in Figure 3.6. This curve is shifted to longer lag times as compared to the ones measured at low dsDNA-PDI4 concentrations indicating formation of bigger structures. This autocorrelation curve however can not be fitted well assuming a single diffusion component and represents the simultaneous diffusion of fluorescent species with different sizes, e.g. single dsDNA-PDI4 helices, dimers and bigger aggregates. This finding is consistent with the AFM results that have shown a variety of aggregates with different size on the mica surface.

3.6 Photophysical study of DNA-PDI hybrids

Dye aggregates are known to exhibit photophysical properties that are sometimes different from the monomers they are composed of.[29]

PDIs usually self-assemble into sandwich-type H-aggregates[30] that exhibit unfavorable, strongly quenched fluorescence properties. J-type packing where the chromophores adopt a slipped configuration accompanied by narrow and bathochromically shifted absorption and high fluorescence quantum yield was only rarely reported for PDIs.[31] In the following the optical properties of the PDIs within the supramolecular DNA scaffold are investigated.

Therefore, steady-state and time resolved photoluminescence (PL) measurements of dsDNA-PDI4 and three controls (ssDNA-PDI (22mer), dsDNA (unlabeled) and dsDNA-PDI1) were carried out (Figure 3.7). The samples were excited at 380 nm and all spectra were recorded at the same concentration of 6 µM. The photophysical study was performed by *Jia Gao* in the group of *Prof. Dr. Maria Loi* (University of Groningen, The Netherlands).

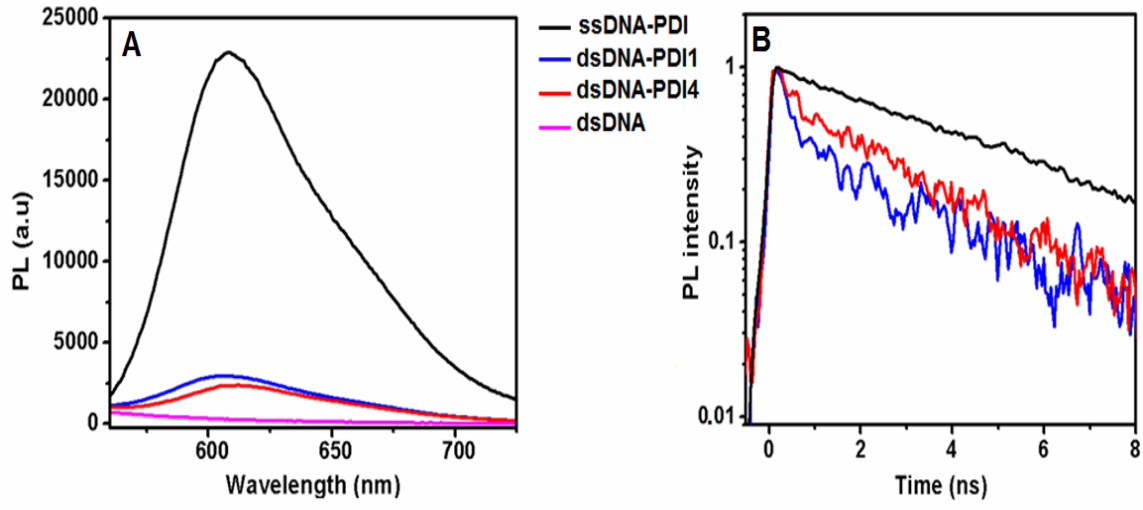

Figure 3.7 Photophysical study of DNA-PDI samples (λ_{ex} = 380 nm). **(A)** PL spectra **(B)** Time traces. Measurements were performed at room temperature.

The steady-state photoluminescence spectra showed that for the dsDNA-PDI1 and dsDNA-PDI4 the emission of the PDIs is strongly quenched, compared to that of ssDNA-PDI. The lifetime of the ssDNA-PDI sample is longer than that of dsDNA-PDI1 and dsDNA-PDI4. The two latter samples revealed a similar

lifetime. All the photophysical measurements above indicate that the emission properties of the PDIs change drastically when the ssDNA is transformed into ds DNA. Since the ds samples with one and four PDIs behave optically very similar it is not clear whether the drop in emission intensity and lifetime resulted from perylene-perylene or perylene-DNA interactions. Hence no clear statement about aggregation of dsDNA-PDI4 can be made from the photoluminescence experiments.

In addition, UV/Vis spectra of dsDNA-PDI4 and the three controls mentioned previously were also carried out (Figure 3.8).

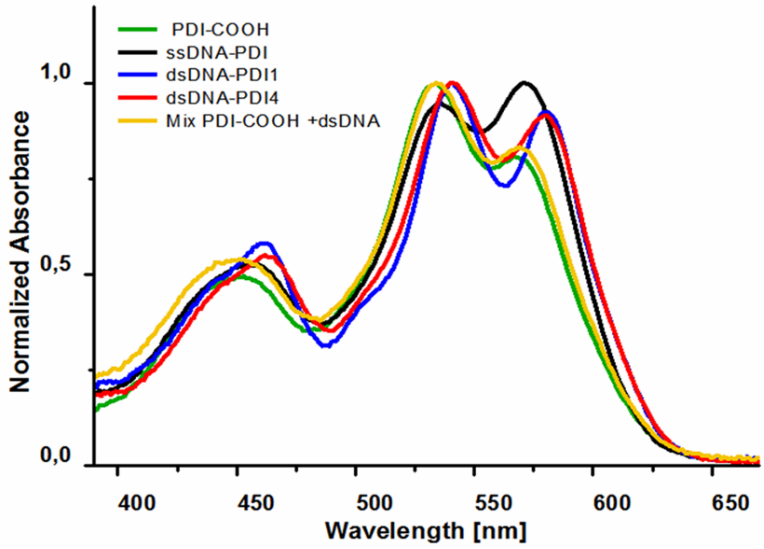

Figure 3.8 UV/Vis spectra of dsDNA-PDI4 and their corresponding controls. Samples were measured in hybridization buffer: NaCl (100 mM), $MgCl_2$ (60 mM) and 0.5 x TAE buffer.

Figure 3.8 shows a slight red shift (~6 nm) of samples dsDNA-PDI4 and dsDNA-PDI1 with respect to the spectrum of the free dye, suggesting aggregation of these dsDNA-PDI structures. This result is in good aggrement with that obtained by PL measurments. Again both samples with one and four PDIs behave very similarly.

3.7 Conclusions

In conclusion, short oligonucleotides that were functionalized with water soluble perylenediimide were successfully hybridized with long complementary DNA templates. The resulting dsDNA-PDI hybrid structures self-assembled into aggregates of higher hierarchy by π-π stacking of the aromatic rings of the perylene chromophores. As a result two parallelly alligned helices were obtained. In this concept of superstructure formation the structural features of DNA play an important role. On the one hand the length of the DNA template determines the overall length of dimeric rods. On the other hand the rigid DNA structure allows to control the orientation of the PDI dyes to one side of the helix, an essential requirement for the formation of the detected rods.

The assembly into dimer aggregates was unequivocally proven by direct visualization with AFM on surfaces. Confirmation of these structures in solution was more difficult. Gel electrophoresis clearly indicated aggregation of DNA double strands that were equipped with four PDI units, however, deducing structural properties of self-assembled objects not exclusively formed by basepairing is rather difficult employing that method.
The FCS results did not reveal aggregation of dsDNA labeled with PDI at low concentrations, but at higher concentrations aggregates of larger size were detected, underligning the fact that the concentration of dsDNA/dye hybrids is a critical factor for the formation of superstructures.

The photophysical investigations of the system with four PDIs aligned on a template revealed considerable quenching of the PDI emission but again due to the simlarity of the results to a control containing only one PDI chromophore no clear statements about the structural properties in solution can be given. The analysis of the system in solution did not indicate clearly the morphology

of the aggregates, if there are dimers, trimers, micelles etc. However these studies served to corroborate the AFM results, demonstrating that new larger structures are present and that the intermolecular interactions between PDIs are necessary for the formation of higher aggregates.

3.8 Experimental Section

3.8.1 Synthesis of ssDNA-PDI conjugate

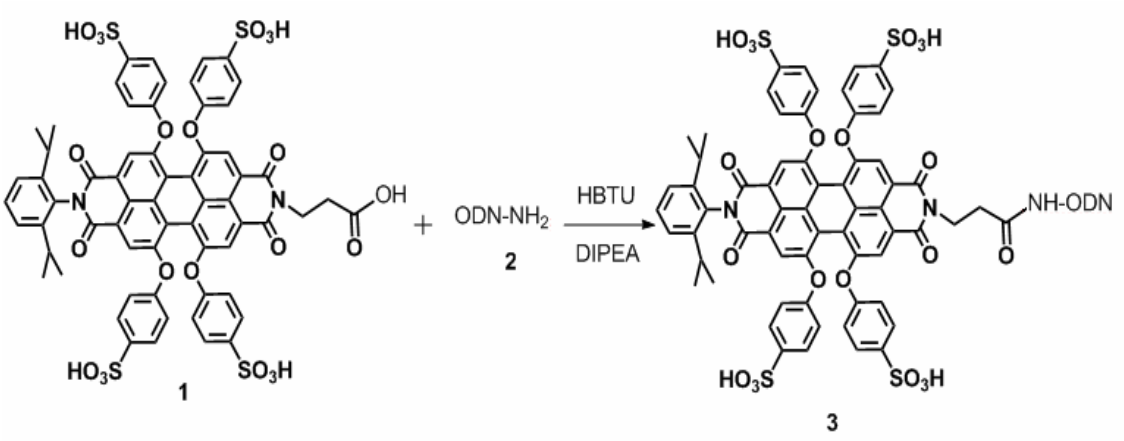

Figure 3.9 Synthesis of ssDNA-PDI conjugate on a solid support by amide bond formation.

10 mg (0.00762 mmol) of carboxyl-functionalized PDI (***1***) (M_W: 1311 g/mol, Figure 3.9) was suspended in 500 µl of dry dimethylformamide (DMF). 9.25 mg O-(1H-benzotriazole-1-yl)-N,N,N',N'-tetramethyluronium hexafluorophosphate (HBTU) was dissolved in 250 µl of a 1:1 mixture of DMF/CH_3CN and combined with the dye solution. Subsequently, 8.6 µl of N-diisopropylamine was added to the reaction mixture. The synthesis was carried out employing a polypropylene column prepacked with a controlled porous glass (CPG) solid support (0.05 µmol) onto which a 22mer C6-amino modified oligonucleotide sequence was attached (5´-NH_2-CCTCGCTCTGCTAATCCTGTTA-3´ (***2***), purchased from Biomers GmbH, Germany). The solution was pushed in and expelled out alternately from the syringes for 1 hour. Then the column was washed with CH_3CN. The product was cleaved from the solid support by incubating the resin with a mixture of t-butylamine/MeOH/H_20 (1:2:1) for 16 h at 55ºC.

After that, the DNA-PDI conjugate was precipitated with a 1:1 ethanol/water mixture, filtered and dried under vacuum.

The resulting material was purified by polyacrylamide gel electrophoresis (PAGE) and desalted with a dialysis membrane with molecular weight cut-off (MWCO) of 1000 g/mol yielding 286 μg (0,036 μmol) of product (***3***) (71%).

The DNA-PDI conjugate was characterized by PAGE, MALDI-TOF mass spectrometry as well as by UV/Vis spectroscopy (Figures 3.10- 3.12).

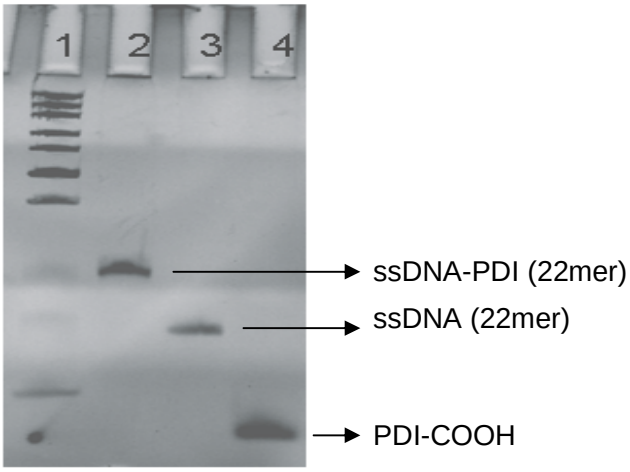

Figure 3.10 20% denaturing PAGE analysis of purified ssDNA-PDI conjugate. *Lane 1*: Ultra low range DNA ladder. *Lane 2*: ssDNA-PDI conjugate (22mer). *Lane 3*: ss DNA(22mer). *Lane 4*: Water soluble PDI.

Gel electrophoresis provides a valuable method for DNA characterization. However, the gel separation is occasionally imperfect due to aberrant mobility of certain fragments, leading to erroneous sequence length determination.

For that reason Matrix-assisted laser desorption/ionization time-of-flight mass spectrometry (MALDI-MS) was employed in this investigation to give additional and precise information about the DNA-hybrids. In MALDI-MS, the sample is embedded in the crystalline structure of small organic compounds (matrix) and deposited on a conductive sample support.[32] The analyte/matrix mixture is irradiated with a nanosecond laser beam. The generated ions are accelerated to the same potential in an electrical field, and are subsequently separated in a field-free drift region according to their mass-over-charge ratio.

DNA is more difficult to analyze under MALDI conditions than peptides, due to their negatively charged phosphate backbone and the possible adduct formation, resulting in a broader distribution of the signal.[33] However, the addition of ammonium-containing additives like ammonium citrate to the matrix reduces cation heterogeneity of analytes,[34] therefore improving the DNA resolution. After several attempts the optimal conditions for MALDI-MS were established. The matrix employed for the DNA-hybrids was the following: 20 mg 3-hydroxypicolinic acid, 2 mg picolinic acid, 3 mg ammonium citrate in 0.5 ml of a mixture of ultra pure water/acetonitrile (7:3) ; ratio sample/matrix = 1:2 (v/v) . The concentration of the DNA solution was 20 µM. Despite that, the same conditions for MALDI-MS were used for all the DNA-hybrid samples, it was observed that longer oligonucleotides (above M_W= 5000 g/mol) presented broader and less-intense signals, as is the case of the Figure 3.11. This observation can be explained taking into account that MALDI imparts large kinetic energies to ions of high mass/charge ratio *(m/z).* However, the method was appropriate for the determination of the molecular weight of the DNA-PDI conjugates.

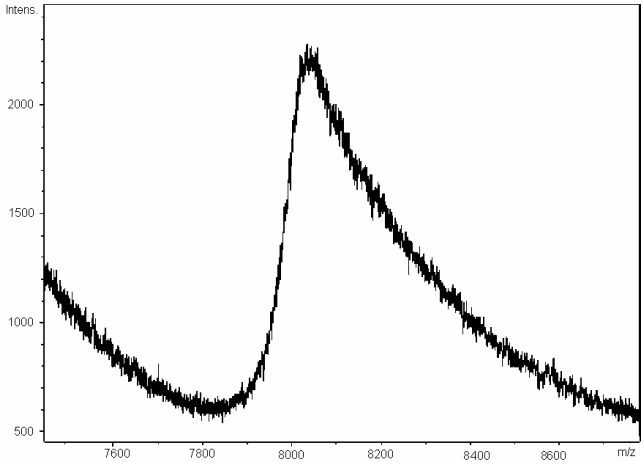

Figure 3.11 MALDI-TOF mass spectrum of ssDNA-PDI conjugate (22mer) (found: 8038 g/mol, calculated: 8035.56 g/mol). Matrix: 3-hydroxipicolin acid.

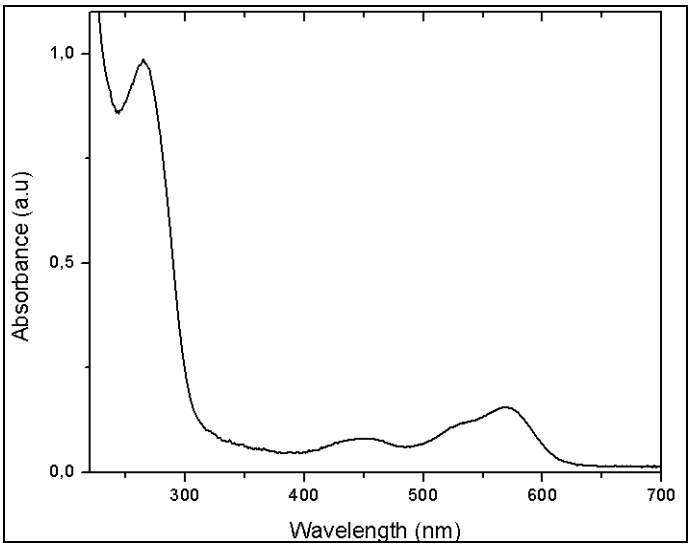

Figure 3.12 UV-visible spectrum of ssDNA-PDI conjugate.

3.8.2 General Hybridization Procedure

The hybridization reaction was carried out by dissolving ssDNA-PDI (22mer) and the long ssDNA template (88mer) in buffer Na^+ (4 mM), Mg^{2+} (24 mM) and 50xTAE buffer (Tris-acetate-EDTA, 20 mM tris(hydroxymethyl)aminomethane-HCl, pH 8.0, 10 mM acetic acid, 0.5 mM EDTA). The template encodes the complementary sequence of the ssDNA-PDI four times. The mixture was heated to 95 ℃ and was cooled one degree per 16 minutes u ntil room temperature in a PCR thermocycler (Biometra GmbH, Germany). The final concentration of ssDNA-PDI was 6 µM.

3.8.3 Samples for AFM, PAGE and Photophysical study

DNA Sequences :

ssDNA-PDI (22mer): 5'- PDI-CCTCGCTCTGCTAATCCTGTTA-3'
Template 88mer (T88): 5'- $(TAACAGGATTAGCAGAGCGAG)_4$ -3'

Labeled Template 88mer (T88-Alexa488):

5'- Alexa488-$(TAACAGGATTAGCAGAGCGAG)_4$ -3'

Template 88 mer (T88c):

5'- $(TGGGCACACACTTATCAATAGA)_3$ -$(TAACAGGATTAGCAGAGCGAG)_1$ -3'

ssDNA (66mer): 5'- $(TCTATTGATAAGTGTGTGCCCA)_3$-3'

dsDNA-PDI4: ssDNA-PDI was hybridized with the complementary template of 88mer (T88).The ratio of the ssDNA-PDI and template was adjusted so that the template encodes four times the ssDNA-PDI. The final concentration of the ssDNA-PDI was 6 μM

dsDNA-PDI1: ssDNA-PDI was hybridized with the 88mer template (T88c) and with an extra 66mer unlabeled ssDNA sequence in a ratio of 1:1:1, forming thus double stranded DNA that includes only one PDI molecule. The T88c encodes only one time the ssDNA-PDI sequence (from 3' to 5'), ensuring that the PDI will be positioned at the 3'-end of the sequence. The final concentration of the ssDNA-PDI was 6 μM.

ds/ssDNA-PDI1: ssDNA-PDI was hybridized with the 88mer template in a ratio of 1:1, so that the predominant form of DNA remains single stranded. The final concentration of the ssDNA-PDI was 6 μM.

3.8.4 Atomic Force Microscope (AFM) Measurements

For the AFM measurements 2 μL of the sample dsDNA-PDI4 (1.5 μM) was deposited onto freshly cleaved mica. After 5 minutes of incubation the sample was rinsed with 200 μL of imaging buffer (10 mM Tris pH = 7.4, 1 mM $NiCl_2$). The

mica sheet was then mounted in the AFM keeping the surface always covered by buffer solution. The measurements were carried out with a Multimode instrument equipped with a 7307E scanner. Oxide-sharpened silicon nitride cantilevers with an integrated tip were used. The images were recorded in soft tapping mode in liquid. The length and width values of the dsDNA-PDI4 were determined with the AFM images (see Table 3.1 and Figures 3.13 and 3.14).

Table 3.1 Length analysis of the dimer structures (dsDNA-PDI4).

Object Nr.	1	2	3	4	5	6	7	8	9	10	11	12	13
Length (nm)	36.3	33.6	24.1	34.6	22.9	40.3	31.9	27.6	33.5	37.5	37.6	31.7	37.7

Mean	**33.0**
SD	5.3

The width of the dimeric structures was measured in the cross section (Figure 3.13). In particular, the width was defined as the distance W between the two maxima from the cross section view along the dimeric structures of AFM images of Figure 3.3. The following relationship was employed: W = 2R+L.

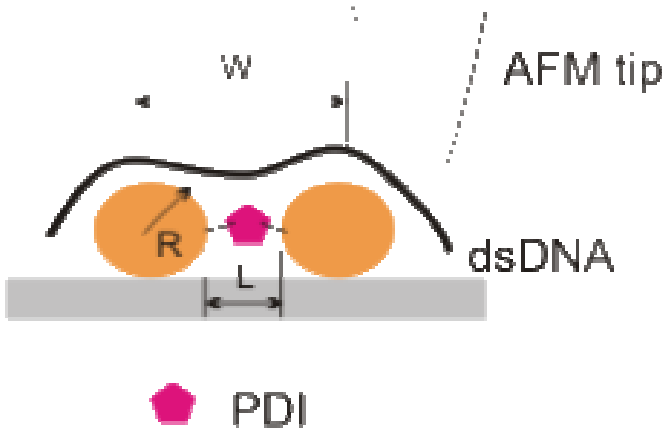

Figure 3.13 Schematic representation of the dsDNA-PDI4 structures width.

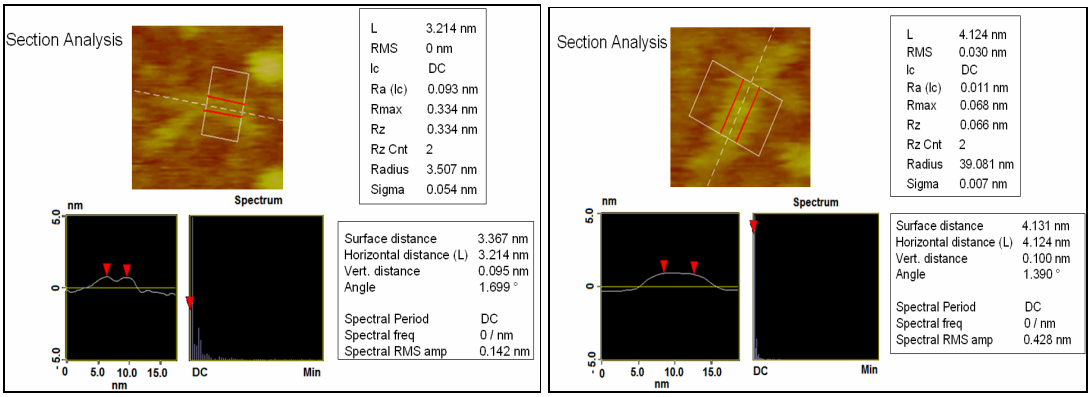

Figure 3.14 The width measurement of the dimeric structures (images show the cross section).

3.8.5 FCS Measurements

A commercial FCS setup manufactured by Carl Zeiss (Jena, Germany) consisting of the module ConfoCor 2 and an inverted microscope, model Axiovert 200 was used. In all experiments a Zeiss C-Apochromat 40x/1.2 W water immersion objective was employed. The Alexa488 labeled DNA molecules were excited by an Argon laser at 488 nm and emission was collected after filtering with a BP505-550 band pass filter. An eight-well, polystyrene chambered cover-glass (Lab-Tek, Nalge Nunc International) was used as sample cell. For each solution series of 10 measurements with total duration 5 min were performed. The optical setup calibration was done using a reference dye with known diffusion coefficient i.e., Rh6G.

3.8.6 Material for FCS Experiments

dsDNA-PDI-Alexa (15 nM): ssDNA-PDI was hybridized with the complementary template of 88mer, which was functionalized with Alexa488 at the 5' end (Sigma Aldrich, Germany) .The ratio of ssDNA-PDI and template carrying the dye was adjusted so that the template encodes four times the ssDNA-PDI. The final concentration of the template was 15 nM.

dsDNA-PDI-Alexa (1.5 μM): ssDNA-PDI was hybridized with the complementary template of 88mer, which was functionalized with Alexa488 at the 5'-end (Sigma Aldrich, Germany), the concentration of the Alexa488 labeled T88 was kept low at 100 nM for a good signal-to-noise ratio. Template (88mer) (1.4 μM) without labeling was also added to complete the hybridization with ssDNA-PDI (22mer). The final concentration of the ssDNA-PDI was 6 μM.

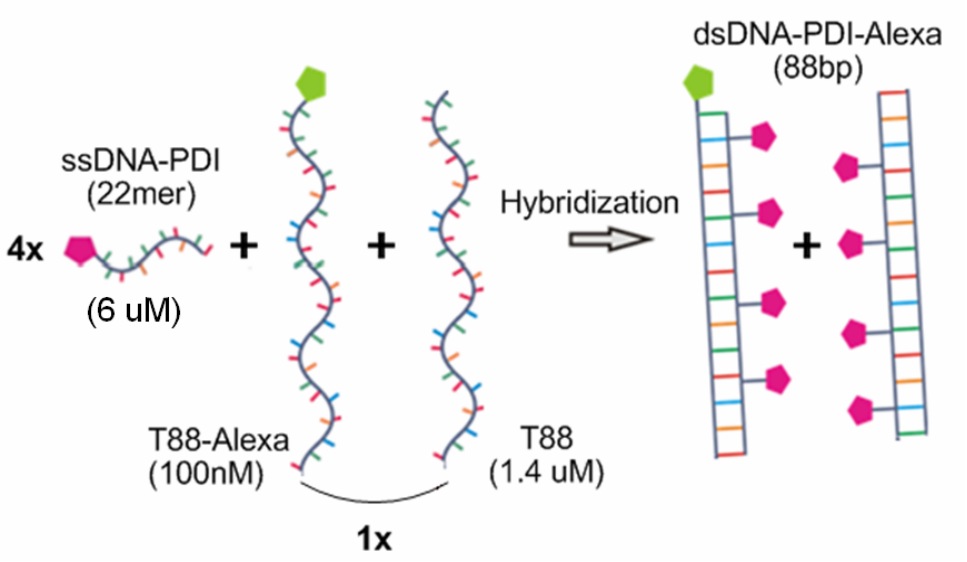

Figure 3.15 Schematic representation of the dsDNA-PDI-Alexa (88 bp) preparation (concentration of 1.5 μM).

3.8.7 Photophysical study of DNA hybridization with PDI

For the steady-state and time resolved photoluminescence measurements, the samples were excited by a 150 fs pulse Kerr mode locked Ti-sapphire laser, doubled at 380 nm. The steady-state PL of the sample was measured with a calibrated Si-CCD detector. The time-resolved PL of each molecule was recorded by Hamamatsu streak camera working in synchroscan mode with the photocathode sensitive in the visible spectral range. All the measurements were performed at room temperature.

3.8.8 Absorption spectra

The UV/Vis spectra of dsDNA-PDI4 and their corresponding controls were recorded with a Perkin-Elmer Lambda 100 UV-Vis spectrophotometer, employing a quartz glass cuvette (light pathlength 10 mm, chamber volume 100 µL , Hellma GmbH, Germany).

3.9 References

[1] K. Adachi, T. Mita, T. Yamate, S. Yamazaki, H. Takechi, H. Watarai, *Languimir* **2009**.

[2] G. Zhang, X. Zhai, M. Liu, Y. Tang, Y. Zhang, *J. Phys. Chem. B* **2007**, *111*, 9301.

[3] M. L. Horng, E. L. Quitevis, *J. Phys. Chem.* **1993**, *97*, 12408.

[4] Y. Fukushima, *Bull. Chem. Soc. Jpn.* **1996**, *69*, 1719.

[5] M. M. Wang, I. Dilek, B. A. Armitage, *Langmuir* **2003**, *19*, 6449.

[6] C. M. Niemeyer, *Curr. Opin. Chem. Biol.* **2000**, *4*, 609.

[7] M. Nakamura, Y. Ohtoshi, K. Yamana, *Chem. Commun.* **2005**, 5163.

[8] M. Nakamura, Y. Murakami, K. Sasa, H. Hayashi, K. Yamana, *J. Am. Chem. Soc.* **2008**, *130*, 6904.

[9] E. Mayer-Enthart, H. A. Wagenknecht, *Angew. Chem., Int. Ed.* **2006**, *45*, 3372.

[10] L.-A. Fendt, I. Bouamaied, S. Thöni, N. Amiot, E. Stulz, *J. Am. Chem. Soc.* **2007**, *129*, 15319.

[11] V. L. Malinovskii, F. Samain, R. Haner, *Angew. Chem., Int. Ed.* **2007**, *46*, 4464.

[12] W. Wang, W. Wan, H. H. Zhou, S. Q. Niu, A. D. Q. Li, *J. Am. Chem. Soc.* **2003**, *125*, 5248.

[13] J. S. Kim, Y. J. Jung, J. W. Park, A. D. Shaller, W. Wan, A. D. Q. Li, *Adv. Mater.* **2009**, *21*, 786.

[14] A. Rademacher, S. Markle, H. Langhals, *Chem. Ber. Recl.* **1982**, *115*, 2927.

[15] M. A. Abdalla, J. Bayer, J. O. Rädler, K. Müllen, *Angew. Chem., Int. Ed.* **2004**, *43*, 3967.

[16] K. Peneva, G. Mihov, F. Nolde, S. Rocha, J. Hotta, K. Braeckmans, J. Hofkens, H. Uji-I, A. Herrmann, K. Müllen, *Angew. Chem., Int. Ed.* **2008**, *47*, 3372.

[17] J. Qu, C. Kohl, M. Pottek, K. Müllen, *Angew. Chem. Int. Ed.* **2004**, *43*, 1528.

[18] C. Jung, B. K. Müller, D. C. Lamb, F. Nolde, K. Müllen, C. Brauchle, *J. Am. Chem. Soc.* **2006**, *128*, 5283.

[19] A. Margineanu, J. Hofkens, M. Cotlet, S. Habuchi, A. Stefan, J. Q. Qu, C. Kohl, K. Müllen, J. Vercammen, Y. Engelborghs, T. Gensch, F. C. De Schryver, *J. Phys. Chem. B* **2004**, *108*, 12242.

[20] T. Tanaka, R. L. Letsinger, *Nucleic Acids Res.* **1982**, *10*, 3249.

[21] R. Vinayak, H. Tang, *Nucleic Acids Symp. Ser.* **2000**, *44*, 257.

[22] F. H. C. Crick, A. Klug, *Nature* **1975**, *255*, 530.

[23] M. Levitt, *Proc. Natl. Acad. Sci. USA* **1978**, *75*, 640.

[24] M. Mandelkern, J. G. Elias, D. Eden, D. M. Crothers, *J. Mol. Biol.* **1981**, *152*, 153.

[25] T. B. Bonne, K. Ludtke, R. Jordan, P. Stepanek, C. M. Papadakis, *Colloid Polym. Sci.* **2004**, *282*, 1425.

[26] T. B. Bonne, K. Ludtke, R. Jordan, C. M. Papadakis, *Macromol. Chem. Phys.* **2007**, *208*, 1402.

[27] K. Koynov, G. Mihov, M. Mondeshki, C. Moon, H. W. Spiess, K. Müllen, H. J. Butt, G. Floudas, *Biomacromolecules* **2007**, *8*, 1745.

[28] M. M. Tirado, J. Garciadelatorre, *J. Chem. Phys.* **1980**, *73*, 1986.

[29] H. Kashida, H. Asanuma, M. Komiyama, *Supramol. Chem.* **2004**, *16*, 459.

[30] D. J. Liu, S. De Feyter, M. Cotlet, U. M. Wiesler, T. Weil, A. Herrmann, K. Müllen, F. C. De Schryver, *Macromolecules* **2003**, *36*, 8489.

[31] T. Kaiser, V. Stepanenko, F. Würthner, *J. Am. Chem. Soc.* **2009**, *131*, 6719.

[32] M. Karas, F. Hillenkamp, *Anal. Chem.* **1988**, *60*, 2299.

[33] F. Kirpekar, E. Nordhoff, L. K. Larsen, K. Kristiansen, P. Roepstorff, F. Hillenkamp, *Nucleic Acids Res.* **1998**, *26*, 2554.

[34] U. Pieles, W. Zurcher, M. Schar, H. E. Moser, *Nucleic Acids Res.* **1993**, *21*, 3191.

Chapter 4

INVESTIGATING THE DYNAMIC BEHAVIOR OF DNA POLYMER CHAINS BY TERMINALLY DYE-FUNCTIONALIZED POLYNUCLEIC ACIDS

4.1 Introduction

DNA plays a special role in polymer science not only because of the highly selective recognition of complementary single DNA strands, but also because bacteria can replicate very long DNA chains yet perfectly monodisperse. DNA properties make it attractive as polymer model particularly for the study of polymer conformation and dynamics.[1-3]

Understanding the physical properties of diluted and concentrated solutions of polymers has long been a major goal of basic and applied research in physics, chemistry, chemical engineering, and material science.[4, 5] Imaging of single DNA molecules has enabled detailed studies of polymer dynamics and rigorous testing of assumptions and predictions of molecular theories.[3, 6] Two of the most widely used theories for polymer melt dynamics describe principally the movement of a single chain in an effective medium. The *Rouse model* is one of the most basic models for polymer dynamics. Linear polymer chains are described as a bead-

spring model with no other interactions between monomers (i.e., beads) than their connectivity along the chain, which is accounted for by harmonic springs.[7, 8] On the other hand, the *reptation model* gives explanations for the dynamics of entangled molecules in a network of fixed obstacles. De Gennes is known as one of the pioneers in this field for his work on reptation of polymer molecules,[9] the dynamics of confined polymer chains,[10] and the dynamics of entangled polymer solutions.[11, 12] Moreover, William Graessley[13, 14] and Doi-Edwards[15-19] reformulated the primary model and extended the investigation specifically in the rheological behavior of semidiluted and concentrated unentangled and entangled polymer solutions.

According to the reptation hypothesis, each polymer is constrained to move within a topological tube due to the presence of the confining surrounding polymers (Figure 4.1). Within this tube, the polymer performs a snake-like motion (therefore the name reptation) and advances in the melt through the diffusion of stored length along its own contour. Within the reptation model, the diffusion process measured by the diffusion coefficient *D* is dominated by the chain length, the degree of polymerization *N* and the chain architecture.

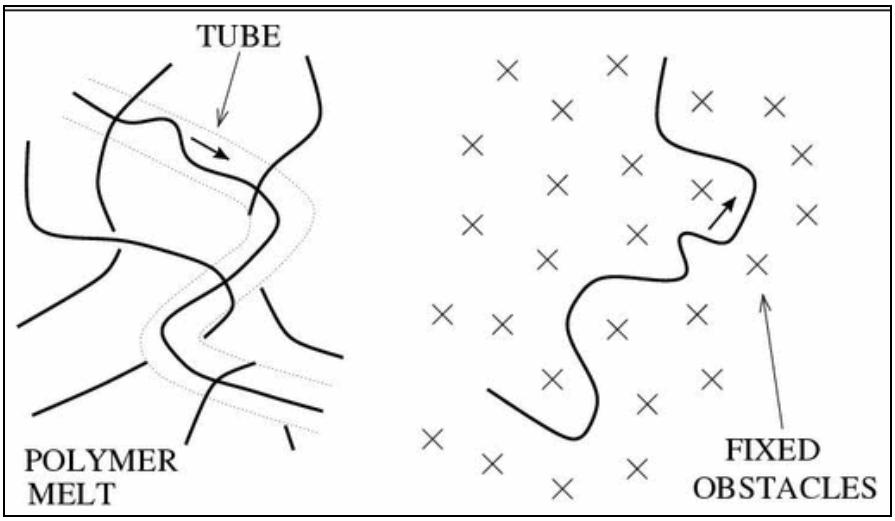

Figure 4.1 Schematic representation of polymer reptation.

Boss et al[20] and Osmers and Metzner[21] identified a critical concentration *C** at which the interaction or overlapping of the domains of the polymer molecules in solution begins. Increasing entanglement and network formation by the dissolved polymer molecules occur as its concentration rises above *C** (Figure 4.2). This provides increasing obstruction to any solute molecules diffusing through the solution. Another important and critical parameter in polymer solution viscosities is $C_{e,}$[22, 23] the polymer entanglement concentration, at which the network becomes "elastically effective", which has clear implications for DNA migration and entanglement dynamics.

The parameters *C* and* C_e define the dilute, semidilute, and entangled regions.

The critical polymer overlap concentration C* is defined as:[24]

$$C^* = \frac{\rho N}{R_g^{\ 3}} \qquad \text{(Equation. 1)}$$

where ρ = 1.1x10^{-21} g/bp is the linear mass per base pair and R_g denotes the radius of gyration of the polymer. The R_g of a polymer coil is given by:[25]

$$R_g = 2L_p\left(N_p/6\right)^{\nu} \qquad \text{(Equation. 2)}$$

where N_p = aN/(2L_p) is the effective number of Kuhn segments, *a* = 3.4 Å corresponds to the length of a base pair, N is the number of base pairs and ν = 0.59 assuming a good solvent whereas ν = 0.5 for a Θ-solvent. The persistence length (L_p) of DNA is assumed as 50 nm.[26, 27]

*C** and C_e are directly related to the number of "blobs" (or chain segments) per entanglement n_e :

$$C_e = n_e^{\ 0.76} C^* \qquad \text{(Equation. 3)}$$

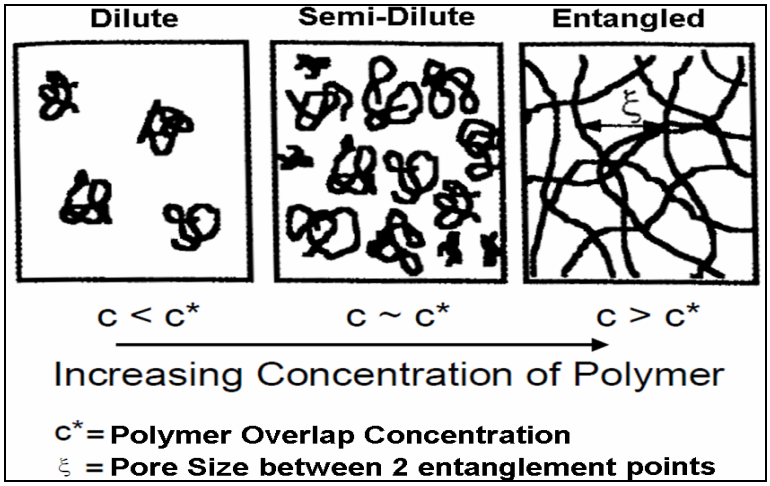

Figure 4.2 Schematic representation of polymer conformations at different concentrations.[24] *Dilute polymers*: the polymer chain is relatively isolated and in a globular state. *Semi-dilute polymers*: Every volume of Rg^3 (Rg=radius of gyration) is occupied by 1 polymer. *Entangled polymers*: Polymer strands interact and develop multiple entanglements, creating a network in which the polymer must snake its way through the matrix via reptation. The pore size ξ is defined as $\xi = 1.43*Rg\ (c/c^*)^{-(1+a)/3a}$.

Graessley also proposed a scheme for the classification of polymer solutions based on concentration and molecular weight of the polymers (Figure 4.3).

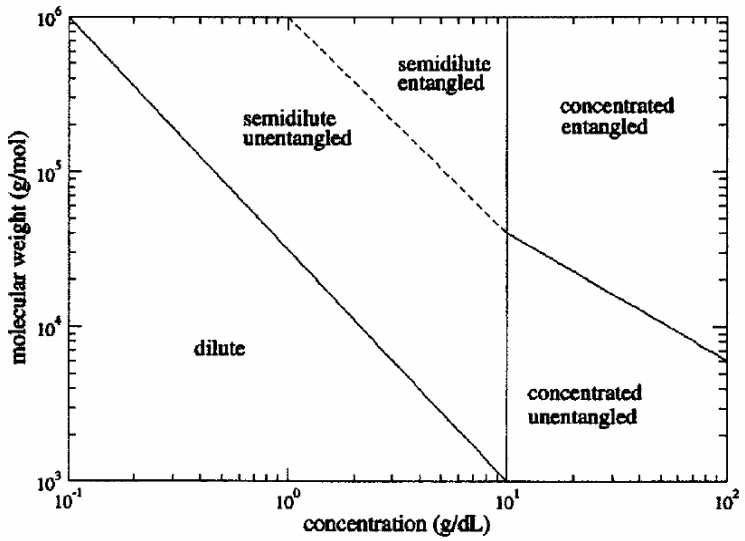

Figure 4.3 Classification of polymer solutions in terms of concentration and molecular weight.[28]

Previous experiments, demonstrated the feasibility of studying single entangled polymer chain dynamics based on observation and manipulation of biopolymers such as DNA[3, 29, 30] or actin[31] molecules.

The motion of a single polymer chain can be followed using wide-field fluorescence microscopy if the polymer is labeled with fluorescent dye molecules at many positions and dispersed in a solution of non-labeled but otherwise identical polymers.[32]

Another possibility to investigate the dynamics of polymer chains is using Förster resonance energy transfer (FRET). For this purpose at least one energy donor and one energy acceptor have to be present at well-defined positions in the polymer chain.

FRET described by Förster in the 1940's[33] is a process by which a fluorophore (the donor), in an excited state, transfers its energy to a neighboring molecule (acceptor) by nonradiative dipole–dipole interaction. The donor molecule emits at (shorter) wavelengths which overlap the absorption spectrum of the acceptor.

The efficiency of energy transfer (E) is defined as the number of quanta transferred to the acceptor, divided by the number of quanta absorbed by the donor. It is described by the expression:[33]

$$E = \frac{1}{1+\left(R/R_0\right)^6} \qquad \text{(Equation. 4)}$$

where R is the distance between the donor and acceptor (in Å) and R_0 – is the distance (in Å) at which energy transfer is 50% efficient, also called the Förster radius.

The formula shows that the rate of energy transfer is inversely proportional to the sixth power of the distance between the donor and acceptor. Therefore, the efficiency of the transfer rapidly declines to zero at distances larger than the Förster radius. In other words, the intensity of the quenched fluorescence between a donor and an acceptor, attached to different segments of the DNA

chain or to its ends, as is the case in the present work, is a strong function of the donor–acceptor separation. This is the basic feature mainly exploited by FRET experiments.
A follow up of the FRET signal which is triggered by a suitable donor excitation source can thus provide information on the Brownian end-to-end motion, or in general, segmental motion of a DNA chain at the molecular level.

The aim of this project was to investigate the reptation of linear labeled 7 kbp DNA on both extremities (2.38 µm in length) and to prove a theory of “end-to-end contacts of macromolecules” at different concentrations in the presence of confining surrounding linear unlabelled DNA, using FRET and wide-field fluorescence microscopy.
The 7 kbp length of the DNA was chosen, considering the optical needs and synthetic accessibility. For optical detection of the polymer a length that is a few times larger then the diffraction limit (500 nm for visible) is requested. On the other hand, the synthesis of higher molecular weight DNA (more than 3 kbp) employing PCR has its limitations.
Previous studies reported reptation of synthetic polymers such polyisocyanopeptides of similar or shorter lengths[34] as the one employed in this investigation. In theory DNA with length of 2.38 µm should be appropriate for reptation experiments.

4.2 PCR technique as strategy to generate fluorescently labeled linear DNA

DNA does not contain intrinsic fluorophores. The most efficient way to site-specifically introduce two terminal fluorophores necessary for FRET is by incorporating pre-labeled short DNA strand(s) as primers in the polymerase chain reaction (PCR).

Via PCR ATTO dyes can be incorporated at both ends of the double helix. This technique allows the production of specific DNA sequences *in vitro* employing a DNA-template, two oligonucleotide primers, the four deoxynucleotide triphosphates (dNTPs), and a thermostable DNA polymerase in a three-step amplification process over several cycles.[35]

A typical PCR experiment starts with the denaturation of the ds DNA at a temperature of about 90 ℃. The reaction is then co oled down in the presence of a large excess of primers, which bind to the complementary end-sequences of the target DNA. The large primer concentration ensures formation of the primer-DNA complexes. The reaction is then heated to the optimal working temperature (70 ℃) of a polymerase from a thermophilic organis m (usually polymerase from *Thermus aquaticus Taq*). The polymerase elongates the primer strand in the presence of all four deoxyribonucleotides (dNTPs). After one cycle the amount of present DNA in the sample has been doubled and the whole PCR cycle can then start again from the beginning. In total, an exponential growth of the DNA sample is obtained over many PCR cycles (Figure 4.4).

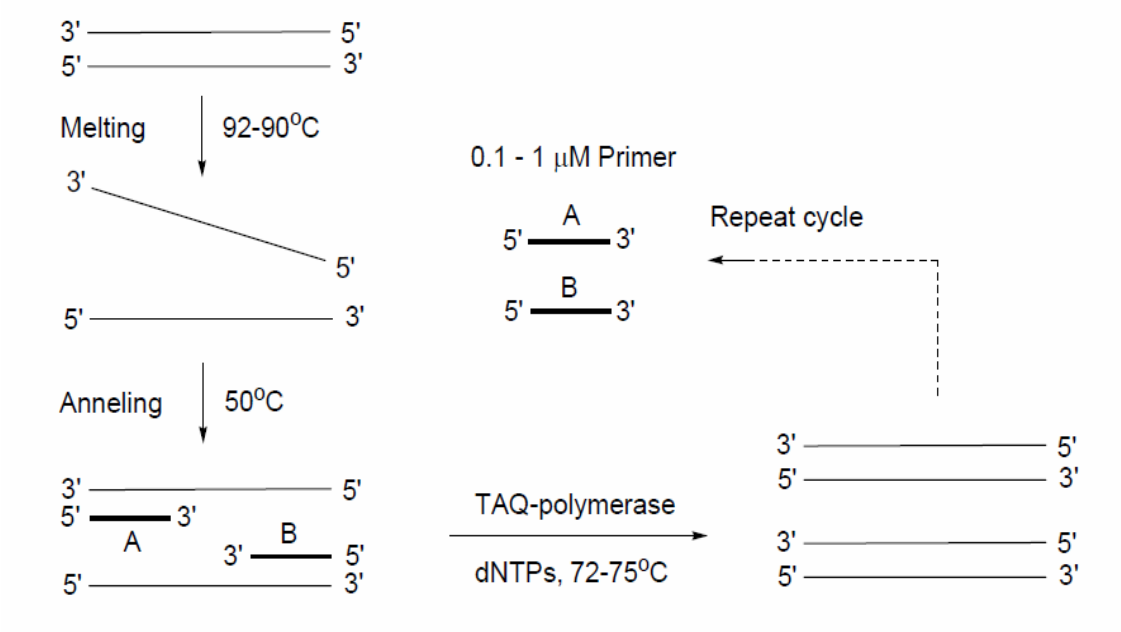

Figure 4.4 Schematic drawing of the PCR cycle.

Because of its extreme sensitivity and specificity, PCR is commonly used in medical and biological research for achieving selective enrichment of a specific DNA sequence by a factor of 106, greatly facilitating a variety of subsequent analytical manipulations. PCR has been used in the detection of hereditary diseases, the identification of genetic fingerprints, the diagnosis of infectious diseases, the cloning of genes and paternity testing[36] and has also been implemented in the last years in polymer chemistry to generate linear multiblock structures up to pentablock architectures.[37, 38]

In order to achieve high specificity and yield, it was necessary to optimize the PCR procedure. Conditions such as temperature, duration time for each cycle, salt concentrations, design of primers, primer concentrations and type of enzyme that should elongate the primers were modified (see experimental section 4.6.1). After several attempts the optimal conditions were established and it was possible to generate well defined labeled DNA, employing a forward primer carrying ATTO-550 dye at the 5'-end as donor and an ATTO-647N derivative attached to the 5'-end of the reverse primer sequence as acceptor. The plasmid (pET44a+) was used as the template for the amplification because of its length that amounts to be 7311 bp.

The most appropriate enzyme for our purpose was contained in the High fidelity polymerase kit from Fermentas GmbH, Germany. High Fidelity PCR Enzyme Mix is a unique blend of *Taq* DNA polymerase and a thermostable DNA polymerase with proofreading activity. The two enzymes act synergistically during PCR to generate more accurate and longer PCR products with greater yields compared to *Taq* DNA polymerase alone.* This set of reagents resulted in formation of dual labeled linear DNA with the ATTO-647N dye at the *5*'-end and ATTO-550 dye at 3'-end of the sequence (Figure 4.5). This nucleic acid structure constitutes of 7000 base pairs (7 kbp), corresponding to a length of 2380 nm. The length of this

* Fermentas GmbH. http://www.fermentas.de/product_info.php?info=p738

nucleic acid segment was determined by the annealing sites of the primers on the template.

The use of the PCR technique in combination with labeled primers to generate such kind of long amplicons with the dyes attached at the 5' and 3' ends is quite novel. Amplification and incorporation of dye-labeled nucleotides[39, 40] or dye-labeled primers[41, 42] for short dye-functionalized PCR products has been already reported. However, few studies describe amplicons longer than 3 kbp containing dye-labeled forward and reverse primers. The amplification of high molecular weight longer than 3000 nucleotides, often fails without an appropriate optimization. Reasons for failure are nonspecific primer annealing, secondary structures in the DNA template, and suboptimal cycling conditions, which have a greater effect on the amplification of longer PCR products than on shorter ones.[43]

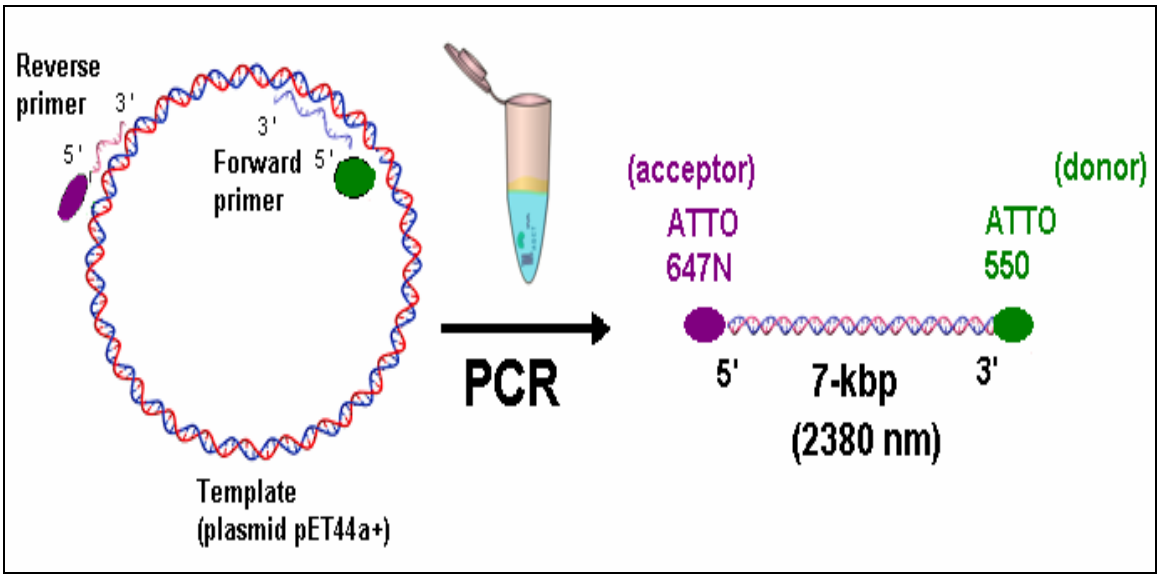

Figure 4.5 Schematic representation of the PCR technique to amplify a 7 kbp DNA chain and for the incorporation of ATTO dyes at the termini of the double helix.

4.3 Preparation and characterization of linear unlabeled DNA on milligram scales by cell transformation

DNA as a model for extended chain molecules offers a lot of advantages, most importantly its highly controllable structure and composition. However, there are also disadvantages associated with its utilization for certain type of physicochemical measurements. To produce well defined DNA of high molecular weight is laborious and costly, especially for studying the dynamics of entangled polymers, which requires milligram quantities of the material.

The unlabelled 7311 bp DNA sequence used in this study was obtained on milligram scale using an *E.coli* bacterial culture. Therefore, the cells were transformed with pET44a+ plasmid. Plasmids (also called vectors) are circular, double-stranded DNA molecules that exist separated from a cell's chromosomal DNA. These extrachromosomal DNAs, occur naturally in bacteria, yeast, and some higher eukaryotic cells.[44] Plasmids range from 1 to 15 kbp and can be replicated in bacteria up to 300 copies per cell.[45] These vectors serve as important tool in genetics and are commonly used to multiply or express particular genes.[46]

Commercially available plasmids are only sold in microgram quantities, which are insufficient for studying reptation with wide field microscopy employing this DNA as unlabeled matrix. However, large quantities of DNA could be obtained by replication of cloned DNA in *E.coli* cells. This is a molecular biology technique, where a foreign plasmid is introduced into bacteria, and used to amplify the plasmid. The cultures grew in Luria Bertani (LB) medium in the presence of a selective antibiotic.

The amplified plasmid was purified employing an alkaline lysis procedure, followed by binding of the plasmid DNA to an anion-exchange resin under low-salt and pH conditions. RNA, proteins and low-molecular-weight impurities were

removed by a wash with buffer of medium salinity. The plasmid was eluted by a buffer of high salinity and then concentrated and desalted by isopropanol precipitation (Figure 4.6). Five liters of bacterial culture yielded 1.5 mg of plasmid pET44a+.

The purified plasmid DNA was linearized using the restriction enzyme EcoRI. This enzyme recognizes one specific DNA sequence of the pET44a+ and cuts the DNA molecule only at one specific point.

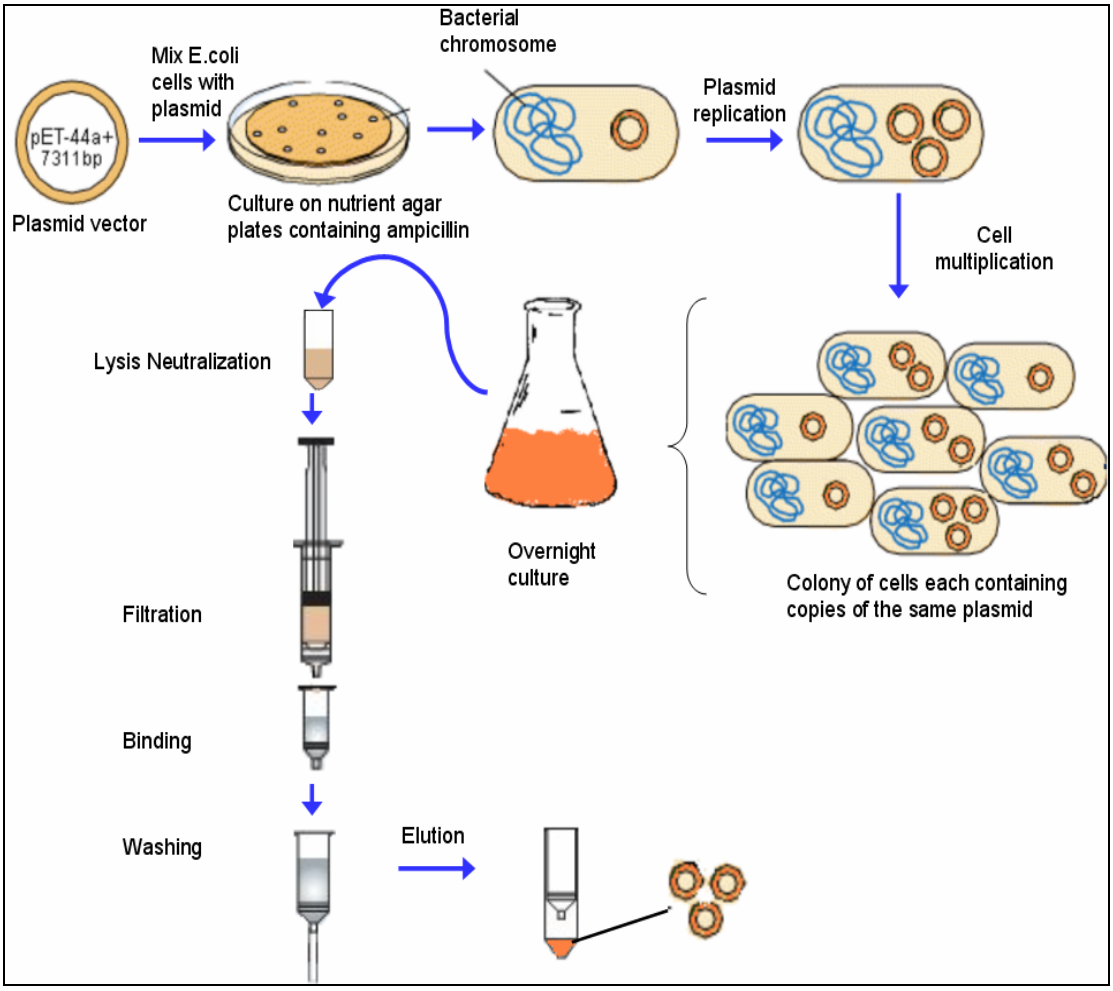

Figure 4.6 Schematic representation of E.coli cell transformation with the plasmid pET44a+ and the corresponding purification using Megaprep Kit (QIAGEN).

The 7 kbp PCR-amplified DNA and the digested plasmid were analyzed using 1 % agarose gel electrophoresis followed by ethidium bromide staining (Figure 4.7). Lanes 1, 2 and 3 show the DNA ladder, the linearized plasmid (digested with the restriction enzyme EcoRI) and the labeled 7 kbp amplified DNA, respectively. The band with the lowest electrophoretic mobility (lane 4) corresponds to the undigested plasmid pET44a+. The difference between the electrophoretic mobility of the circular and the linear DNA confirmed the successful digestion of the plasmid. Additionally, the size of the PCR-amplified DNA and the linearized plasmid was corroborated by comparing the bands with the DNA size marker.

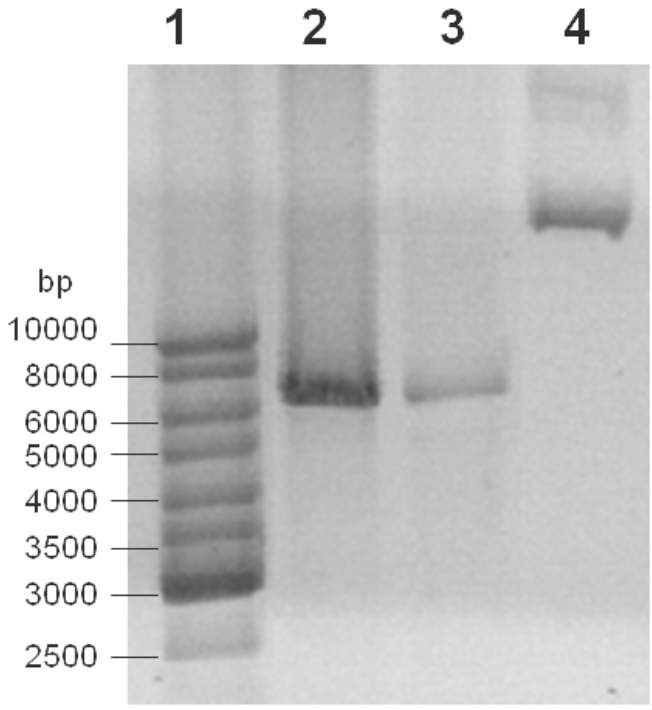

Figure 4.7 Agarose Gel analysis of pET44a+ plasmid and labeled 7000 bp DNA with terminal ATTO dyes. *Lane 1*: DNA ladder. *Lane 2*: Digested plasmid pET44a+ linearized with the restriction enzyme EcoRI. *Lane 3*: Amplified DNA (7000 bp) labeled with ATTO dyes employing PCR. *Lane 4*: Undigested plasmid pET44a+ (circular DNA of 7311 bp) amplified with bacteria.

4.4 Single–molecule FRET and wide-field fluorescence microscopy measurements

Single molecules of DNA, like λ-DNA, are of sufficient size (tens of micrometers) that they can be directly visualized by fluorescence microscopy with efficient, tightly bound fluorescent dyes.[47]

M. Yanagida and colleagues were the first to image single DNA molecules with fluorescence techniques.[48] They observed that the DNA formed a coiled structure at equilibrium and noted its Brownian motion.[49, 50] S. Chu and colleagues were the first to demonstrate simultaneous manipulation and visualization of single DNA molecules combining optical tweezers, microfluidics, and fluorescence microscopy. [47, 51]

As already mentioned, for this investigation the donor ATTO-550 (D) and acceptor ATTO-647N (A) fluorophores were conjugated to the DNA strand, being separated by 7000bp.
The ATTO dyes exhibit high fluorescence quantum yields combined with high thermal-and photo-stabilities. Donor and acceptor are on the opposite side of the double helix ends and they should be suited to visualize the end-to-end contact events when the two labels are closer than the Förster-radius R_0. When they are more separated no FRET signal will be detected. For the fluorophores used in this work, ATTO-550 and ATTO-647N, the Förster-radius R_0 was determined to be 65Å[†]. Figure 4.8 shows the absorption and emission spectra of these dyes.

[†] ATTO TEC Ro Values
https://www.atto-tec.com/fileadmin/user_upload/Katalog_Flyer_Support/R0Values.pdf

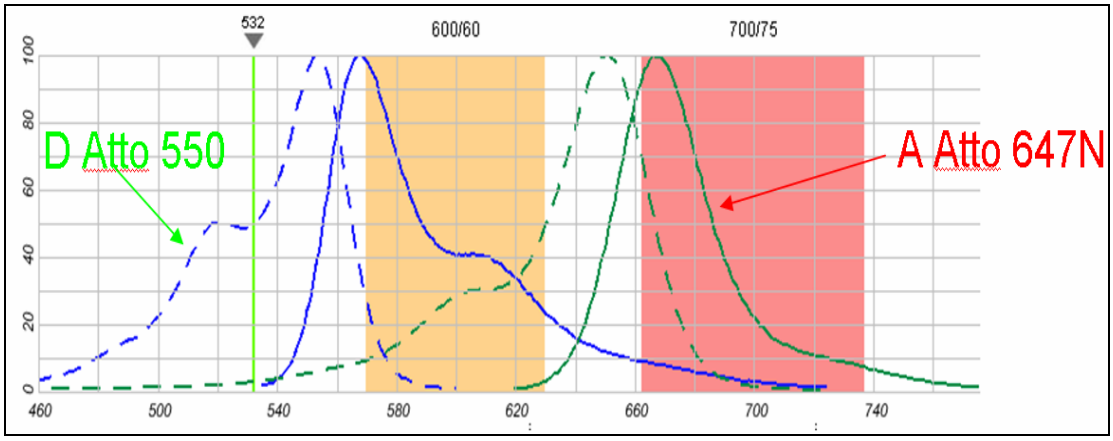

Figure 4.8 Absorption (dashed lines) and emission (plain lines) spectra of ATTO-550 (donor) and ATTO-647N (acceptor) dyes.

The unlabeled DNA (u-DNA) consisted of the linearized plasmid pET44a+ dissolved in ultra pure water. The solution for the analysis of the reptation process contained fluorescently labeled DNA (D-dsDNA-A) surrounded by u-DNA.

The radius of gyration R_g and the critical concentration (C*) of the labeled DNA was calculated employing equations 1 and 2. Table 4.1 summarizes the important properties of the probe DNA used in the subsequent optical experiments.

Table 4.1 Characteristics of the labeled DNA (D-dsDNA-A).

Sample	C* [mg/ml]	bp / length [nm]	R_g [nm]	M_w [g/mol]
D-dsDNA-A	0.67	7000 / 2380	225.4	4316737

Initially, the fluorescence decay at the emission wavelength of the donor was measured directly on a confocal microscope in order to obtain the fluorescence lifetime of the donor in presence of the acceptor (Figure 4.9). The measurements were performed by *Dr. Jean-Alexis Spitz* in the group of *Prof. Dr. Hofkens* (Katholieke Universiteit Leuven).

The final concentration of the D-dsDNA-A was 1 nM and the fluorescence decay was measured at different concentrations of unlabeled DNA (0, 0.1, 1, 10, 50 and 80 nM).

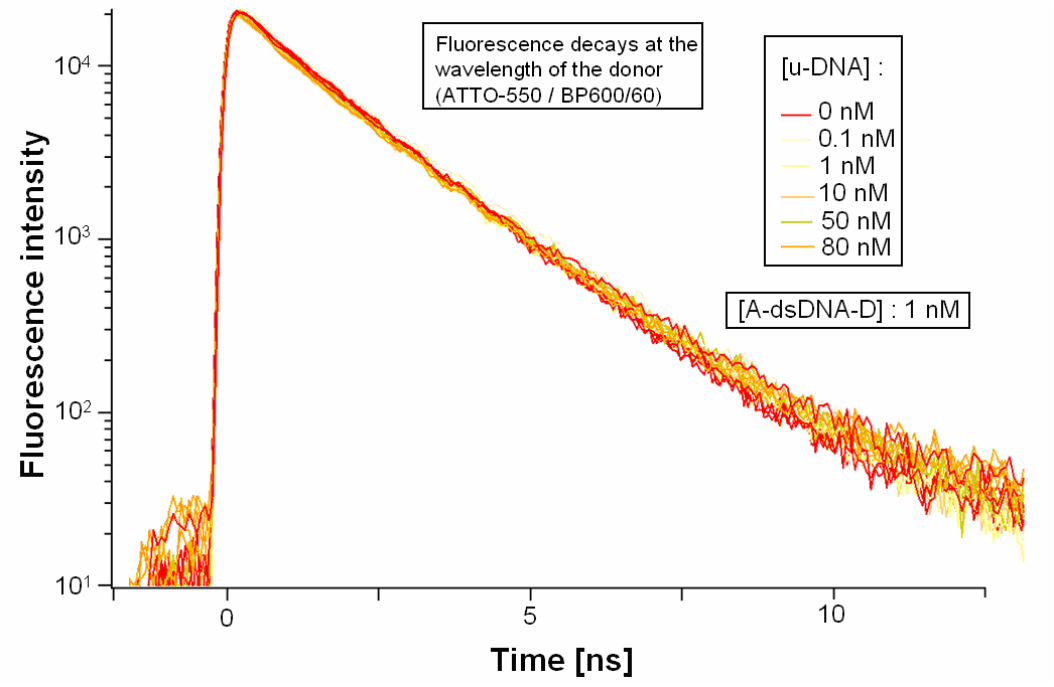

Figure 4.9 Fluorescence decay (at the wavelength of the donor) of 1nM labeled DNA in respectively 0, 0.1, 1, 10, 50 and 80 nM of unlabeled DNA.

All the decay curves of the donor in presence of the acceptor were almost superimposed. The lifetime was 3.6 ns. In the case of increased numbers and durations of end-to-end contacts, a quenching in the lifetime of the donor is expected with an increased of unlabeled DNA concentration. The decay time should become shorter with increasing DNA concentration because of FRET. One explanation why there is almost no effect on the donor lifetime is that the first experiments were carried out at concentrations of the unlabeled DNA below the critical concentration C* (0.67 mg/mL). Further experiments with concentrations of u-DNA larger than C* were carried out because of insufficient quantities of the material.

Since the confocal measurement tends to average the results of single molecules, the simultaneous motions of individual molecules were directly observed using wide-field fluorescence microscopy in the next step.

To investigate the 7 kbp DNA the concentration of the labeled DNA was maintained at $4.3*10^{-3}$ mg/mL (1 nM) and the concentration of the unlabeled DNA was increased to 5 mg/mL (~7.5 times higher than the critical concentration C*). The experiment was carried out employing the following set-up:

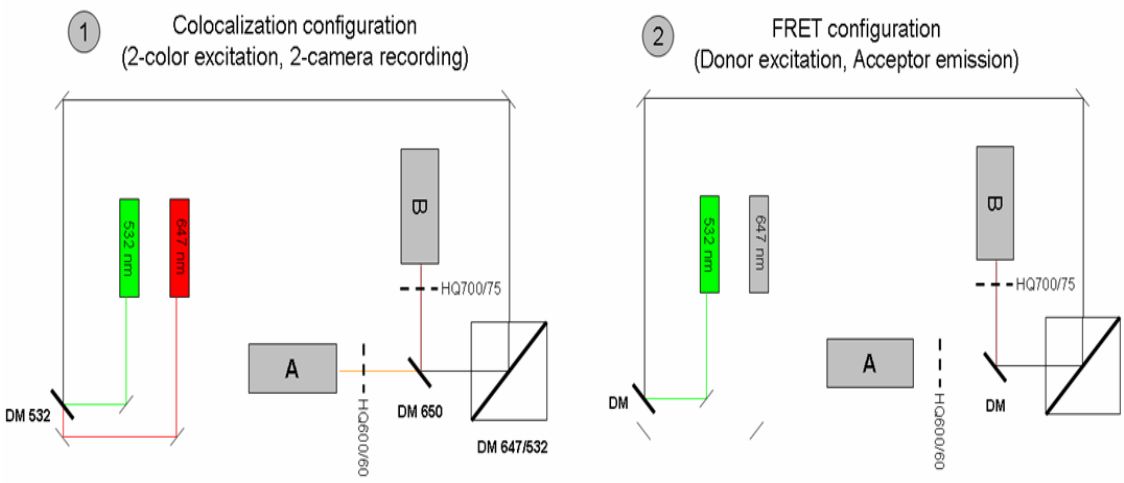

Figure 4.10 Set-up of the wide-field microscopy experiments. Two color excitations, two color recordings could be used to follow slower motions and colocalize the two labels on each molecule. Donor excitation and acceptor recording could be used to measure FRET events in the case of end-to-end contacts. DM: Dichroic mirror, Band Pass (BP) filter: Highest Quality (HQ): center of the band / width of the band.

The cameras A and B (Figure 4.10) allowed the detection of the D-dsDNA-A via two different wavelength ranges. The fluorescence light of the sample was splitted by the Dichroic Mirror (DM) and was then sent to two different cameras. The lower wavelengths range was recorded by camera A, while higher wavelengths were monitored by camera B. By employing a two camera set-up in combination with appropriate filters it was possible to detect two spectral ranges

separately, i.e. the fluorescence signal from the non-FRET state (1) and the FRET state (2).

Despite the higher concentration of unlabeled DNA used in this experiment (above the critical overlap concentration C*) and the viscous appearance of the sample, the movement of the labeled DNA was very rapid and most probably purely diffusive. No reptation was observed in the videos (each frame was recorded for 75 ms). At this recording rate of the camera, the polymer movement was too fast to be fully analyzed in detail. At a frame rate of 30 ms which is the maximum time resolution of the camera, the signal was too weak to be detected (not enough photons were emitted during the time of 30 ms). When exciting only the donor, a weak fluorescence blinking signal was visible in the acceptor channel, indicating a possible FRET taking place. But again, the dynamics were quite fast and tracking was not possible.

Diverse studies investigated the mobility and Brownian diffusion of DNA in gel electrophoresis.[52-54] However, only few reports have focused on the effects of the topology in the diffusion of entangled DNA. In none of these experiments the length of DNA was determined at which the chains get entangled in solution.
The results of the present experiments suggest that the onset of entanglements and reptation depend on the effect and also on the chemical nature of the polymer. The concentration of the unlabeled 7311 bp DNA was approximately 7.5 times higher than C*, indicating that theoretically the chains could become entangled. However, no reptation behavior was observed. Thus, it is possible that in the real experiment the 7311 bp DNA molecules are too short to effectively become entangled. Looking at the chemical structure of DNA, it might be possible that the charged nature of the polymer strongly affects the intermolecular chain interactions. Due to the high number of charges these are strong repulsive forces between individual polymers, which might suppress effective entanglement. Since the formula for estimating C* does not take into account this forces it might be possible that the entangled polymer regime is

reached for nucleic acids only at much higher concentration C* calculated from the model.

4.5 Conclusions

In conclusion, the PCR technique was an appropriate method to amplify a 7 kbp DNA and to incorporate the ATTO dyes at the ends of the double helix in a good yield. The generation of labeled PCR products longer than 3 kbp, represents a step forward regarding the synthesis of dye functionalized DNA and complements previous DNA synthesis methods, in which fluorescence labeled nucleotides and *Taq* DNA polymerase were used.

The results for polymer reptation were not as predicted by theory. Even with a sample that contained DNA at significantly higher concentrations than the theoretical overlap concentration C*, no entanglement of DNA chains was observed. The FRET events remained quite rare and weak and the moving of polymer chains was dominated by free diffusion. These experiments indicate that a 7 kbp DNA fragment is too short to study reptation.

For future investigations it is suggested to prepare longer dual labeled DNA (e.g. around 45 kbp /15.3 nm) and unlabeled DNA constructs of similar lengths. For polynucleic acids of that size reptation was detected.[29] The PCR method has its target length limitations and amplification of such lengths would be not feasible employing this technique. For that reason the synthesis of longer DNA would be possible by linearization of fosmids or cosmids, i.e hybrid plasmids that contain *cos* sequences derived from Lambda phage. The DNA could be linearized using a blunt romo enzyme, being possible to incorporate the dyes into DNA employing a ligation procedure. The cosmids or fosmids consist of 37 to 52 kbp of DNA and can be replicated in bacteria to obtain milligram scales products.

4.6 Experimental Section

4.6.1. Synthesis of labeled ds DNA 7000 bp

Labeled dsDNA (7000 bp) was synthesized by standard PCR procedure employing two labeled primers (**ssDNA-ATTO647N** and **ssDNA-ATTO550)**. The labeled primers were purchased from Sigma Aldrich, Germany (Table 4.2).

Table 4.2 Sequences of the labeled primers.

Name	Primer	DNA sequence 5'-3'-direction
ssDNA-ATTO647N	Reverse Primer	CCTCGCTCTGCTAATCCTGTTA
ssDNA-ATTO550	Forward Primer	CAAATATGTTCCGCTCATGAGAC

A total of ten PCR reactions (each one of 100 µL) contained 0.2 mM dNTPs, 5 U High fidelity polymerase kit (Fermentas GmbH), 2 ng plasmid DNA pET44a+, 1 µM forward and reverse primers, PCR buffer (100 mM Tris-HCl, 500 mM KCl and 0.8% Nonidet P40), and 2 mM of magnesium chloride were subjected to thermal cycling (4 min at 95 ℃ and then 35 cycles of 30 se c at 95 ℃ for denaturation, 30 sec at 54 ℃ for annealing and 7 min at 68 ℃ for e xtension) in a thermocycler (Biometra GmbH, Germany). The PCR amplified products were purified by QIAquick Gel Extraction Kit from Qiagen GmbH (Germany) using deionized water for eluting the amplicons.

4.6.2 Transformation of *E.coli* cells with plasmid pET44a+

Competent *E.coli* cells in LB-medium were placed on ice and mixed with 5 ng of plasmid pET44a+ (7311 bp) and incubated for 20 min on ice. A heat shock was applied by placing the cells in 42 ℃ water bath fo r 90 seconds and subsequent

cooling on ice. This procedure induces uptake of the vector into the cells.[55] LB-Media was added (1 mL) and the mixture was incubated 45 min at 37 ℃. 200 µL of the mixture were platet on agar containing ampicillin. The plates were incubated overnight at 37 ℃.

A single colony was picked from the plate and inoculated in a starter culture of 5 mL LB medium containing ampicillin. The solution was incubated for approximately 8 h at 37 ℃ with vigorous shaking (250 rpm). This 5 mL culture was grown in 200 mL LB media overnight at 37 ℃. The bacterial culture (200 mL) was divided in aliquots of 40 mL and was transfered to 1 L LB media with ampicillin, to complete 5 L bacterial culture. This solution was incubated again at 37 ℃ with vigorous shaking (250 rpm) overnight. Afterwards, the bacterial cells were pelleted at 5000 rpm at 4 ℃ for 20 min and the supernatant was discarded.

4.6.3 Purification of plasmid pET-44a+

The plasmid was purified employing a kit from QIAGEN GmbH (Germany). The pellet was resuspended in 120 mL suspension buffer, followed by the addition of 120 mL lysis buffer. Afterwards, 120 mL neutralization buffer was added to the suspension and the mixture was incubated for 5 min on ice. The lysate was centrifuged at 10000 rpm for 1 hour at 4 ℃. The supernatant contained the amplified plasmid. The clear supernatant was applied to a NucleoBond AX500 column. The plasmid DNA was bound to the macroporous anion-exchange resin in the column. Cellular impurities were eluted from the column with a high salt wash. Finally, the plasmid DNA was eluted from the column. The recovered DNA was precipitated, concentrated and desalted by isopropanol precipitation. The DNA was washed with 70% ethanol and redissolved in 3.5 mL of MilliQ-water. 2 mg of pure plasmid DNA was obtained. The purified plasmid was cut on a specific location using the restriction enzyme EcoRI. Table 4.3 shows the reaction components employed for the digestion.

Table 4.3 Reaction components for the plasmid digestion

Plasmid DNA	1 mL (~ 150 µg)
Restriction Enzyme (EcoRI)	200 µL (10 U/µl)
10x buffer for EcoRI	150 µL
Water, nuclease-free	150 µL
Total volume	1.5 mL

Ten solutions of a final volume of 1.5 mL were mixed gently and were subsequently incubated at 37 ℃ for 12 h. The liner alized plasmid was purified by QIAquick PCR Purification Kit from QIAGEN GmbH (Germany).

4.6.4 Wide-field fluorescence microscopy

The microscope employed was an inverted microscope IX71 from Olympus and the hyper sensitive cameras used were from Hamamatsu Photonics (ImagEM-CCD). Excitation was achived by diode lasers from Spectra Physics with wavlengths of 647 nm and 532 nm. All mirrors were purchased from New Focus and all optics were mounted on New Port Holders. Filters (Dichroic Mirrors and Band Pass filters) are all from Chroma. All the set up was mounted on a vibration-isolated optic table from New Port.

4.7 References

[1] R. Pecora, *Science* **1991**, *251*, 893.

[2] H. Qian, E. L. Elson, *Biophys. J.* **1999**, *76*, 1598.

[3] S. Laib, R. M. Robertson, D. E. Smith, *Macromolecules* **2006**, *39*, 4115.

[4] R. B. Bird, C. F. Curtiss, R. C. Armstrong, O. Hassager, *Dynamics of Polymeric Liquids, Vol. 2*, 2 ed., Wiley, New York, **1987**.

[5] J. D. Ferry, *Viscoelastic Properties of Polymers* 3ed., Wiley, New York, **1980**.

[6] D. N. Fuller, D. M. Raymer, J. P. Rickgauer, R. M. Robertson, C. E. Catalano, D. L. Anderson, S. Grimes, D. E. Smith, *J. Mol. Biol.* **2007**, *373*, 1113.

[7] P. E. Rouse, *J. Chem. Phys.Vol.* **1953**, *21*, 1272.

[8] P. E. Rouse, K. Sittel, *J. Appl. Phys.* **1953**, *24*, 690.

[9] P. G. deGennes, *J. Chem. Phys.* **1971**, *55*, 572.

[10] F. Brochard, P. G. Degennes, *J. Chem. Phys.* **1977**, *67*, 52.

[11] P. G. deGennes, *Macromolecules* **1976**, *9*, 587.

[12] P. G. deGennes, *Macromolecules* **1976**, *9*, 594.

[13] W. W. Graessley, *Adv. Polym. Sci.* **1974**, *16*.

[14] W. W. Graessley, *Adv. Polym. Sci.* **1982**, *47*, 67.

[15] M. Doi, S. F. Edwards, *J. Chem. Soc., Faraday Trans.2* **1978**, *74*, 1789.

[16] M. Doi, S. F. Edwards, *J. Chem. Soc., Faraday Trans.2* **1978**, *74*, 1802.

[17] M. Doi, S. F. Edwards, *J. Chem. Soc., Faraday Trans.2* **1978**, *74*, 1818.

[18] M. Doi, S. F. Edwards, *J. Chem. Soc., Faraday Trans.2* **1978**, *74*, 918.

[19] M. Doi, S. F. Edwards, *J. Chem. Soc., Faraday Trans.2* **1978**, *74*, 560.

[20] B. D. Boss, E. O. Stejskal, J. D. Ferry, *J. Phys. Chem.* **1967**, *71*, 1501.

[21] H. R. Osmers, A. B. Metzner, *Ind. Eng. Chem. Fundam.* **1972**, *11*, 161.

[22] Y. Heo, R. G. Larson, *J. Rheol.* **2005**, *49*, 1117.

[23] E. Jimenez-Regalado, J. Selb, F. Candau, *Macromolecules* **2000**, *33*, 8720.

[24] P. G. deGennes, *Scaling Concepts in Polymer Physics*, Cornell University Press: Ithaca, NY, **1979**.

[25] M. Doi, S.F.Edwards, *The Theory of Polymer Dynamics*, Oxford University Press, Oxford UK, **1986**.

[26] P. J. Hagerman, *Annu. Rev. Biophys. Biophys. Chem.* **1988**, *17*, 265.

[27] P. J. Hagerman, *Biopolymers* **1981**, *20*, 1503.

[28] W. W. Graessley, *Polymer* **1980**, *21*, 258.

[29] R. M. Robertson, D. E. Smith, *Proc. Natl. Acad. Sci. USA* **2007**, *104*, 4824.

[30] D. Smith, T. Perkins, S. Chu, *Phys. Rev. Lett.* **1995**, *75*, 4147.

[31] J. Kas, H. Strey, E. Sackmann, *Nature* **1994**, *368*, 226.

[32] D. Woll, E. Braeken, A. Deres, F. C. De Schryver, H. Uji-i, J. Hofkens, *Chem. Soc. Rev.* **2009**, *38*, 313.

[33] T. Förster, *Ann. Phys.* **1948**, *2*, 55.

[34] L. Leger, H. Hervet, F. Rondelez, *Macromolecules* **1981**, *14*, 1732.

[35] R. K. Saiki, D. H. Gelfand, S. Stoffel, S. J. Scharf, R. Higuchi, G. T. Horn, K. B. Mullis, H. A. Erlich, *Science* **1988**, *239*, 487.

[36] H. Ahern, *Scientist* **1996**, *10*, 18.

[37] F. E. Alemdaroglu, W. Zhuang, L. Zöphel, J. Wang, R. Berger, J. P. Rabe, A. Herrmann, *Nano Lett.* **2009**, *9*, 3658.

[38] M. Safak, F. E. Alemdaroglu, Y. Li, E. Ergen, A. Herrmann, *Adv. Mater.* **2007**, *19*, 1499.

[39] T. Obayashi, M. M. Masud, A. N. Ozaki, H. Ozaki, M. Kuwahara, H. Sawai, *Bioorg. Med. Chem. Lett.* **2002**, *12*, 1167.

[40] H. Yu, J. Chao, D. Patek, R. Mujumdar, S. Mujumdar, A. S. Waggoner, *Nucleic Acids Res.* **1994**, *22*, 3226.

[41] T. Weimer, in *United States Patent Vol. 6248526*, USA, **2001**.

[42] J. Y. Ju, C. C. Ruan, C. W. Fuller, A. N. Glazer, R. A. Mathies, *Proc. Natl. Acad. Sci. USA* **1995**, *92*, 4347.

[43] D. Löffert, S. Karger, N. Seip, J. Kang, QIAGEN News, Germany, **1998**.

[44] J. D. Watson, R. M. Myers, J. A. Witkowski, A. A. Caudy, A. A. Caudy, *Recombinant DNA: Genes and Genomics: A Short Course*, 3rd Edition ed., Freeman, W. H. & Company, New York, **2006**.

[45] T. Maniatis, J. Sambrook, E.F. Fritsch, *Molecular Cloning: A Laboratory Manual*, 2 ed., Cold Spring Harbor, New York, **1989**.

[46] D. W. Russell, J. Sambrook, in *Cold Spring Harbor Laboratory.* (Ed: C. S. Harbor), N.Y, **2001**.

[47] T. T. Perkins, D. E. Smith, S. Chu, *Science* **1994**, *264*, 819.

[48] K. Morikawa, M. Yanagida, *J. Biochem.* **1981**, *89*, 693.

[49] S. Matsumoto, K. Morikawa, M. Yanagida, *J. Mol. Biol.* **1981**, *152*, 501.

[50] M. Yanagida, Y. Hiraoka, I. Katsura, *Cold Spring Harbor Symp. Quant. Biol.* **1982**, *47*, 177.

[51] S. Chu, *Science* **1991**, *253*, 861.

[52] J. Rousseau, G. Drouin, G. W. Slater, *Electrophoresis* **2000**, *21*, 1464.

[53] N. Pernodet, B. Tinland, J. Sturm, G. Weill, *Biopolymers* **1999**, *50*, 45.

[54] J. Sturm, A. Pluen, G. Weill, *Biophys. Chem.* **1996**, *58*, 151.

[55] S. N. Cohen, A. C. Y. Chang, L. Hsu, *Proc. Natl. Acad. Sci. USA* **1972**, *69*, 2110.

Chapter 5

TUNABLE HYDROPHOBICITY IN DNA MICELLES: DESIGN, SYNTHESIS AND CHARACTERIZATION OF A NEW FAMILY OF DNA AMPHIPHILES*

5.1 Introduction

Amphiphilic molecules represent one of the fundamental building blocks of self-assembled materials. They are able to form a variety of structures of different morphology and size, depending on the hydrophobic volume and the size of the head group as well as other variables such as concentration, temperature, pH and solvent. Many such structures are present in nature and play important roles in biological processes, for instance phospholipids in the bilayers of cell membranes and intracellular vesicles. A range of these self-assembled aggregates have been reproduced *in vitro* and employed for potential applications such as nano-reactors,[1] gene therapy,[2, 3] catalyst encapsulation and drug delivery.[2, 4-6]

A more recent development in this field is the generation of hybrid micellar aggregates based on biopolymers, namely peptides and oligonucleotides (ODNs), covalently attached to hydrophobic moieties such as poly(propylene oxide),[7, 8] polystyrene,[9] linear and branched alkyl chains,[10, 11] poly(butyl

* This chapter was accepted for publication in Chemistry - A European Journal (2010).

acrylate)[12] and poly(*D*,*L*-lactic-*co*-glycolic acid) (PLGA).[13] Among those hybrids, DNA-based materials are especially appealing because of the sequence programmability, self-recognition and mechanical properties of DNA, as well as its only moderate resistance to degradation.[14] A model amphiphilic DNA-based system, the DNA block copolymer, has shown great potential for drug delivery.[15, 16] Such micellar structures allow both facile functionalization through DNA hybridization and internalization of hydrophobic payloads.[17]

Another related class of amphiphiles is based on low molecular weight hydrophobic groups attached to ODNs or individual nucleotides. The latter are known as nucleolipids and have been extensively studied for their interactions with membranes and potential biomedical applications[18] as well as their supramolecular organization, both into monolayers[19] and micelles.[20-22] The ability of these aggregates to carry information is limited by the presence of only individual nucleosides, but nucleobases modified at the 5-position with a range of hydrophobic moieties have also been integrated into DNA sequences using solid phase synthesis.[23, 24] The focus of these efforts, however, was not on supramolecular aggregation but rather on the effect of distribution of hydrophobic moieties on duplex stability.

A more common motif for this class of DNA amphiphiles is the terminal functionalization along the sugar-phosphate backbone, for instance with cholesterol[25] or long alkyl chains[26] for anchoring into lipid bilayers. Another such material containing pyrene and diacyllipid groups was recently shown to form micelles, once more with an affinity for cell membranes.[27] A final strategy utilizes solid phase DNA synthesis with custom phosphoramidites in which the bulky hydrophobic group completely replaces the nucleobase.[28] It is clear, then, that micellar systems of DNA amphiphiles are particularly under-investigated, with hardly any fundamental studies on the role of the hydrophobic blocks of DNA amphiphiles, for instance in determining the morphology of aggregates, their size

and stability under dilution and the effects of hybridization on the physical characteristics of the DNA micelles.

In light of this, the synthesis and characterization of a family of DNA amphiphiles containing a hydrophobically modified nucleobase and an initial investigation of the influence of the positioning of these groups on micellar properties was studied. Specifically, dodec-1-yne (-$C_{12}H_{22}$) was attached to the 5-position of uracil to impart hydrophobicity, akin to reported structures.[23, 24] The design of this modified uracil nucleobase allows the precise and easy introduction of hydrophobic units at arbitrary positions in a DNA sequence via conventional solid-phase synthesis. Three asymmetric lipid-DNAs were efficiently prepared through this synthetic procedure. They differed in the number and positions of modified bases along a fixed 12mer sequence and all self-assembled into micelles at room temperature above a Critical Micelle Concentration (CMC). The aggregates were studied with Atomic Force Microscopy (AFM), Dynamic Light Scattering (DLS) and Polyacrylamide Gel Electrophoresis (PAGE) before and after hybridization with complementary DNA (cDNA). A strong dependence of micellar size and dilution stability on the volume of hydrophobic units, as opposed to their location in the sequence, was thereby revealed. In the following a detailed outline of these experiments is given starting with the synthesis of lipidified DNA, prepared via automated solid phase DNA synthesis.

5.2 Solid phase DNA synthesis

The solid phase synthesis of DNA is a combination of the effective solid phase chemistry and phosphoramidite methodology that allows fast and efficient production of oligonucleotides.[30, 31] In this procedure the desired oligonucleotide sequence is synthesized onto an inert solid support, from which it is cleaved after the synthesis has been completed.[32]

The principal advantage of solid-phase synthesis is the facility with which immobilized products can be separated from other reactants and by-products

employing simple filtration and washing steps. The method is ideal for the synthesis of linear molecules, which require the repetition of the same steps for every chain extension. DNA synthesis begins with attachment of a 3'-hydroxyl nucleoside to a solid Controlled-Pore Glass (CPG) support via a long spacer. The CPG support is functionalized with a primary amine.
The synthesis is divided into several steps which make up a characteristic synthesis cycle (Figure 5.1).[33]

1. **Detritylation**: removal of the 5'-dimethoxytitryl group (DMTr) to obtain a hydroxyl group by treatment with $CHCl_2COOH$ (dichloroacetic acid).

2. **Coupling**: Activation of the amidites with tetrazole and formation of the 3`-5` phosphodiester bond of the growing oligonucleotides.

3. **Capping**: all free reactive groups are blocked using acetylation, thus eliminating them as reactive partners in the further course of the synthesis.

4. **Oxidation**: The internucleotide phosphit group that has been created in the coupling step is oxidized to its phosphate using iodine solution. A new synthesis cycle is started from step (1) again.

Between the reactions, washing steps with acetonitrile are introduced, to rinse out residual reagents. The reactions (1-4) are repeated until the desired oligonucleotide sequence has been produced. After accomplishing the synthesis, cleavage of the oligonucleotide from the solid support is induced by treating the support-bound oligonucleotide with concentrated ammonia solution.

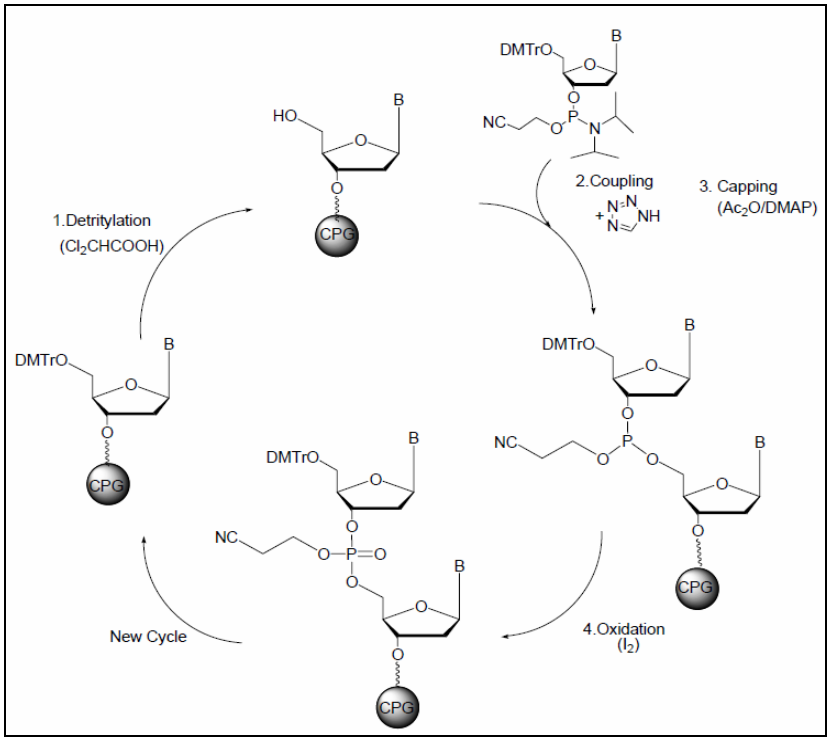

Figure 5.1 Automated solid phase synthesis of DNA.

In the next paragraph the synthesis of oligonucleotides is described employing the protocol described above. The sequences contain modified phosphor amidite building blocks.

5.3 Synthesis and micellization of lipid-DNAs

A building block analogous to deoxyuridine (**1**) was synthesized, containing 5-dodec-1-ynyluracil with a dimethoxytrityl (DMT) group at the 5'- and phosphoramidite at the 3'-position of the deoxyribonucleoside (Figure 5.2). The modified base was synthesized as is described in section 5.9.1 of the experimental section. Three different 12mer sequences were designed: **U2M** (5'-TCCUUGGCGCAG-3') and **U2T** (5'-UUTGGCGGATTC-3') with two modified uracil bases and **U4T** (5'-UUUUGCGGATTC-3') with four (U represents the modified uracil base, see Figure 5.2b). Conventional solid-phase synthesis was

employed using an automated DNA synthesizer. This investigation was performed in collaboration with *Minseok Kwak* (University of Groningen).

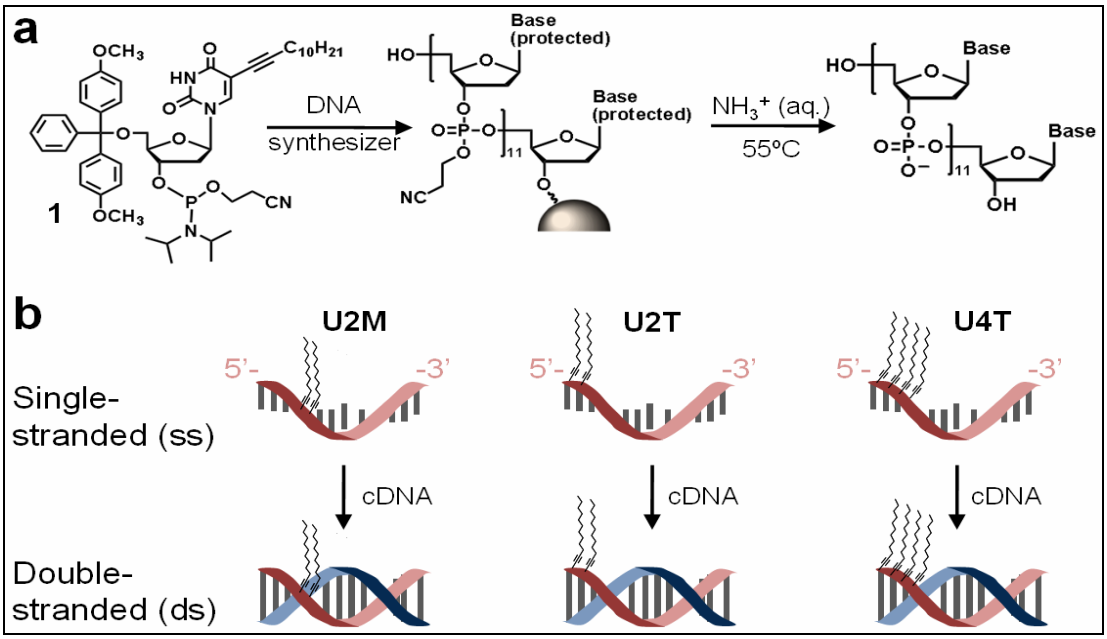

Figure 5.2 Synthetic scheme and representation of lipid-DNAs. **(a)** The precursor, 5-dodec-1-ynyluracil deoxyribo phosphoramidite (left) was used in conventional solid-phase DNA synthesis (center) and the deprotection yielded lipid-DNA (right). **(b)** Schematic representation of ss and ds lipid-DNA amphiphiles (**U2M**, **U2T**, and **U4T**) investigated.

The crude mixtures were purified by anion-exchange chromatography (Figure 5.9 in experimental section), with the molecular weights of the isolated products measured by MALDI-TOF mass spectrometry (Figure 5.10 in experimental section). Here, again MALDI-MS was chosen as a precise quantitative method for the determination of the molecular weight of the DNA-amphiphiles. As mentioned in section 3.8.1 of *Chapter 3,* MALDI analysis of DNA is not straightforward, however the use of novel matrices, such as hydroxipicolinic acid combined with ammonium acetate can improve DNA resolution. The MALDI-TOF spectra of the DNA-amphiphiles show narrow and well resolved signals, indicating that MALDI-TOF is an appropriate method for such kind of short

modified oligonucleotides. MALDI offers a potential advantage over electrospray ionization (ESI), in that biomolecules of large mass can be ionized and analyzed readily.[59] Additionally, ESI has difficulty in analyzing mixtures of compounds in the presence of salts, buffers, detergents, and other additives which reduce its sensitivity. MALDI-TOF is reasonably tolerant to the presence of salts, buffers, and other additives. [60]

Analytical HPLC results of the crude lipid-DNAs showed efficient coupling of the modified base during DNA synthesis comparable to that attained with commercial unmodified DMT-nucleoside phosphoramidite chemicals. Furthermore, the ratio of product to byproduct in the HPLC graphs was shown to be exceptionally high. It turned out that the product band in the chromatogram showed significantly better separation from impurities than that of natural ODN, presumably due to the presence of dodec-1-ynyl chains. Another effect of the modified nucleotides was found through UV/Vis spectroscopy on the lipid-DNAs (Figure 5.3). The **U2T** and **U4T** spectra showed broadened absorption bands and a bathochromic shift relative to a reference DNA containing unmodified dU. The degree of broadening and red shift corresponded well to the number of modified bases in the lipid-DNAs. For further studies, the lipid-DNA solutions were heated to 95 ºC and subsequently cooled to r.t. to generate micelles of uniform size.

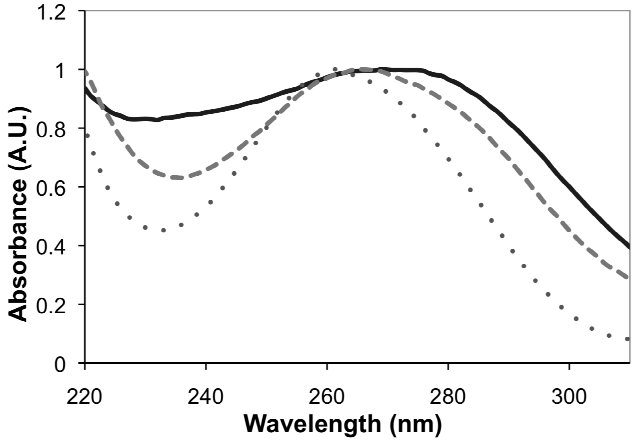

Figure 5.3 Normalized absorption spectra of **U4T** (solid, λ_{max} = 269 nm), **U2T** (dashed, λ_{max} = 265 nm), and DNA without modified base (dotted, λ_{max} = 261 nm).

5.4 Morphological characterizations by AFM and DLS

The morphologies of all the materials in this study were characterized by AFM in Tapping Mode in fluid phase. This provided confirmation of micellization, as well-defined round particles were observed on the mica surface in all cases (Figure 5.4). The AFM images were recorded by *Andrew Musser* (University of Groningen).

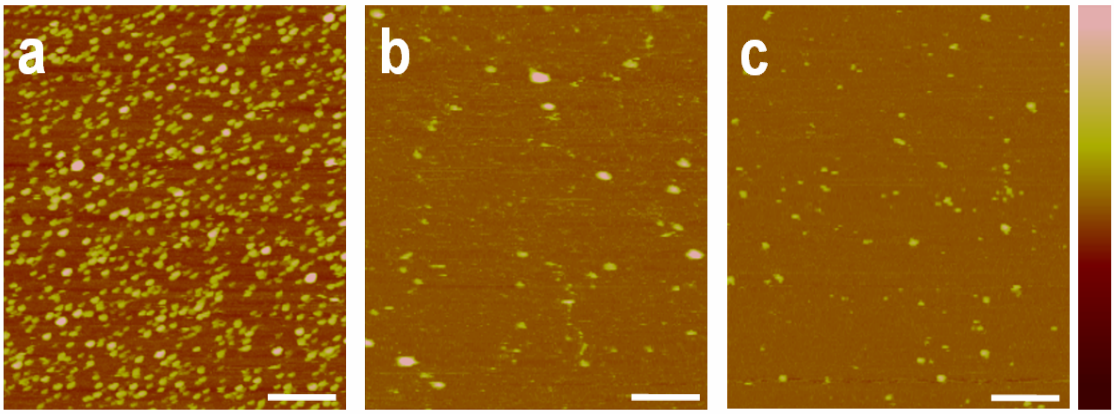

Figure 5.4 AFM height images of single-stranded lipid-DNA micelles. (a) **U2M.** (b) **U2T**. (c) **U4T**. Imaging conditions were optimized for each material separately, see experimental section. All scale bars are 200 nm. Vertical scale is 20 nm.

However, in spite of the close structural and chemical similarity of the three lipid-DNAs used in this study, they exhibit markedly different responses to the complicated mixture of electrostatic interactions and vertical tip forces. Indeed, a wide variation in salt and lipid-DNA concentration is observed in their optimum imaging conditions, as determined based on the coverage of well-defined micellar objects on the surface. It is already known that AFM is not an ideal tool for the quantitative characterization of soft micellar materials, as surface immobilization and compressive forces from the tip result in significantly reduced particle sizes.[34] A further complication with the materials presented here and, presumably, other DNA-based micelles, is the strong observed variation of

particle size with the concentration of immobilization salt and DNA material, in some cases by nearly 50% (see experimental section 5.9.4 for the size statistics). Without a systematic investigation of the effects of salt concentration, hydrophobicity and material concentration on observed height, rigorous micelle size data can not be extracted from AFM studies of such a family of amphiphilic materials as presented here. In light of these considerations, the utility of AFM in this study is restricted primarily to showing the presence of reasonably uniform micelles and highlighting the contrasts between materials. For a more reliable quantitative characterization, the much less invasive technique of DLS was employed. Size distributions obtained from DLS yielded larger diameters than those obtained by AFM, as expected,[27, 35] and are presented in Figure 5.5.

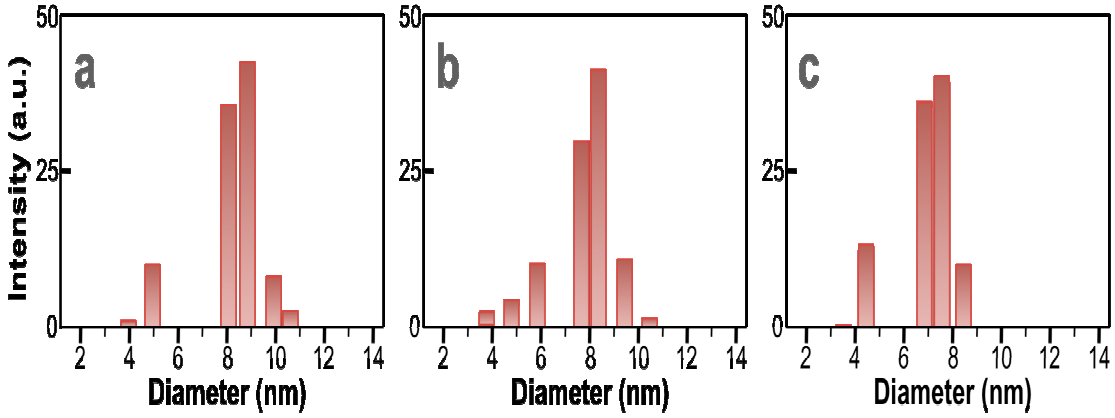

Figure 5.5 Dynamic light scattering (DLS) diameter distributions, analyzed by number, of ss lipid-DNA micelles (a: **U2M**, b: **U2T** and c: **U4T**).

The average hydrodynamic diameters for **U2M**, **U2T** and **U4T** were 7.6, 7.9, and 6.7 nm, respectively. The diameter of **U4T**, containing four modified bases, is distinctly smaller (approximately 15%) than that of the lipid-DNAs with only two modifications. This observation suggests that an increase in the number of alkyl chains (of the same length) generates higher attractive hydrophobic interactions, thereby favoring the exclusion of a greater volume of polar head groups and water from the core,[36-38] which is reflected as a reduction of the micelle size. On

the other hand, the sizes of the sequences containing two alkyl chains, whether in the middle (**U2M**) or at the terminus (**U2T**), did not differ notably. Such a result suggests that the position of the alkyl chains in these particularly short sequences has at most a weak influence on morphology. This conclusion merits further investigation with a family of longer sequences with the hydrophobic bases in a range of different positions. The high-yield fully automated synthetic strategy presented here would be well suited to such a study.

5.5 Determination of critical micelle concentration

The CMC affords a direct measurement of the resistance of a micellar system to dissociation into unimers upon dilution, and it is commonly used to evaluate the stability of micelles.[39, 40] Indeed, the CMC can be viewed as effectively equivalent to the free energy of micellization,[39] with low values denoting particularly strong intermolecular interactions and favorable aggregation. The CMC of lipid-DNAs was determined here by the internalization and fluorescence of pyrene, a well-known hydrophobic probe.[13, 41, 42] The pyrene concentration was maintained constant (0.6 µM) and the lipid-DNA concentrations were varied from 0.5 g/L to 0.5 mg/L.

From the fluorescence spectra of pyrene (λ_{exc} = 339 nm) (see spectra in Figure 5.13 in experimental section), the change in the intensity ratio of the first and the third peak (I_1 at 373 and I_3 at 383nm) was analyzed. The I_3/I_1 ratio is dependent on the polarity of the pyrene microenvironment and thus provides information about of the presence of micelles.[43] I_3/I_1 was plotted against the logarithm of the lipid-DNA concentration, and the CMC was determined from the intersection of the lower horizontal asymptote of the sigmoidal curve with the tangent at the inflection point (Figure 5.6).

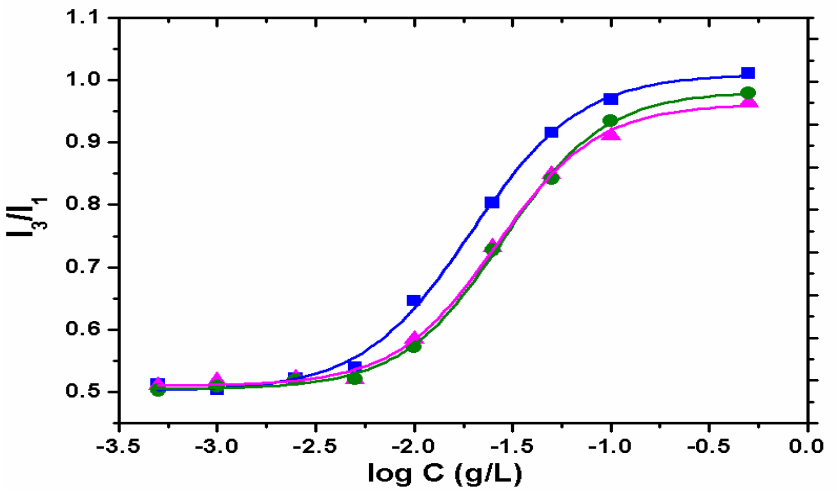

Figure 5.6 The change of the intensity ratios (I_3/I_1) from pyrene fluorescence (λ_{exc} = 339 nm) as a function of the ss lipid-DNA concentration in water (**U2M**: triangle, **U2T**: circle and **U4T**: square).

The CMC value decreased upon an increase in the number of lipid-modified bases present in the sequence, from 7.9 and 8.1 (**U2M** and **U2T**, respectively) to 5.4 mg/L (**U4T**). The relatively low CMC of **U4T** shows that the micelles with four alkyl chains are thermodynamically more stable and formed more readily than those with two, due to increased hydrophobic interactions. Moreover, little difference was observed between the CMC values of **U2M** and **U2T** - apparently the proportion of hydrophobic moieties in the sequence is by far the more important determinant of micellar stability. Previously reported micelles based on DNA and diacyllipid groups,[27] polypropylene oxide (PPO)[7] or poly(*D*,*L*-lactic-*co*-glycolic acid) (PLGA),[13] yielded CMCs of 0.04-0.2, 5-6 and 10 mg/L, respectively. Although the CMCs of the micelles described in this investigation are higher than that of ODN/diacyllipid micelles, the values (5.4 to 8.1 mg/L) compare favorably with those of DNA diblock copolymer micelles.[44, 45] More significantly, the results suggest that the CMC can be easily tuned by the modular incorporation of the appropriate number of modified nucleobases into the sequence. Further studies will be necessary, however, to probe the full range and precision of such tuning.

5.6 Hybridization with complementary DNA

The primary utility of DNA based micellar systems is the potential for functionalization through DNA hybridization.[15, 29] For this reason, complementary DNA was hybridized onto the corona of lipid-DNA micelles to study the effects of this process on their physical characteristics, for instance morphology and stability. Successful hybridization was confirmed using fluorescence measurements in the presence of an asymmetric positively-charged cyanine dye, SYBR Green I (λ_{em} = 525 nm). This dye shows exponentially greater fluorescence upon preferential binding to double-stranded (ds) DNA over ss DNA[46, 47] with a sequence-specific response[48] and is thus widely used for DNA staining.[49, 50] Previous studies reported the detection of DNA mutations using SYBR Green I, demonstrating that the method is sufficiently sensitive to distinguish completely hybridized Watson-Crick duplexes from unstable mismatch sequences.[47] In light of this, SYBR Green I fluorescence also allows a comparison between pristine ds DNA and ds lipid-DNAs to investigate the influence of the modified uracil bases with alkyl chains on the completeness of hybridization.

U2M, **U2T** and **U4T** were hybridized with the respective cDNA sequences by annealing in a 1:1 molar ratio, and compared to a series of SYBR Green I-containing control samples: ss lipid-DNA, pristine ss DNA, pristine ds DNA and an unannealed mixture of ss lipid-DNA and its cDNA. All fluorescence spectra were collected with the same concentration of SYBR Green I (1x) and DNA (15 µM) in 1 x TAE buffer (pH 8.5). Figure 5.7 exhibits the results for each lipid-DNA and its controls. For all three materials, SYBR Green I showed greater fluorescence intensity after hybridization, demonstrating successful formation of lipid-DNA duplexes. There is no significant intensity difference between ds lipid-DNA and ds DNA – the slight decrease of the fluorescence intensity for lipid-DNA versus pristine DNA can be attributed to molecular weight differences. The close

agreement between the peak intensities indicates that complete hybridization was accomplished along the full sequence. Additionally, there is a clear blue shift (approximately 6 nm for **U2M** and **U2T** and 10 nm for **U4T**) in the emission maximum of modified DNAs relative to those of pristine DNAs. Such a hypsochromic shift was observed in a previous study with benzimidocarbocyanine dyes containing *N*-alkyl chains and the effect was attributed in part to the local hydrophobic environment.[51] The hydrophobicity of the modified base may play a similar role in the photophysical behavior observed here, but further investigations with a series of lipid-modified phosphoramidite precursors are required to conclusively determine the origin of this phenomenon. Nevertheless, from the SYBR Green I fluorescence result it is unambiguous that the lipid-DNAs have the full ability to hybridize.

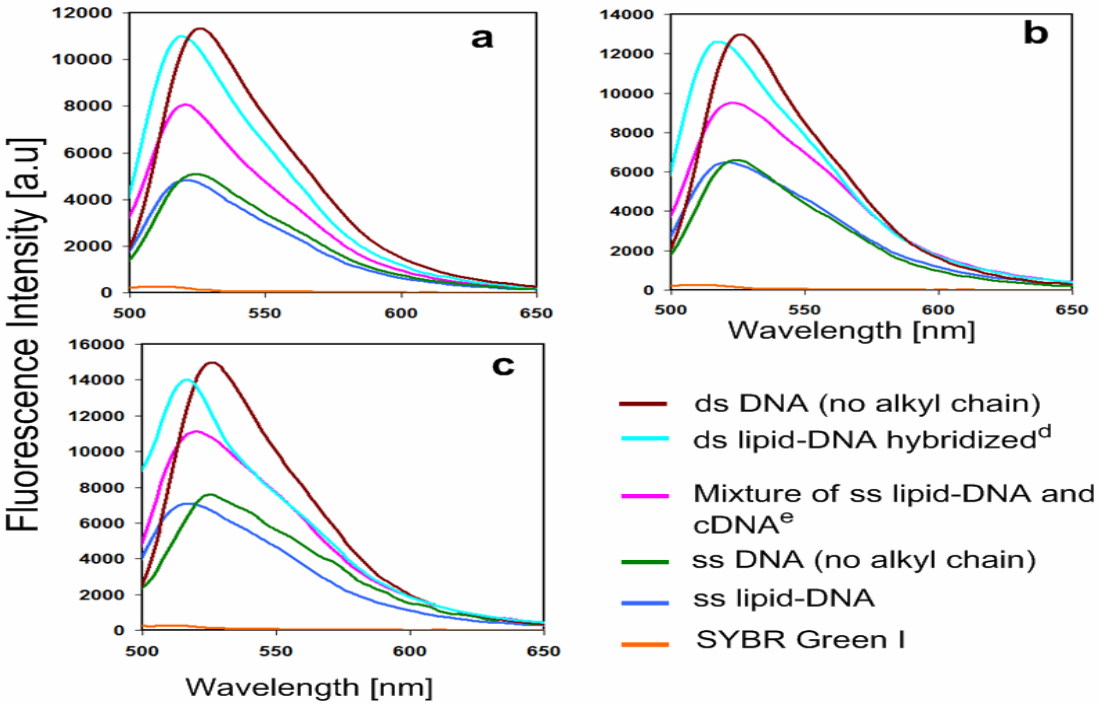

Figure 5.7 Fluorescence spectra of lipid-DNAs (a: **U2M**, b: **U2T** and c: **U4T**) in the presence of SYBR Green I and their corresponding controls. [d]Lipid-DNA and the cDNA were hybridized by heating the mixture to 95 ℃ and subsequent cooling down to r.t. [e]Same mixture as *d* but without the thermal treatment.

The hybridization properties of the materials were further analyzed by 20% PAGE (Figure 5.8). The gel shows discrete bands under ethidium bromide staining, corresponding to the hybridization products of the lipid-DNAs with their respective cDNA (lanes 5, 6 and 7). The electrophoretic mobilities in these lanes differ significantly from those of the starting materials (lanes 2, 3 and 4), another indication of successful duplex formation. Indeed, in none of the lanes for ds lipid-DNA is residual ss starting material visible –virtually all of the material must thus be hybridized. Additionally, it was observed that increased incorporation of hydrophobic chains in the DNA sequences resulted in lower migration in the gel, relative to unmodified ODNs. Previous studies of spermine-modified DNA have revealed similar behavior during PAGE analysis.[52, 53] In the present experiment the mobility retardation is not due to charge neutralization but rather increased molecular weight or hydrophobic interactions with the gel matrix. Furthermore, the extreme retardation of **U4T** and its hybridization product suggests that the hydrophobic interactions between these molecules are so strong that micelles are present even in the electrophoresis conditions.[27] In any case, the well-resolved bands in the gel provide a clear additional confirmation of successful hybridization.

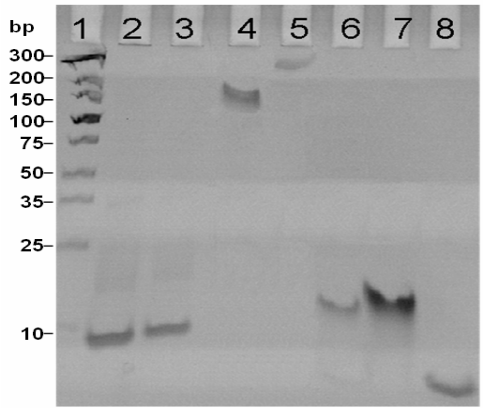

Figure 5.8 20% non-denaturing PAGE of ss- and ds lipid-DNAs. *Lane 1*: Ultra low range ladder (10-300 bp), *Lane 2*: **U2M**, *Lane 3*: **U2T**, *Lane 4*: **U4T**, *Lanes 5-7*: hybridization products of U4T, U2M and U2T with their corresponding complementary sequences (cDNA), and *Lane 8*: unmodified 12mer DNA sequence (control).

5.7 Morphological characteristics of ss- and ds DNA-lipids

After the confirmation of lipid-DNA hybridization by fluorescence spectroscopy and electrophoresis, the morphology and CMC of the ds lipid-DNAs were characterized by AFM, DLS and pyrene solubilization. Once more, well-defined round structures were observed in AFM, indicating that DNA duplex formation does not hinder micellization (see experimental section table 5.2 for the AFM images and size histograms of the ds lipid-DNAs). It should be noted that the slight increase of particle sizes observed in AFM for **U2T** and **U4T** (Table 5.1) does not necessarily reflect growth of the micelles, as the increased persistence length of ds DNA versus ss DNA[54-56] also results in greater resistance of the micelles to compression under the AFM tip.

Thus, DLS is again the preferred method here to evaluate the sizes of the micelles. As shown in Table 5.1, all micelles revealed only a slight increase in diameter upon hybridization, as is consistent with reports on other DNA amphiphile micelles.[7] This is to be expected, since the close confinement of the negatively-charged ss DNA strands in the corona leads to high electrostatic repulsion and consequent extension into solution. Thus the additional rigidity imparted by hybridization does not necessarily result in significant lengthening of the DNA. The micelles of **U4T** are again somewhat smaller than those with fewer alkyl chains, indicating that the degree of hydrophobicity remains the major factor in determining micelle size even after hybridization. Likewise, the number of hydrophobic groups still appears to be the dominant factor in the stability of the hybridized micelles, with no significant change in molar CMC observed after hybridization.

Table 5.1 Characteristics of ss- and ds lipid-DNA micelles.

Lipid-DNA	CMC (mg/L)[b]		Diameter by DLS (nm)		Height by AFM (nm)	
	ss	ds	ss	ds	ss	ds
U2T	8.1	15.1	7.9 ± 2.6	8.3 ± 3.9	5.1 ± 1.4	7.9 ± 3.6
U2M	7.9	15.8	7.6 ± 2.1	8.1 ± 2.7	7.3 ± 1.9	6.9 ± 2.2
U4T	5.4	10.2	6.7 ± 2.5	7.3 ± 1.9	4.2 ± 0.9	6.6 ± 1.2

[b] Note that higher CMC of ds samples are due to the molar mass of hybridized cDNAs. The conversion into molar CMC is presented in experimental section Table 5.3.

5.8 Conclusions

In conclusion, the synthesis of a modified nucleotide and its precise modular incorporation into short ODN sequences using automated solid phase DNA synthesis was presented. The three lipid-DNA molecules characterized here contained either two or four dodec-1-ynyluracil units at different positions in the sequence, and all formed micelles at room temperature. The lipid-DNA structures were studied with Atomic Force Microscopy (AFM), Dynamic Light Scattering (DLS) and Polyacrilamide Gel Electrophoresis (PAGE). The Critical Micelle Concentration (CMC) of the three systems was also determined as evaluation parameter of the micelle stability. Investigation of micellar size and stability showed that these parameters primarily depend on the degree of hydrophobicity, with the greater number of dodec-1-ynyl chains resulting in smaller, thermodynamically more stable micelles. In contrast, the position of hydrophobic units in the short ODN proved to have little influence.

The possible functionalization of the DNA micelles with any molecule conjugated to the complementary sequence is of a great interest especially for the design of micellar carrier systems for drug delivery. For that reason, each ss lipid-DNA was hybridized with its complementary sequence. The alkyl chains were found to not interfere with DNA hybridization, and the same trends in micelle characteristics were observed for double-stranded micelles.

The more significant outcome of this modified base method, though, is the ability to systematically introduce well-defined hydrophobic nucleotides into DNA amphiphiles and thereby alter their supramolecular properties. This study represents the first such investigation of the fundamental role of hydrophobic moieties in determining aggregation behavior in ODN micelle systems. Further application of this strategy may eventually allow precise tuning of these structures and their physical properties. For instance, analogous to other amphiphilic superstructures,[57] it should be possible to form self-assembled nanofibers covered with DNA and to template chemical reactions using reactive groups introduced into the nucleobases. [58]

5.9 Experimental Section

5.9.1 Synthesis of modified uridine phosphoramidite

5'-O-(4,4'-Dimethoxytrityl)-5-iodo-2'-deoxyuridine *(1)*

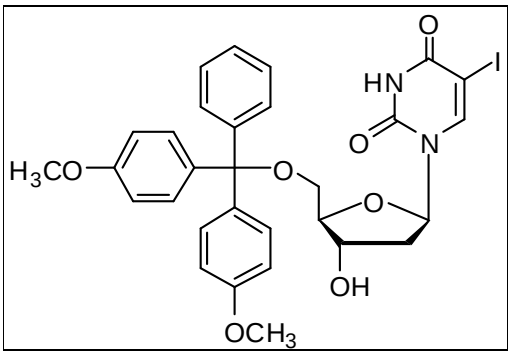

5-Iodo-2'-deoxyuridine (5 g, 14.12 mmol) was dissolved in 80 ml pyridine and was reacted with 4,4'-dimethoxytrityl chloride (DMT-Cl) (5.76 g, 17.01mmol) overnight at room temperature. Afterwards, ice-cold water (50 ml) was added to the solution and the resulting mixture was extracted twice with 50 ml dichloromethane. The organic layer was washed with water, dried over $MgSO_4$ and the solvent was evaporated under reduced pressure.
The residue was purified by silica gel column chromatography, eluted with Hexane/EtOAc (1:1) to give 8.43 g (91%) of pure product.

^{1}H-NMR (250 MHz, $CDCl_3$-d_1): δ = 2.24 (m, 2H, 2'-H), 3.32 (m, 2H, 5'-H), 3.72 (s,6H, OCH3), 4.01 (m, 1H, 3'-H), 4.47 (m, 1H, 4'-H), 6.24 (t, J_1 = 6.7Hz, 1H, 1'-H), 6.77 (d, J = 8.9 Hz, DMTr aromatic protons, 4H), 7.08 to 7.42 (m, 9H, DMTr aromatic protons), 8.07 (s, 1H, 6-H), 8.77 (s, N3-H,1H) ppm.

^{13}C-NMR (63 MHz, $CDCl_3$-d_1): δ = 40.3, 55.3(2C), 63.51, 68.94, 70.3, 85.05, 86.92, 87.5, 113.21(4C) 125.9, 127.56(2C), 127.68(2C), 128.9(4C), 132.35, 135.38, 144.19, 144.71, 150.1, 159.2(2C), 160.52 ppm

FD-MS: m/z calculated for $C_{30}H_{29}IN_2O_7$ = 656.46 g/mol; found: 656.2.

5-[Dodec-1-ynyl] -5'-O-dimethoxytrityl-2'-deoxyuridine *(2)*

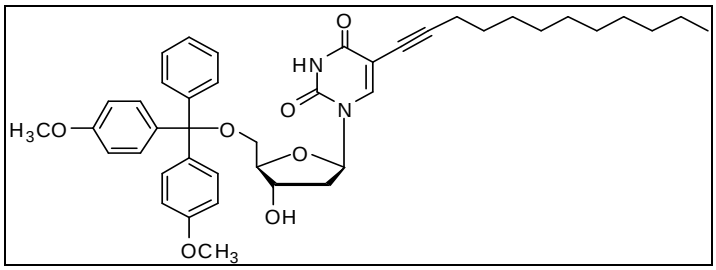

5'-O-(4,4'-Dimethoxytrityl)-5-iodo-2'-deoxyuridine ***(1)*** (8 g; 12.19 mmol) was dissolved in degassed anhydrous DMF (100 ml) and argon was bubbled through this solution for 10 min. *Tetrakis*(triphenylphosphine)palladium(0) (1.41 g; 1.22 mmol, 10 mol%) was added and Argon was bubbled through the solution for another 5 min. Amberlite-IRA67 (20 g) was introduced, followed by addition of 1-dodecyne (6.1 g; 36.56 mmol) and copper(I)iodide (0.46 g; 2.44 mmol, 20 mol%). The mixture was stirred for 18 hours at room temperature under exclusion of light. The solid was filtered and washed with MeOH/CH_2Cl_2 1:1 (10 ml). The solvent was evaporated and the residue was purified by silica column chromatography. The product was eluted with Hexane/EtOAc (1:1) to yield 5.96 g (70%) of the target component as a white solid.

^{1}H-NMR (250 MHz, CD_2Cl_2-d_2): δ = 0.8 (t, J = 7.3Hz, 3H, $1CH_3$), 1.16 (s, 14H, $7CH_2$), 1.5 (t, J = 6.6Hz, 2H, $1CH_2$), 1.99 and 2.20 (2 sets of multiplets, 2H, 2'H), 2.31 (m,2H,$1CH_2$), 3.25 (m, 2H,$1CH_2$, 5'H), 3.48 (m, 2H, 3'-H and 3'-OH), 3.70 (s, 6H ,2OCH3), 4.43 (m, 1H, 4'-H), 6.17 (dd, J_1=7.6Hz,J_2=5.5Hz, 1H, 1'-H), 6.74 (d,4H, J = 8.8Hz, DMTr aromatic protons), 7.25 (m, 9H, DMTr aromatic protons), 7.83 (s,1H, H-6), 8.56 (s,N3-H,1H) ppm.

^{13}C-NMR (63 MHz, $CDCl_3$-d_1): δ = 14.3, 19.8, 23.1, 28.93, 29.73, 32.23, 41.70, 55.6, 63.99, 71.14, 72.69, 86.03, 87.00, 87.31, 87.9, 93.4, 94.60, 95.55, 101.1, 113.64, 116.8, 126.4, 127.25, 128.29, 128.40, 130.29, 135.92, 136.07, 145.26, 151.08, 153.08, 156.00, 159.45, 160.35 ppm

FD-MS: m/z calculated for $C_{42}H_{50}N_2O_7$ = 694.86 g/mol; found: 694.4.

5-(3"Dodecyne)-5'-O-dimethoxytrityl-2'deoxyuridine 3'[(2-cyanoehtyl)-N,N-diisopropylphosphoramidite] ***(3)***

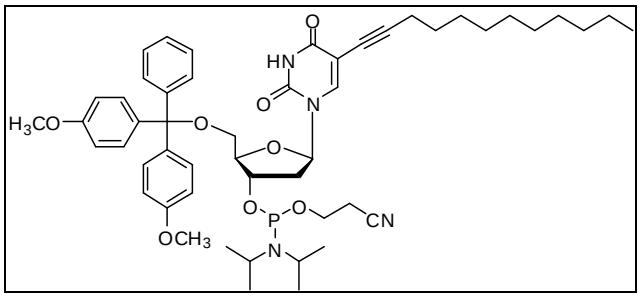

5-[Dodec-1-ynyl] -5'-O-dimethoxytrityl-2'-deoxyuridine ***(2)*** (5.64 g, 8.12 mmol) was dissolved in dry THF and reacted with N-diisopropyl-2-cyanoethyl-chlorophosphoramidite (2.31 g, 9.74 mmol) in the presence of diisopropylethylamine at room temperature. The reaction mixture was stirred for 3 hours under argon atmosphere. The mixture was poured into saturated Na_2CO_3 solution and washed with water (3×) and brine (3×). The organic layers were combined and dried over $MgSO_4$. After evaporation of the solvent the product was dried under high vacuum and yielded (***3***) quantitatively. The product was used immediately for the solid phase DNA synthesis.

^{31}P-NMR (100 MHz, THF-d_8): 149.65 ppm

5.9.2 DNA Synthesis

The modified 5-dodec-1-ynyluracil containing phosphoramidite ***(3)*** (7 g) was dissolved in CH_3CN (52 mL) to adjust the concentration to 0.15 M, in the presence of 3 Å molecular sieve. The acetonitrile solution was directly connected to the DNA synthesizer prior to starting the DNA synthesis. The synthesis of **U2M**, **U2T** and **U4T** was performed in 50 µmol scale.

General procedure: after every detritylation step, 1.5 equivalents of the nucleoside phosphoramidite were passed through the column reactor and further recycled for 3 min (coupling and recycling steps). Subsequently oxidation and capping steps were performed.

5.9.3 DNA-amphiphile purification and characterization

5.9.3.1 Analytical anion exchange (AIEX) chromatography

Analytical AIEX chromatography (Figure 5.9) was performed using a HiTrap Q HP 1 mL column (GE Healthcare) through linear gradient using buffer A (25 mM Tris-HCl, pH 8.0) and buffer B (25 mM Tris-HCl and 1.0 M NaCl, pH 8.0). According to each analytical chromatogram of DNA-amphiphile, HiTrap Q HP 5 mL was used during purification of the crude mixtures.

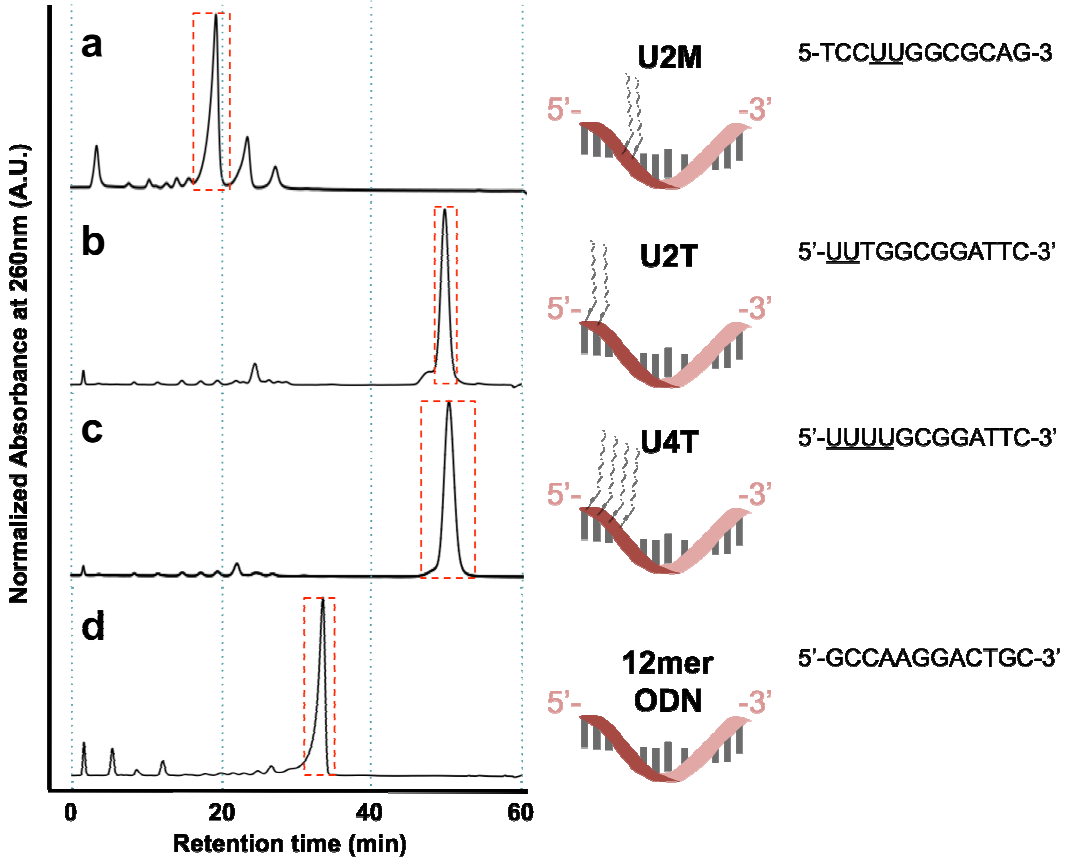

Figure 5.9 AIEX elution graphs of the crude reaction mixtures. (a) **U2M**. (b) **U2T**. (c) **U4M**. (d) Pristine 12mer with same sequence. The product fraction of each crude mixture is marked. Numbers beside the fraction represent the percentage of product area versus total area integrated from the eleugram.

5.6.3.2 MASS SPECTRA

Molecular weights of the DNA sequences were determined using matrix-assisted laser desorption/ionisation time of flight (MALDI-TOF mass spectrometry) (Figure 5.10). The spectra were recorded on a Bruker MALDI-TOF (Reflex-TOF) mass spectrometry. See *Chapter 3* for the description of the matrix.

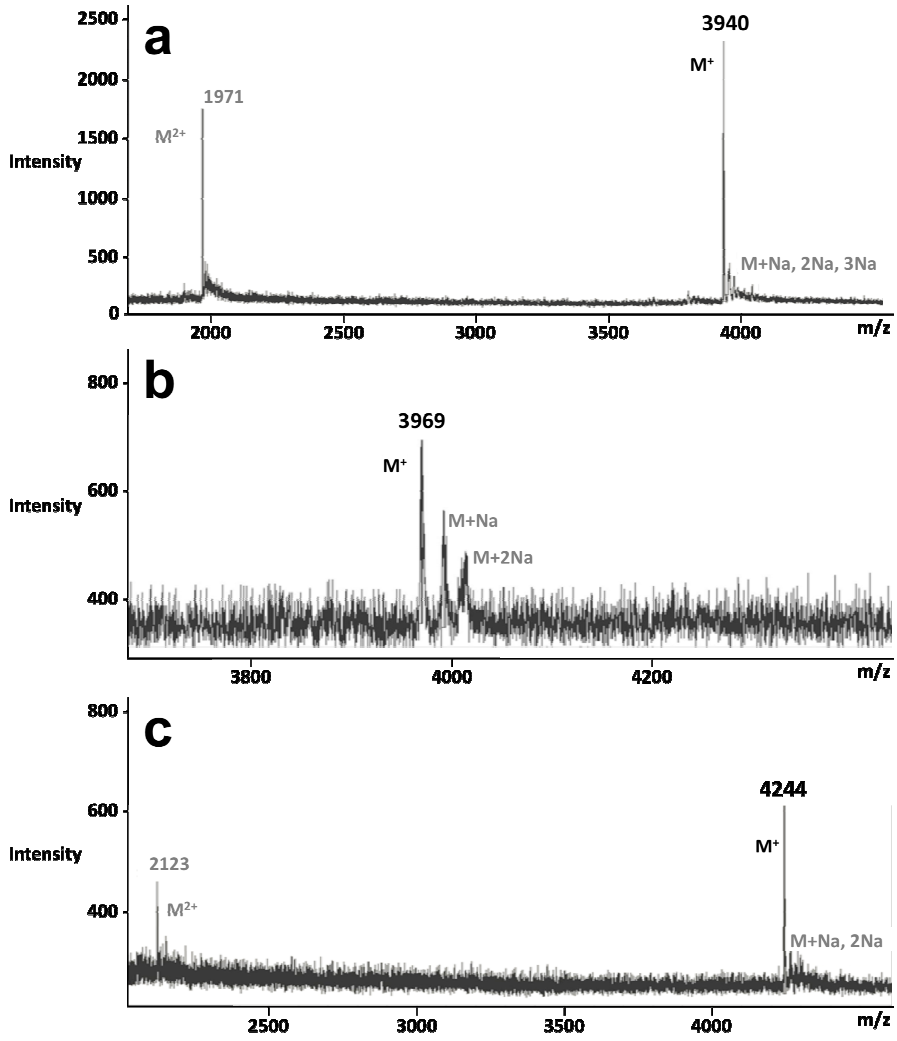

Figure 5.10 MALDI-TOF spectra of the lipid-DNAs. (a) **U2M** (found: 3940 g/mol, calculated: 3938 g/mol), (b) **U2T** (found: 3969 g/mol, calculated: 3968 g/mol) and (c) **U4T** (found: 4244 g/mol, calculated: 4244 g/mol).

5.9.4 Characterization of the DNA micelles

5.9.4.1 AFM images

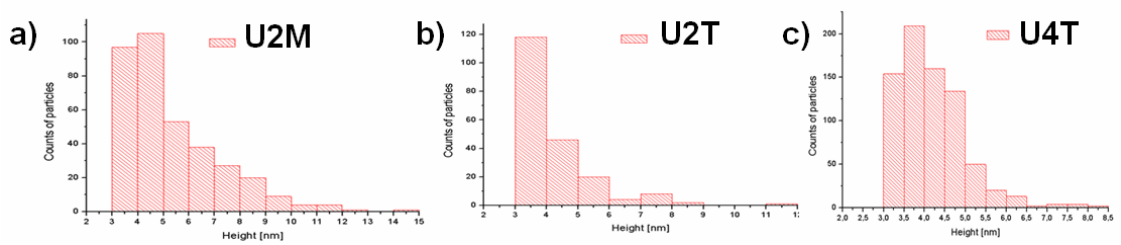

Figure 5.11 Size histograms of single stranded DNA-amphiphiles. (a) **U2M** (5.2 ± 1.3 nm) (b) **U2T** (4.2 ± 2.0 nm) and (c) **U4T** (4.2 ± 0.18 nm).

In order to compare the height of the ss- and ds DNA amphiphiles (measured by AFM), the ss and ds materials were prepared under the same conditions:
U2M: A freshly cleaved mica surface was covered with 40 µL of 5 mM $MgAc_2$ and blown dry after 5 minutes. Subsequently, 50 uL of a ~10 µM solution of the material in 500 µM $MgAc_2$ was deposited on fresh mica and allowed to incubate for 20 minutes. Images were then collected (Table 5.2, first row).

U2T: A freshly cleaved mica surface was covered with 40 µL of 5 mM $MgAc_2$ and blown dry after 5 minutes. Subsequently, 50 µL of a ~50 µM solution of the material in ultra pure water was then immediately deposited on the surface and allowed to incubate for 20 minutes. Images were collected for ~1 hour, and then the excess solution was gently shaken off and replaced with 50 µL ultra pure water, after which these images were collected (Table 5.2, second row).

U4T: A freshly cleaved mica surface was covered with 40 µL of 5 mM $MgAc_2$ and blown dry after 5 minutes. Subsequently, 50 µL of a ~1.3 µM solution of the material in ultra pure water was then immediately deposited on the surface and allowed to incubate for 20 minutes. Images were then collected (Table 5.2, third row).

Table 5.2 AFM images and size histograms of the DNA micelles before and after hybridization.

	ss DNA amphiphiles	ds DNA amphiphiles
U2M	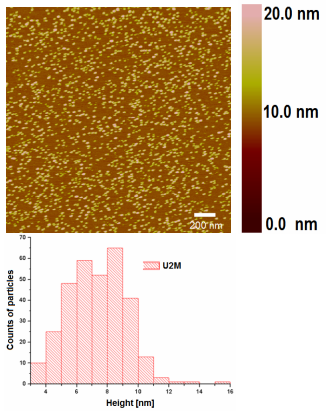 Mean: 7.3±1.9 nm	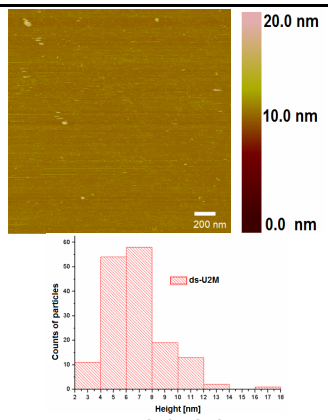 Mean: 6.9±2.2 nm
U2T	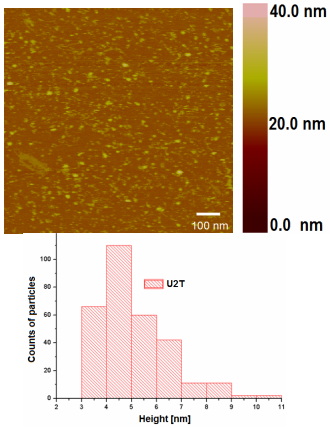 Mean: 5.1±1.4 nm	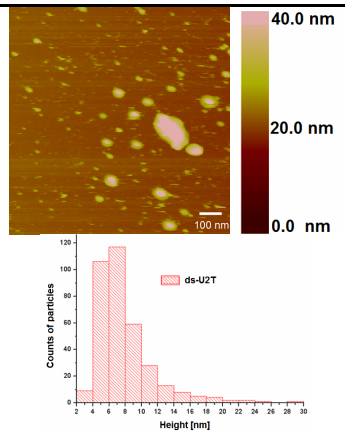 Mean: 7.9±3.6 nm
U4T	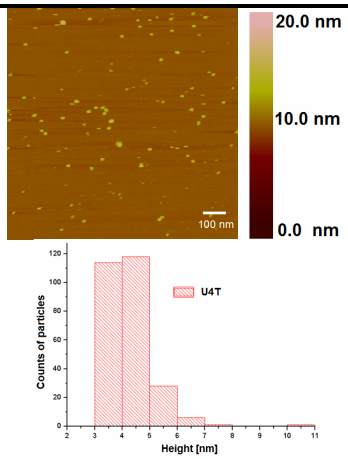 Mean: 4.2±0.9 nm	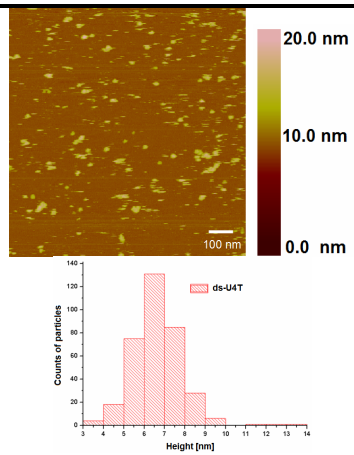 Mean: 6.6±1.2 nm

5.9.4.2. DLS measurements

The size distribution of the micelles (before and after hybridization) was determined by DLS at room temperature and at a scattering angle of 90° employing a ZetaSizer 3000HS (Malvern Instruments Ltd., Malvern, UK) equipped with a He-Ne ion laser (633 nm). All the solutions (2.5 mg/mL) were filtered through a 0.45 μm filter before the experiment and were heated up to 95 ℃ and cooled down to room temperature overnight. T he correlation function was analyzed by the CONTIN method and the number intensity distribution was chosen for evaluation of the data.

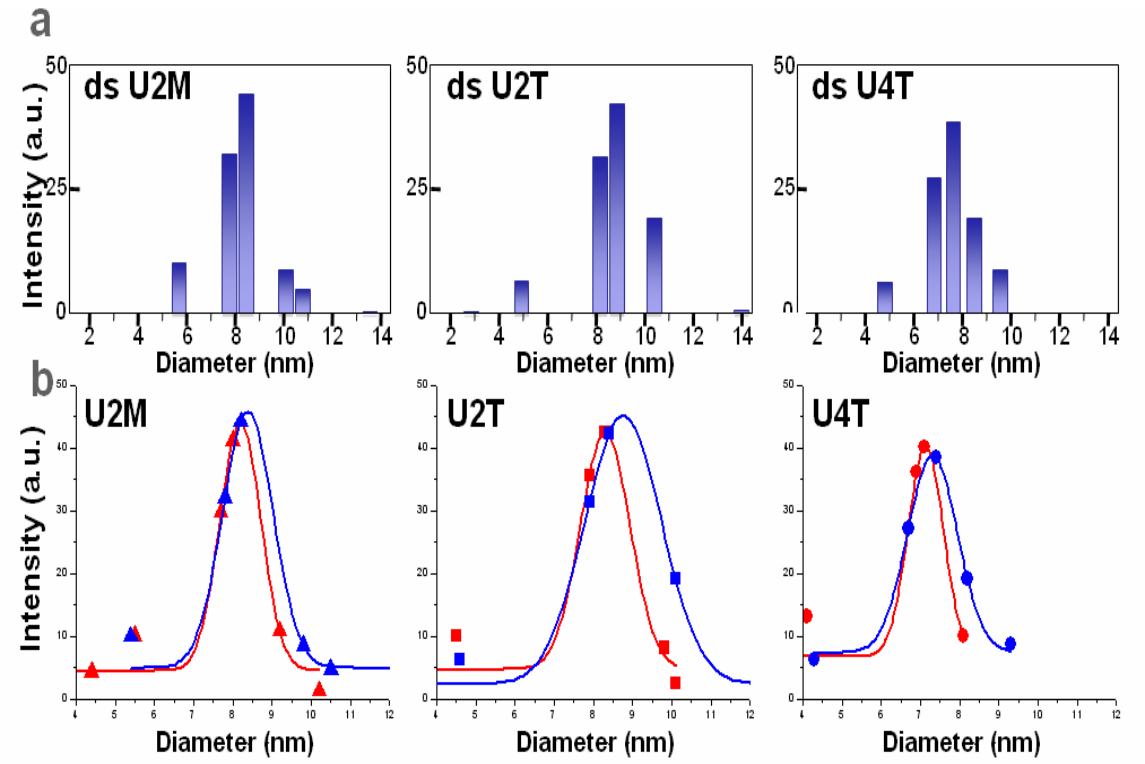

Figure 5.12 Dynamic light scattering (DLS) diameter distributions, analyzed by number. **(a)** Diameter distribution histograms of ds lipid-DNA micelles. **(b)** Gaussian-fitted curves (red: ss lipid-DNAs, blue: ds lipid-DNAs) of hydrodynamic size correlation data obtained from DLS measurements.

5.9.4.3. CMC determination before and after hybridization

A known amount of pyrene was dissolved in acetone and added to several eppendorf tubes. The acetone was allowed to evaporate for 4 h at 45 ℃ and a solution of the different DNA amphiphiles (concentrations ranging from 0.0005 to 0.5 g/L) was added to the tubes, yielding a final pyrene concentration of 0.6 µM. The solutions were incubated at 95 ℃ for 10 minutes in the dark and slowly cooled down to room temperature. The fluorescence spectra were recorded at room temperature using an excitation wavelength of 339 nm. The fluorescence spectrum was measured by use of a Fluoroscan FL 3095 spectrometer (J&M, Germany). Figure 5.13 shows the fluorescence spectra of pyrene in the presence of decreasing concentration of **U2T.** Figure 5.14 displays the change of the intensity ratio I_3/I_1 from pyrene emission of the hybridized lipid-DNAs.

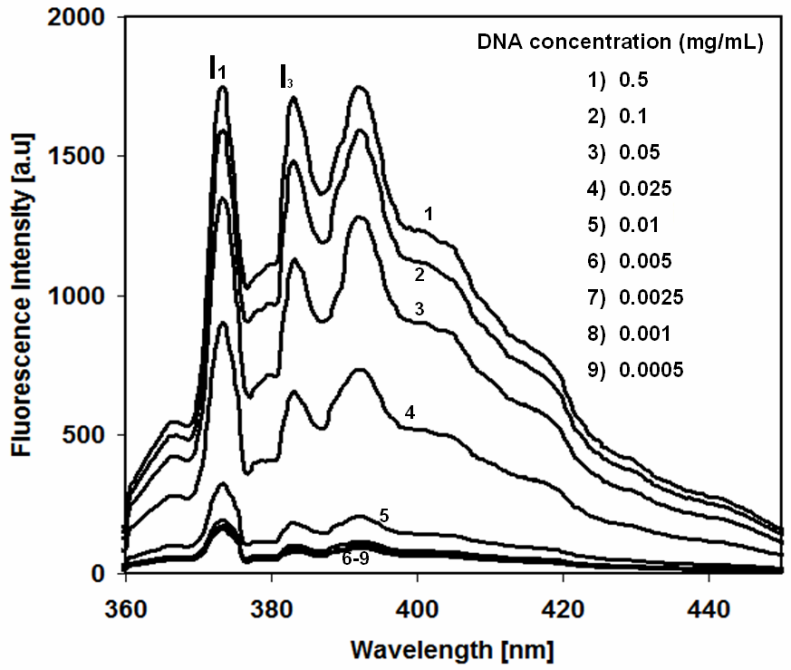

Figure 5.13 Fluorescence spectra (λ_{ex} = 339 nm) of pyrene-loaded **U2T** micelles (pyrene concentration: 0.6 µM) at different **U2T** concentrations. Fluorescence spectra of the other pyrene-loaded micelles are not shown (see Table 5.3 for molar CMC determination of all micellar structures).

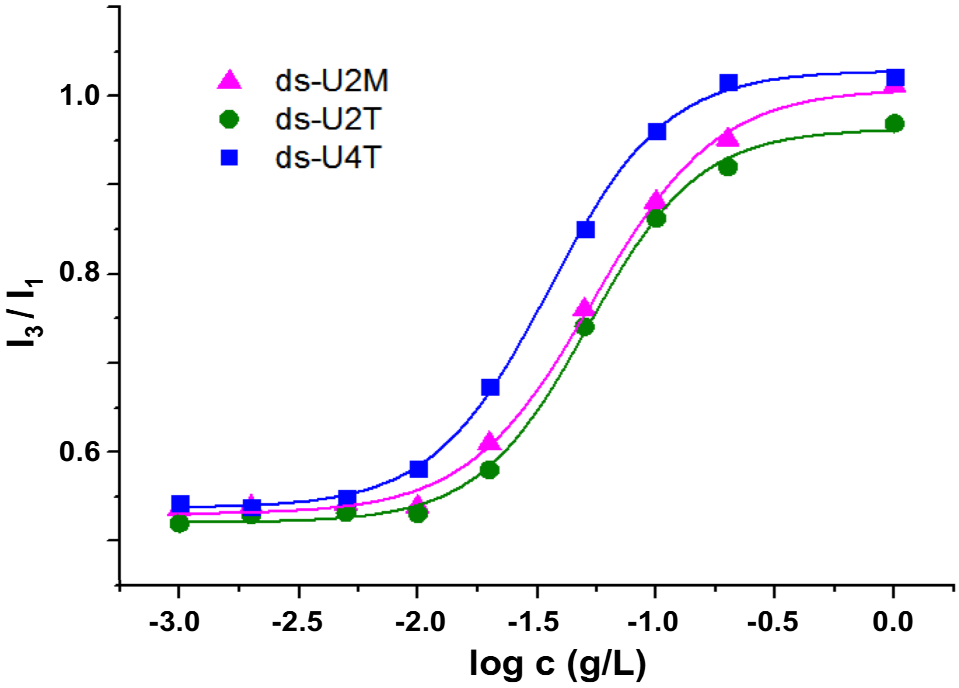

Figure 5.14 The change of the intensity ratio I_3/I_1 from pyrene fluorescence (λ_{ex} = 339 nm) as a function of the ds lipid-DNA concentration in ultra pure water (**U2M**: triangle, **U2T**: circle and **U4T**: square).

Table 5.3 Molar CMC of ss- and ds lipid-DNA micelles.

Lipid-DNA	**CMC (10^{-6} M)**	
	ss	ds
U2M	2.01	2.01
U2T	2.04	2.09
U4T	1.27	1.29

5.10 References

[1] V. Kotzabasakis, E. Georgopoulou, M. Pitsikalis, N. Hadjichristidis, G. Papadogianakis, *J. Mol. Catal. A: Chem.* **2005**, *231*, 93.

[2] J. A. Wolff, J. E. Hagstrom, S. D. Monahan, V.Budker, D. B. Rozema, P. M. Slattum, in *United States Patents, Vol. US 6.740.643 B2*, **2004**.

[3] P. S. Kuhn, Y. Levin, M. C. Barbosa, *Physica A* **1999**, *274* 8.

[4] R. Savic, L. B. Luo, A. Eisenberg, D. Maysinger, *Science* **2003**, *300*, 615.

[5] Y. Kakizawa, K. Kataoka, *Adv. Drug Deliv. Rev.* **2002**, *54*, 203.

[6] K. Kataoka, A. Harada, Y. Nagasaki, *Adv. Drug Deliv. Rev.* **2001**, *47*, 113.

[7] F. E. Alemdaroglu, K. Ding, R. Berger, A. Herrmann, *Angew. Chem., Int. Ed.* **2006**, *45*, 4206.

[8] K. Ding, F. E. Alemdaroglu, M. Börsch, R. Berger, A. Herrmann, *Angew. Chem., Int. Ed.* **2007**, *46*, 1172.

[9] Z. Li, Y. Zhang, P. Fullhart, C. A. Mirkin, *Nano Lett.* **2004**, *4*, 1055.

[10] T. Gore, Y. Dori, Y. Talmon, M. Tirrell, H. Bianco-Peled, *Langmuir* **2001**, *17*, 5352.

[11] Y. C. Yu, P. Berndt, M. Tirrell, G. B. Fields, *J. Am. Chem. Soc.* **1996**, *118*, 12515.

[12] M. G. J. ten Cate, H. G. Börner, *Macromol. Chem. Phys.* **2007**, *208*, 1437.

[13] J. H. Jeong, T. G. Park, *Bioconjugate Chem.* **2001**, *12*, 917.

[14] J. I. Sheu, E. Y. Sheu, *AAPS Pharmscitech* **2006**, *7*.

[15] F. E. Alemdaroglu, N. C. Alemdaroglu, P. Langguth, A. Herrmann, *Adv. Mater.* **2008**, *20*, 899.

[16] F. E. Alemdaroglu, N. C. Alemdaroglu, P. Langguth, A. Herrmann, *Macromol. Rapid Commun.* **2008**, *29*, 326.

[17] M. Kwak, A. J. Musser, J. Lee, A. Herrmann, *Chem. Commun.* **2010**, (Online early access) DOI:10.1039/c0cc00855a.

[18] H. Rosemeyer, *Chem. Biodivers.* **2005**, *2*, 977.

[19] U. Rädler, C. Heiz, P. L. Luisi, R. Tampe, *Langmuir* **1998**, *14*, 6620.

[20] D. Berti, P. Barbaro, I. Bucci, P. Baglioni, *J. Phys. Chem. B* **1999**, *103*, 4916.

[21] G. Zandomeneghi, P. L. Luisi, L. Mannina, A. Segre, *Helv. Chim. Acta.* **2001**, *84*, 3710.

[22] P. Baglioni, D. Berti, *Curr. Opin. Colloid Interface Sci.* **2003**, *8*, 55.

[23] L. Ötvös, J. Sági, G. Sági, A. Szemző, *Nucleos. Nucleot.* **1999**, *18*, 1929.

[24] F. Seela, M. Zulauf, *Helv. Chim. Acta.* **1999**, *82*, 1878.

[25] I. Pfeiffer, F. Höök, *J. Am. Chem. Soc.* **2004**, *126*, 10224.

[26] Y. H. M. Chan, B. van Lengerich, S. G. Boxer, *Proc. Natl. Acad. Sci. USA* **2009**, *106*, 979.

[27] H. P. Liu, Z. Zhu, H. Z. Kang, Y. R. Wu, K. Sefan, W. H. Tan, *Chem. Eur. J.* **2010**, *16*, 3791.

[28] U. Jakobsen, A. C. Simonsen, S. Vogel, *J. Am. Chem. Soc.* **2008**, *130*, 10462.

[29] M. Kwak, I. J. Minten, D. M. Anaya, A. J. Musser, M. Brasch, R. J. M. Nolte, K. Müllen, J. J. L. M. Cornelissen, A. Herrmann, *J. Am. Chem. Soc.* **2010**, *132*, 7834.

[30] S. L. Beaucage, M. H. Caruthers, *Tetrahedron Lett.* **1981**, *22*, 1859.

[31] W. Bannwarth, *Chimia* **1987**, *41*, 302.

[32] http://www.biomers.net/en/index/Technical_Information/Synthesis.html.

[33] S. L. Beaucage, D. E. Bergstrom, G. D. Glick, R. A. Jonesly, *Current Protocols in Nucleic Acid Chemistry*, Wiley, **2000**.

[34] X. M. Liang, G. Z. Mao, K. Y. S. Ng, *Colloids Surf., B* **2004**, *34*, 41.

[35] C. M. Hoo, N. Starostin, P. West, M. L. Mecartney, *J. Nanopart. Res.* **2008**, *10*, 89.

[36] C. Tanford, *Proc. Natl. Acad. Sci. USA* **1974**, *71*, 1811.

[37] J. C. Leroux, A. S. Benahmed, in *United States Patents, Vol. US 6.338.859*, **2002**.

[38] C. Tanford, *J. Phys. Chem.* **1974**, *78*, 2469.

[39] P. Sehgal, O. Kosaka, H. Doe, D. E. Otzen, *J. Dispersion Sci. Technol.* **2009**, *30*, 1050.

[40] L. Chun-Liang, L. Sheng-Jie, T. Hsieh-Chih, C. Wei-Hsiang, T. Cheng-Hung, C. H. D. Cheng, H. Ging-Ho, *Biomaterials* **2009**, *30*, 3961.

[41] M. Wilhelm, C. L. Zhao, Y. C. Wang, R. L. Xu, M. A. Winnik, J. L. Mura, G. Riess, M. D. Croucher, *Macromolecules* **1991**, *24*, 1033.

[42] G. Kwon, M. Naito, M. Yokoyama, T. Okano, Y. Sakurai, K. Kataoka, *Langmuir* **1993**, *9*, 945.

[43] K. Kalyanasundaram, J. K. Thomas, *J. Phys. Chem.* **1977**, *81*, 2176.

[44] Y. Y. Li, X. Z. Zhang, J. L. Zhu, H. Cheng, S. X. Cheng, R. X. Zhuo, *Nanotechnology* **2007**, *18*.

[45] T. Inoue, G. H. Chen, K. Nakamae, A. S. Hoffman, *J. Controlled Release* **1998**, *51*, 221.

[46] X. Jin, S. Yue, K. S. Wells, V. L. Singer, *Biophys. J.* **1994**, *66*, A159.

[47] T. Maruyama, T. Takata, H. Ichinose, L. C. Park, N. Kamaiya, M. Goto, *Biotechnol. Lett* **2003**, *25*, 1637.

[48] R. S. Tuma, M. P. Beaudet, X. K. Jin, L. J. Jones, C. Y. Cheung, S. Yue, V. L. Singer, *Anal. Biochem.* **1999**, *268*, 278.

[49] J. Skeidsvoll, P. M. Ueland, *Anal. Biochem.* **1995**, *231*, 359.

[50] A. E. Kiltie, A. J. Ryan, *Nucleic Acids Res.* **1997**, *25*, 2945.

[51] U. D. Rossi, J. Moll, J. Kriwanek, S. Daehne, *J. Fluoresc.* **1994**, *4*, 53.

[52] D. A. Barawkar, K. G. Rajeev, V. A. Kumar, K. N. Ganesh, *Nucleic Acids Res.* **1996**, *24*, 1229.

[53] K. G. Rajeev, V. R. Jadhav, K. N. Ganesh, *Nucleic Acids Res.* **1997**, *25*, 4187.

[54] Y. Lu, B. Weers, N. C. Stellwagen, *Biopolymers* **2001**, *61*, 261.

[55] S. W. Kowalczyk, M. W. Tuijtel, S. P. Donkers, C. Dekker, *Nano Lett.* **2010**, *10*, 1414.

[56] B. Tinland, A. Pluen, J. Sturm, G. Weill, *Macromolecules* **1997**, *30*, 5763.

[57] L. C. Palmer, S. I. Stupp, *Acc. Chem. Res.* **2008**, *41*, 1674.

[58] T. Dwars, E. Paetzold, G. Oehme, *Angew. Chem., Int. Ed.* **2005**, *44*, 7174.

Chapter 6

VIRUS PARTICLES TEMPLATED BY DNA MICELLES: A GENERAL METHOD FOR LOADING VIRUS NANOCARRIERS*†

6.1 Introduction

Virus capsids (VCs) or virus-like particles are a relatively new class of natural biomaterials with great potential for materials science and nanotechnology. They form precisely defined stable cage structures, permit coat protein (CP) manipulation through mutagenesis or chemical modification and can be easily produced. Such exceptional characteristics make them particularly strong candidates for applications in biomedicine.[1-3] The natural container-like properties of viruses, as well as their ability to specifically target individual cells, have been attractive for gene delivery and are now being harnessed for therapeutic delivery. While some VCs have been investigated and chemically modified to probe targeting behavior,[4] scant work has been dedicated to loading these nanocontainers.[5] An excellent model system in this regard is the Cowpea Chlorotic Mottle Virus (CCMV). As with other VCs, CCMV evolved to encapsulate

* This chapter was accepted for publication *J. Am. Chem. Soc.* **2010**, *132*, 7834.

† This study was performed in collaboration with Minseok Kwak (University of Groningen) and members of Prof. Dr. Cornelissen's group (University of Twente, Enschede and Raboud University, Nijmegen) in the Netherlands.

and transport RNA. In its natural state it consists of 180 identical CPs, which self-assemble around the central RNA into 28 nm icosahedral particles. These can be described according to the Caspar and Klug T (triangulation) number as T = 3 particles.[6] It has been shown that such capsids can also be readily made to self-assemble around large polyanions, resulting in smaller T = 1 icosahedral particles of 18 nm.[7, 8] CCMV is unique in that capsid assembly can be induced in acidic conditions even in the absence of nucleic acids, allowing the possibility of loading more diverse cargos such as enzymes.[9] Nonetheless, the porous walls of the shell severely complicate the loading and retention of small molecules. A still more severe limit is imposed by solvent incompatibilities, which prevent the loading of hydrophobic drugs except through covalent modification of the protein or complexation with polyanions.[10] The success of engineered virus nanoparticles as delivery vehicles will hinge in large part on the resolution of these issues and the development of efficient loading strategies for small molecules and macromolecular entities.

6.2 Loading of CCMV capsids using DNA amphiphiles

The aim of this study was to find a strategy for the facile self-assembly and loading of CCMV capsids using DNA amphiphiles. This investigation was performed in collaboration with *Minseok Kwak* from the University of Groningen. As seen in the previous chapters, the DNA-amphiphiles aggregate into micelles with a hydrophobic core and an anionic DNA corona. The negatively charged particles induce capsid formation, allowing the entrapment of a large number of small oligonucleotides (ODNs) as a constituent part of the micellar template. Furthermore, preloading of the micelles with hydrophobic or hydrophilic entities enables encapsulation of various small molecules inside VCs (Figure 6.1). In the following sections a detailed outline will be given how DNA micelles template the formation of virus-like particles and how this process allows to incorporate small molecules into the nano-containers.

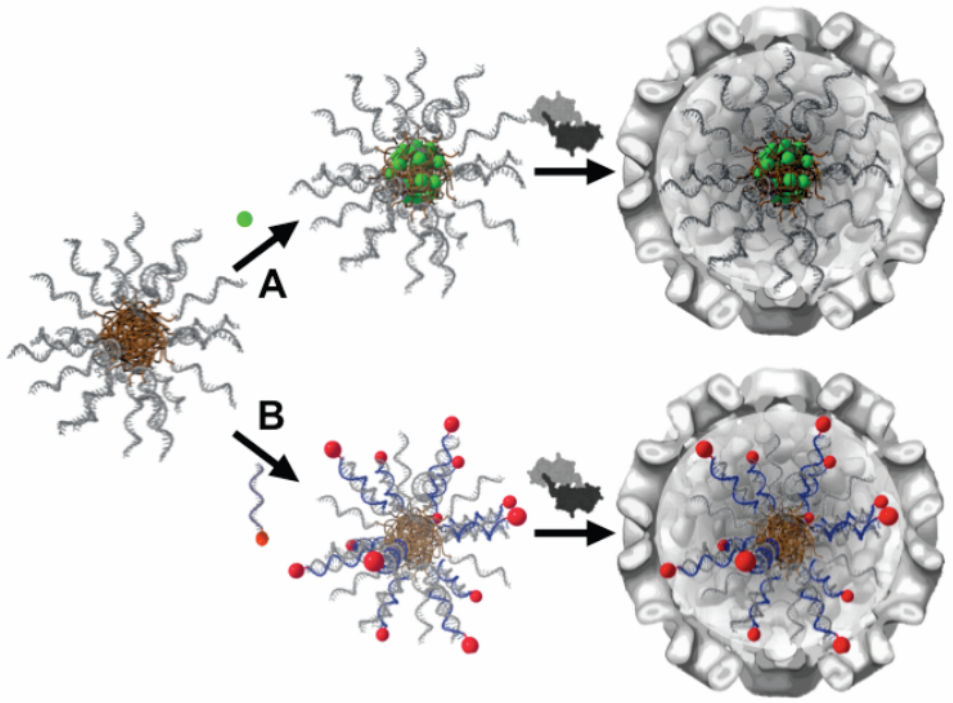

Figure 6.1 Schematic representation of VC formation induced by DNA micelle templates **(A)** Loading hydrophobic molecules (green) into the core. **(B)** Equipping moieties (red) attached to complementary DNA by hybridization. Coat proteins encapsulate the micelle by simple mixing at neutral pH.

Two classes of DNA amphiphiles known to self-assemble into larger aggregates should be distinguished, though representatives of both were investigated in this chapter. The first class consists of low molecular weight hydrophobic molecules that are attached to ODNs.[11] Here a lipid-DNA (11mer, sequence: 5'-UUTGGCGTCTT-3', **UU11**) containing two 5-dodec-1-ynyluracil nucleobases (Figure 6.2A) at the 5'- end was synthesized. The modified uridine phosphoroamidite was synthesized according the method described in *Chapter 5* (experimental section 5.9.1).

The other class of DNA amphiphiles is a linear DNA block copolymer (DBC) in which a nucleic acid sequence is covalently connected to a hydrophobic organic polymer via complementary end groups.[12] Here two DBCs containing polypropylene oxide blocks of the same molecular weight (M_W = 6800 g/mol) but different lengths of ODNs were employed, namely an 11mer (5'-AAGATATCTTT-

3', **P11**) and a 22mer (5'-CCTCGTCTGCTAATCCTGTTA-3', **P22**) sequence (Figure 6.2B).

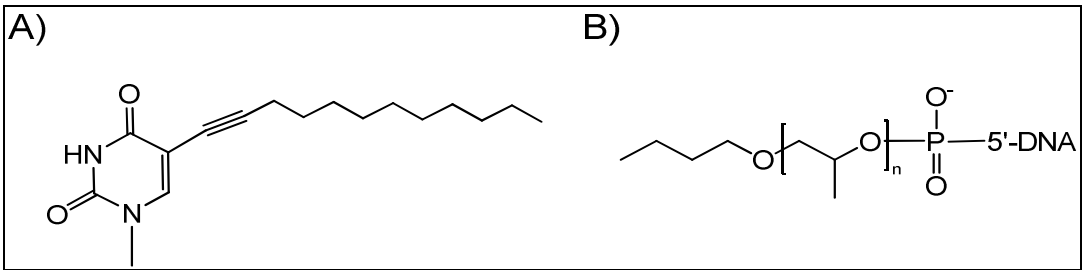

Figure 6.2 Key chemical structures of DNA amphiphiles. **(A)** The chemical structure of modified uracil nucleobases of UU11 and **(B)** The chemical structure of hydrophobic PPO block attached to 11 and 22mer ODNs.

All three amphiphiles formed micellar structures at room temperature. These structures were characterized by anion exchange chromatography and PAGE (Figures 6.3 and 6.4). The chromatograms document well the purity of the samples. All materials elute as single peaks. In case of the DNA block copolymers the pristine DNA controls undoubtedly prove the attachment of the hydrophobic polymer segment. The PAGE analysis shows individual bands for **UU11** and **P22**. All the DNA samples modified with hydrophobic groups (dodec-1-ynyl chains or PPO) exhibit a lower electrophoretic mobility than the pristine DNA controls.

The particle sizes of the micelles were determined using dynamic light scattering (DLS). From the DLS measurements (Figure 6.5) that were carried out at room temperature and at a scattering angle of 90 ℃ the size of **UU11** micelles was determined to be 10 nm analyzing the diameter distributions by number. The DLS data were confirmed by AFM measurements (Figure 6.6). These revealed the formation of spherical aggregates that appeared as bright dots in the images. Again, as in the previous chapter no exact size data can be extracted from these measurements. AFM measurements were carried out by *Andrew Musser* (University of Groningen).

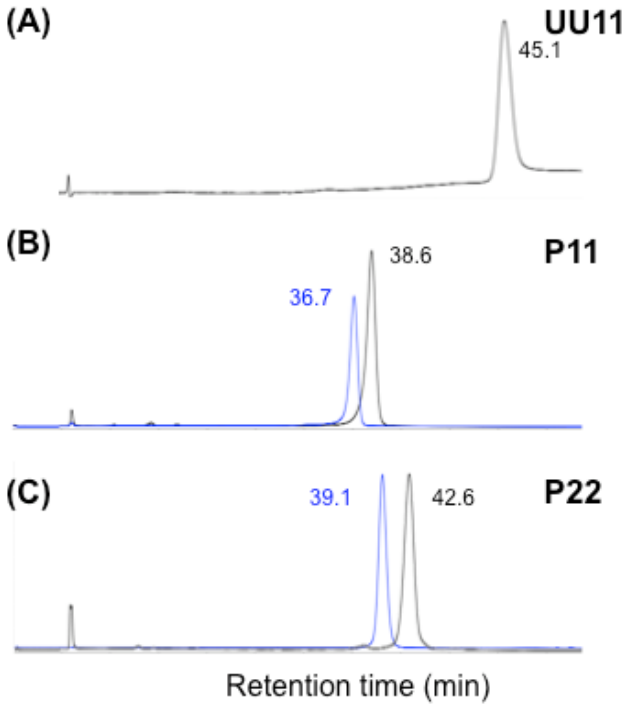

Figure 6.3 AIEX chromatograms of DNA materials (**UU11**, **P11**, and **P22**). Curves are traces of OD_{260}. Numbers represent corresponding retention time of the peak. Blue curves are pristine DNA controls with same lengths as modified DNA or block copolymer.

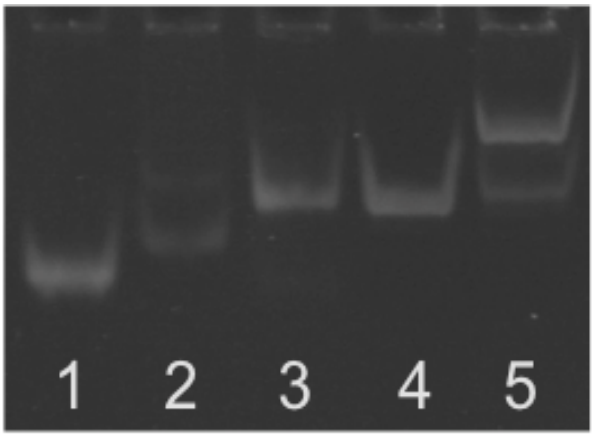

Figure 6.4 Denatured 15% TBU (Tris, boric acid, and urea) PAGE. *Lane 1*: 11mer ODN, *Lane 2*: **UU11**, *Lane 3*: **P11**, *Lane 4:* 22mer ODN, and *Lane 5*: **P22**. The gel was stained with EtBr.

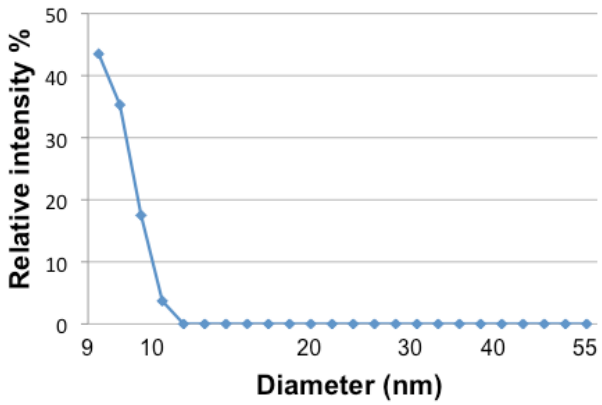

Figure 6.5 DLS size distribution of **UU11** (2 mg/ml) analyzed by number.

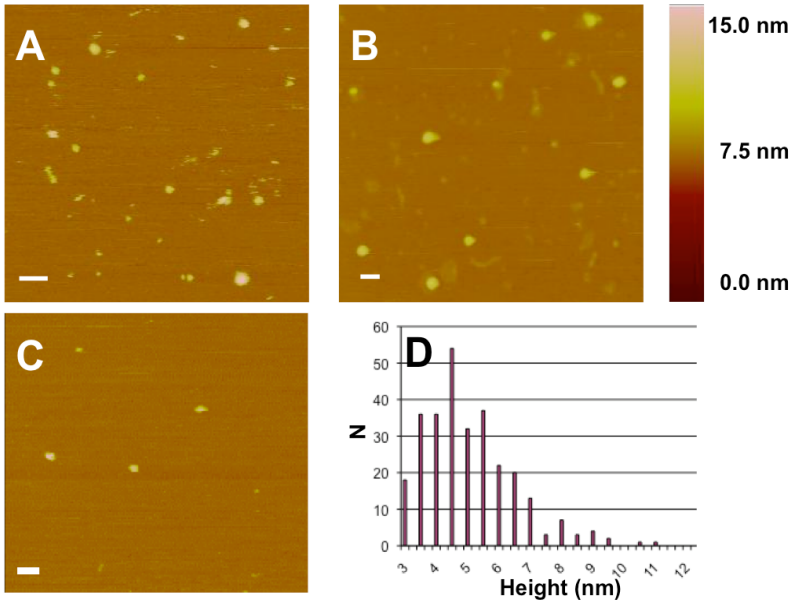

Figure 6.6 AFM images of the DNA micelles. (A) **UU11** in fluid cell. (B) **UU11** in air. (C) **P11** in fluid cell. (D) Size histogram of **P11**. The scale bars are 50 nm.

To assess the ability of these DNA particles to template VC formation both systems were combined through a simple mixing procedure. In most experiments DNA amphiphiles were mixed with CP in a 1 : 2.3 molar ratio at pH 7.5 and incubated for 30 min at 4 ºC. It should be stressed that in these conditions VC formation can only be attributed to the organizing role of the micelles. The resulting materials were isolated by fast protein liquid chromatography (FPLC).

Transmission electron microscopy (TEM) analysis revealed successful envelopment of all DNA micelle species by the CCMV capsid protein (Figures 6.7 and 6.8). Particles eluted at 1.3−1.4 ml exhibited a size of 19.9 ± 3.1 nm (Figure 6.7A). This size suggests that the objects have T = 2 symmetry. Also, a small proportion of the particles formed a T = 1 architecture. The TEM micrographs and their statistical analysis (Figure 6.9) provided additional evidence of loaded VCs, as empty cores appear dark under the negative staining conditions.[9] Moreover, a fraction that eluted at 1.6 ml could be clearly identified as **UU11** micelles from the size distribution, 8.1 ± 1.6 nm (Figure 6.7B), in agreement with DLS measurements.

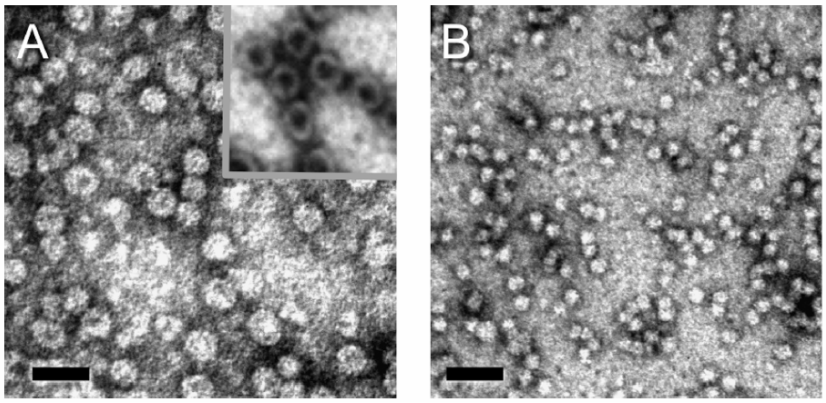

Figure 6.7 TEM micrographs, stained by uranyl acetate, of UU11-VC FPLC fractions eluted at (A) 1.4 ml, VCs, and (B) 1.6 ml, UU11 micelles. Scale bars are 40 nm.

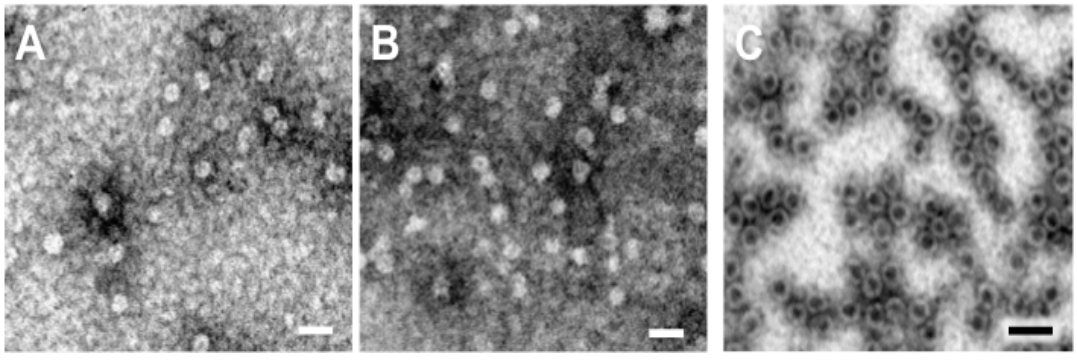

Figure 6.8 TEM images of (A) **P11**-VC, (B) **P22**-VC and (C) Wild type capsid assembled at pH 5. The scale bars: 40 nm.

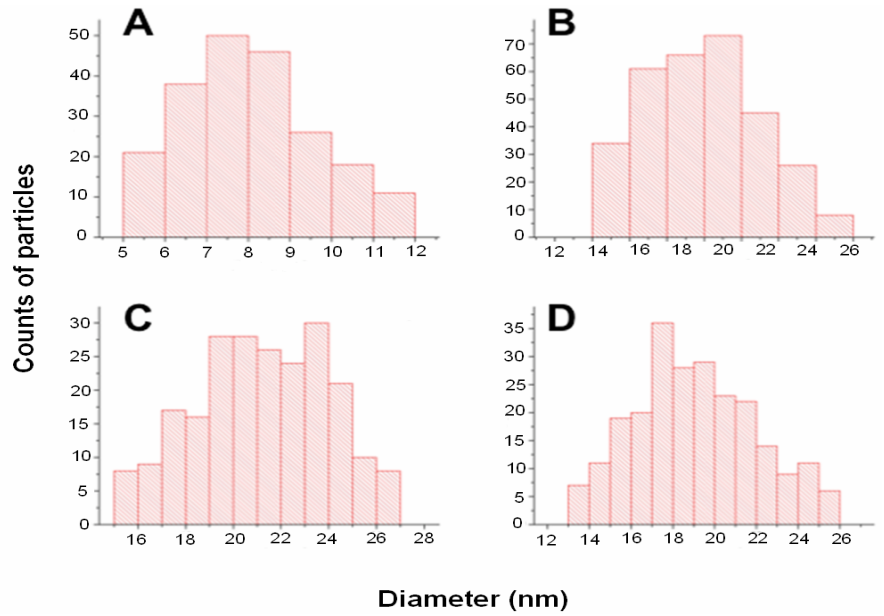

Figure 6.9 Size distribution histograms of **UU11** micelle (A, 8.1 ± 1.6 nm) and **UU11** VC (B, 19.9 ± 3.1 nm), **P11** VC (C, 21.2 ± 2.8 nm), and **P22** (D, 19.2 ± 3.5 nm) VC from TEM images.

6.2.1 Loading of small hydrophobic molecules into DNA aggregates

After confirming the loading of VCs with DNA amphiphile aggregates, these scaffolds were further exploited for incorporation of other moieties. Since hydrophobic drugs are known to accumulate within the hydrophobic core of DBC amphiphiles, the fluorescent aromatic compound pyrene was introduced into **UU11** aggregates as a model for hydrophobic small molecules (see experimental section 6.4.6 for the preparation of the loaded micelles). Templated assembly of VCs was subsequently carried out as described above. During the FPLC elution of pyrene-loaded **UU11**-VC (Figure 6.10A), a fraction around 1.3 ml was identified as containing capsid since it showed clear pyrene absorption. The fluorescence spectrum of the chosen fraction showed sharp and well-resolved pyrene emission bands demonstrating the presence of the fluorophore within **UU11** aggregates and thus also inside VCs (Figure 6.10B).

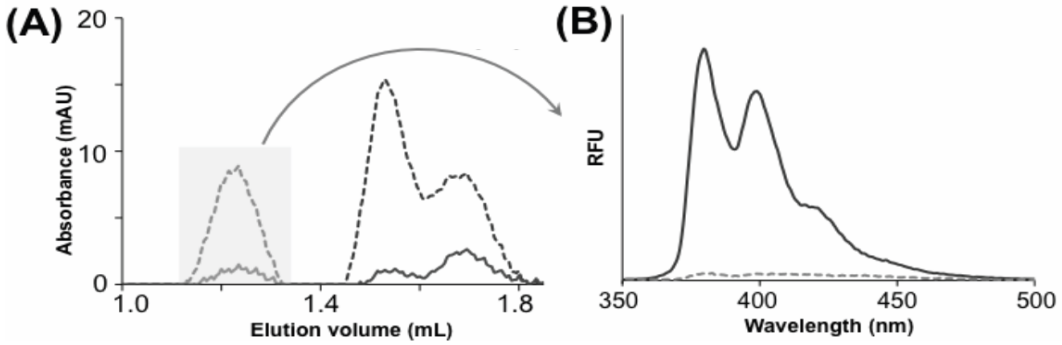

Figure 6.10 FPLC elugram and fluorescence spectra of pyrene-loaded UU11-VC. **(A)** Absorbance of protein (280 nm, dashed) and pyrene (342 nm, solid). **(B)** Fluorescence spectra (λ_{ex} = 342 nm) of the highlighted fraction (solid) and pristine CP (dashed).

Similar measurements were carried out using micelles loaded with a membrane staining dye 1,1'-dioctadecyl-3,3,3'3'-tetramethylindocarbocyanine perchlorate (DiI) that is also hydrophobic. Size exclusion chromatography of the crude VC mixture is shown in Figure 6.11. Again a significant absorption signal of the dye that is localized in the hydrophobic interior of the micelles is detected in the FPLC elugram where fully formed capsids elute.

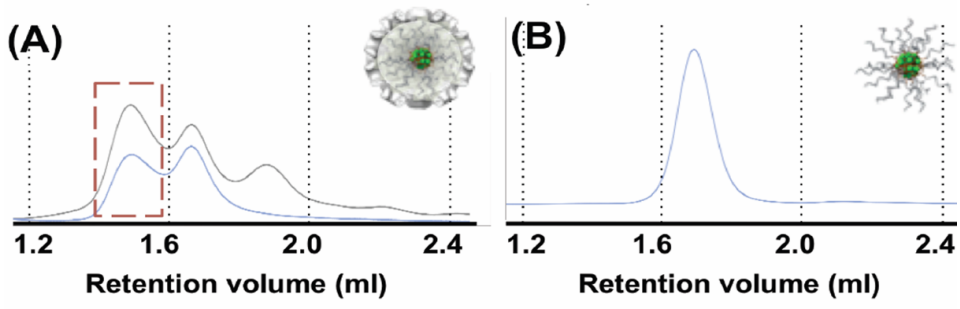

Figure 6.11 FPLC graphs **(A)** DiI loaded UU11-VC crude mixture. **(B)** DiI loaded UU11 only. The ordinate corresponds to the normalized absorbance. The highlighted section represents the elution volume where capsids are present. The black curve corresponds to the protein absorbance at 280 nm and the blue curve is the corresponding DiI signal monitored at 549 nm, loaded in the DNA micelle. The integrated area of figure (A) shows that around 56% of the micelles are encapsulated into VCs.

The FPLC fractions of DiI loaded UU11-VP and non-encapsulated UU11 were further analyzed on a SDS-PAGE and detected by silver-staining (Figure 6.12). This gel showed the presence of capsid protein in the DiI loaded UU11-VP fraction at 1.4 mL (lane 3). Capsid protein dimers are known to elute at 1.8 mL (lane 5). Heavy degradation was observed, while the wild-type capsid protein (wt CP) stored at pH 5.0 and the DiI loaded UU11-VP only show light degradation. Wt CP is known to degrade fairly quickly at pH 7.5, but not at pH 5.0. A possible reason is that at pH 5.0 the N-terminus that is prone to degradation points inwards into the capsid and is thus protected from the environment. Since the capsid proteins envelope the micelle, the same mechanism probably protects the capsid proteins of the DiI loaded UU11-VP from degradation. Like the DiI loaded UU11-VP, the dimers that did not form around the micelle were left at room temperature for at least an hour, which accelerated their degradation. The capsid proteins in the second lane were also at pH 7.5 for several hours, but they were stored at 4 ºC. The TEM images corroborated the analysis above for pristine micelle-loaded VCs.

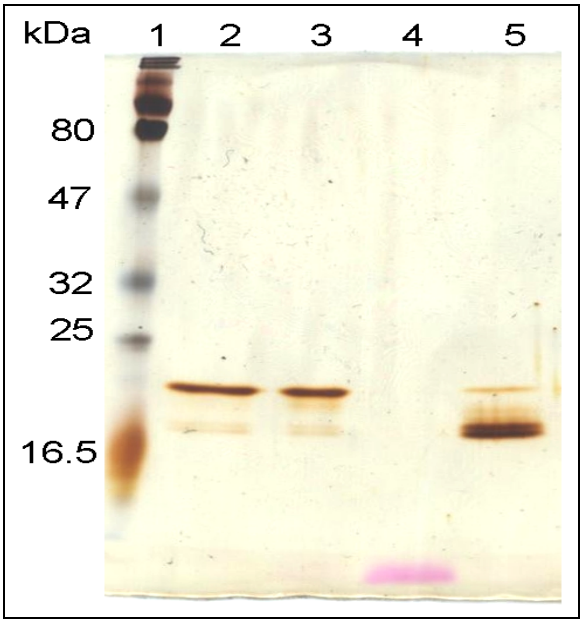

Figure 6.12 Silvers protein stained gel of UU11 fractions in SEC. *Lane 1*: Marker; *Lane 2*: Wt CP (wild type capsid protein); *Lane 3*: UU11, SEC fraction at 1.4 mL; *Lane 4*: UU11, SEC fraction 1.6 mL and *Lane 5*: Wt CP: UU11, FPLC fraction 1.8 mL.

6.2.2 Loading of VC with hydrophilic molecules by hybridization of DNA micelles

Finally the challenge of loading small hydrophilic moieties in VC was addressed. DNA micelles can be equipped by hybridization with almost any molecule conjugated to the complementary DNA sequences. Many functionalities are commercially available or can be easily synthesized. As a proof of concept, **UU11** micelles were labeled with 6-carboxylic-X-rhodamine (ROX), a hydrophilic fluorescent dye, by hybridization with a complementary ROX-DNA conjugate. VCs were formed employing the same general encapsulation procedure. Again FPLC analysis confirmed successful envelopment of functionalized micelles (Figure 6.13).

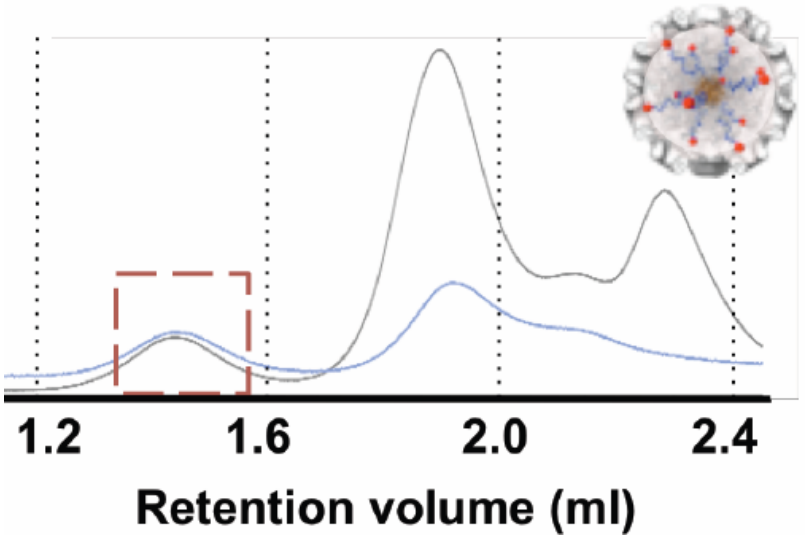

Figure 6.13 FPLC graph of ROX-DNA hybridized **UU11**-VC (crude VC mixture). Ordinate represents normalized absorbance. The highlighted section is the fraction collected for further measurement. The black curve corresponds to the protein absorbance at 280 nm and the blue curve is the corresponding absorbance monitored at 575 nm where ROX shows an absorption maximum when, loaded in DNA micelles.

With the help of the ROX label and dylight functionalized CP, the aggregation number Z of micelles as well as the DNA content within the VC could be calculated (see experimental section 6.4.5). It turned out that Z amounted to be 25, which is in very good agreement with a geometrical calculation. Assuming a T= 2 configuration, the ODN content to capsid was 6% by weight.

6.3 Conclusions

The loading and self-assembly of CCMV capsids using different DNA amphiphiles was investigated. The first class of amphiphiles consisted of low molecular weight hydrophobic molecules (5-dodec-1-ynyluracil) attached to the ODNs. The second class of DNA amphiphiles employed were the linear DNA block copolymers (DCB) in which oligonucleotides of two different lengths were covalently attached to the hydrophobic polymer poly(propylene oxide) monobutyl ether (PPO). The amphiphilic nature of this kind of DNA structures enabled the formation of micelle aggregates, containing a hydrophobic core and a hydrophilic DNA corona. Such micellar structures allowed the functionalization through DNA hybridization as well as internalization of hydrophobic payloads. In this regard, the lipid-DNA micelles were loaded with hydrophobic (pyrene and DiI) or hydrophilic (ROX) entities, allowing the subsequent encapsulation of small molecules inside the virus capsids, through a simple mixing procedure. TEM images, fast protein liquid chromatography (FLPC) and gel electrophoresis analysis were used to confirm the successful envelopment of the functionalized micelles by the CCMV virus capsid.

The combination of short ODNs with virus-like particles was already reported. VC networks were formed by hybridization employing virus like particles that were chemically modified with nucleic acid sequences at the outside.[13] Incorporation of pristine ODNs into VC was demonstrated for polyomavirus. However, the loading procedure was cumbersome because packaging required osmotic shock

treatment as well as acidic pH.[14] The approach presented herein is much simpler since a high number of ODNs were preassembled by attached hydrophobic units, i.e. alkyl chains or polymers, acting as an efficient soft matter template and avoiding the need of altering environmental conditions.

Moreover, copackaging of various small molecules is achieved either by hybridizing them onto the micelles or incorporating them into the core. This novel loading strategy marks a significant step towards virus-based targeted therapeutics. This is especially true for hydrophobic drugs, which are difficult to couple chemically to water-soluble capsid proteins due to solvent incompatibilities.

With the general loading strategy presented in this investigation, it is possible to fully explore diverse applications, especially the potential of these nanocarriers as a high-impact drug delivery system.

6.4 Experimental Section

6.4.1 Laboratory Equipment

- **AFM and TEM grids**

AFM images were collected with a MultiMode-II AFM connected with Nanoscope IIIa controller (Veeco) in a fluid-cell filled with Milli-Q water, filtered with 0.2 µm syringe filter prior to use. V-1 grade mica plates were purchased from Electron Microscopy Sciences (USA). Silicon nitride cantilevers with silicon tips and spring constant of 0.32 N/m (SNL-10) were acquired from Veeco (France).

TEM grids (Formvar-Carbon) were exposed to an electron discharge treatment using a Cressington Carbon coater and power unit. The sample was applied to the grids by adding a 5 µL drop of sample solution (~ 0.2 mg/mL) to the grid and carefully removing it after 1 minute immersion using a filter paper. The grid was allowed to dry for at least 15 minutes before applying 5 µL of a 2% (w/v) uranyl acetate aqueous solution, which was removed after 15 s. The grid was again allowed to dry for at least 15 min. Samples were studied on a JEOL JEM-1010 TEM (Jeol, Japan).

- **FPLC (Fast protein liquid chromatography)**

FPLC measurements were performed using a Superose 6 PC 3.2/30 analytical column from GE lifesciences, on an Amersham Ettan LC system, fitted with a fractionating device. Buffers for FPLC were filtered with a Millipore 0.2 µm filter before use.

- **DLS (Dynamic light scattering)**

DLS measurements were performed on a Zetasizer Nano S and Zetasizer 5000 (Malvern Instruments Ltd, England). Crude VC mixtures were first purified by FPLC and subsequently measured.

- **UV-VIS spectrophotometer**

Protein concentrations were determined with a Cary 50 Conc (Varian, Middelburg) UV-VIS spectrophotometer using a quartz cuvette with a path length of 3 mm.

- **Size Exclusion Chromatography of Crude VC Mixtures**

Size exclusion chromatography was performed on FPLC system equipped with a Superose 6 column using the pH 7.5 capsid buffer. Multiple wavelengths were monitored during elutions.

A capsid buffer pH 7.5 (0.5 M NaCl, 0.05 M Tris-HCl, 0.01 M $MgCl_2$ and 0.001 M EDTA) was used in all VC formation experiments.

6.4.2. Preparation of CCMV coat protein

The purification of the CCMV virus and the removal of its RNA were carried out according to literature procedures.[15] CP was labeled with Dylight-647 (ε = 250,000 $cm^{-1}M^{-1}$) following the procedure outlined in the product manual, in 16.7% coupling efficiency.

6.4.3 Synthesis of UU11 and P11/P22

P11 and **P22** DNA diblock copolymers with poly(propylene oxide) monobutyl ether (PPO, M_W = 6800 g/mol) were prepared according to a previous report.[12] The modified uridine phosphoroamidite was synthesized according the method described in *Chapter 5.*

- **DNA Synthesis**

The 11mer DNA synthesis (UU11) was carried out like described in *Chapter 5.* The **UU11** synthesis was performed in 50 µmol scale with an overall yield of 16%, as calculated from the AIEX chromatogram. Solvents and reagents for DNA synthesis were purchased from Novabiochem (Merck, UK) and SAFC (Sigma-aldrich, Netherlands).

6.4.4 Characterization of UU11 and P11/P22

- **Anion exchange chromatography**

Analytical AIEX chromatography was performed using a HiTrap Q HP 1 ml column (GE Healthcare) through a linear gradient using elution buffers (A: 25 mM Tris and B: 25 mM Tris and 1.0 M NaCl).

6.4.5 Calculation of aggregation number Z of UU11 micelles

- **Calculation of Z using molar extinction coefficient (ε) of two dyes attached to DNA and CP**

According to Beer-Lambert rule, A = *εcl*, molarity ratio of **UU11** : CP = 1 : 4.82 was derived from the absorbance of ROX on complementary DNA (4.30 mAU, 50% hybridized) and Dylight647 on CP (85.5 mAU, 17% labeled) at 1.28 ml elution of Figure 6.13. This value means there are ca. 25 **UU11** molecules present in the cavity when 120 CPs form a single T = 2 VC which was found in the TEM images. From Z = 25, the weight percent of nucleotides in the cavity *vs.* VC was derived to 6%.

- **Geometrical estimation of Z**

For the purposes of estimating the aggregation number of **UU11** micelles, the single-stranded DNA strands of the corona were each assumed to be confined to spheres of radius 2 nm.[16, 17] For a micelle radius of 10.5 nm as observed in DLS, this yields an approximate aggregation number (Z = 32), which corresponds to 6 nucleobases per CP dimer in the case of T = 2 VC.

6.4.6 Preparation of Loaded Micelles

DiI or pyrene was dissolved in acetone. A drop of dye solution (400 µg/ml) was added to a tube and subsequently evaporated. **UU11** micellar solution was added to the tube and mixed overnight at room temperature.
50 mol percent of ROX-ODN was hybridized with **UU11** in $MgAc_2$ (10 mM) buffer at pH 7.5. 6-Carboxylic-X-rhodamine (ROX, ε = 80,000 $cm^{-1}M^{-1}$) at 5'-hydroxy end modified oligonucleotide (5'-AAGACGCCAAA-3') was purchased from biomers, Germany.

6.4.7 Preparation of VCs

- **General procedure of VC formation:**

In the molar ratio of a DNA amphiphile : CP = 1 : 2.3, both solutions (Table 6.1) were mixed in the pH 7.5 capsid buffer (0.5 M NaCl, 0.05 M Tris-HCl, 0.01 M $MgCl_2$ and 0.001 M EDTA), and the mixtures were allowed to form capsids for 1 h at 4 ºC.

Table 6.1 Mixed volume and concentration of VCs.

Amphiphile used for VC formation (molar ratio of the amphiphile : CP)	DNA amphiphile	Coat protein
Pyrene/**UU11** (1 : 2.3)	19.6 µL (208.58 µM)	100 µL (94.2 µM)
DiI/**UU11** (1 :3.6)	8.1 µL (400 µM)	100 µL (148 µM)
ROX-ODN/**UU11** (1 : 2.3)	19.6 µL (208.58 µM)	90 µL (83.1 µM)

6.5 References

[1] T. Douglas, *Science* **2003**, *299*, 1192.

[2] I. W. Hamley, *Angew. Chem., Int. Ed.* **2003**, *42*, 1692.

[3] P. Singh, M. J. Gonzalez, M. Manchester, *Drug Dev. Res.* **2006**, *67*, 23.

[4] E. Strable, M. G. Finn, *Viruses and Nanotechnology* **2009**, *327*, 1.

[5] Y. F. Hu, R. Zandi, A. Anavitarte, C. M. Knobler, W. M. Gelbart, *Biophys. J.* **2008**, *94*, 1428.

[6] L. O. Liepold, J. Revis, M. Allen, L. Oltrogge, M. Young, T. Douglas, *Phys. Biol.* **2005**, *2*, S166.

[7] F. D. Sikkema, M. Comellas-Aragones, R. G. Fokkink, B. J. M. Verduin, J. J. L. M. Cornelissen, R. J. M. Nolte, *Org. Biomol. Chem.* **2007**, *5*, 54.

[8] I. J. Minten, Y. J. Ma, M. A. Hempenius, G. J. Vancso, R. J. M. Nolte, J. J. L. M. Cornelissen, *Org. Biomol. Chem.* **2009**, *7*, 4685.

[9] M. Comellas-Aragones, H. Engelkamp, V. I. Claessen, N. A. J. M. Sommerdijk, A. E. Rowan, P. C. M. Christianen, J. C. Maan, B. J. M. Verduin, J. J. L. M. Cornelissen, R. J. M. Nolte, *Nature Nanotech.* **2007**, *2*, 635.

[10] Y. Ren, S. M. Wong, L. Y. Lim, *Bioconjugate Chem.* **2007**, *18*, 836.

[11] C. Xu, P. Taylor, M. Ersoz, P. D. I. Fletcher, V. N. Paunov, *J. Mater. Chem.* **2003**, *13*, 3044.

[12] F. E. Alemdaroglu, K. Ding, R. Berger, A. Herrmann, *Angew. Chem., Int. Ed.* **2006**, *45*, 4206.

[13] E. Strable, J. E. Johnson, M. G. Finn, *Nano Lett.* **2004**, *4*, 1385.

[14] S. Henke, A. Rohmann, W. M. Bertling, T. Dingermann, A. Zimmer, *Pharm. Res.* **2000**, *17*, 1062.

[15] J. J. Bujarski, *Bromovirus isolation and RNA extraction*, Humana Press, **1998**.

[16] C. Gosse, A. Boutorine, I. Aujard, M. Chami, A. Kononov, E. Cogne-Laage, J. F. Allemand, J. Li, L. Jullien, *J. Phys. Chem. B* **2004**, *108*, 6485.

[17] F. Delie, R. Gurny, A. Zimmer, *Biol. Chem.* **2001**, *382*, 487.

Chapter 7

SINGLE-MOLECULE REDOX BLINKING OF PERYLENE DIIMIDE DERIVATIVES IN WATER*

7.1 Introduction

The use of fluorescence microscopy in life-sciences and nano-technology has tremendously increased during the past decades and a great variety of experimental techniques is currently available for the characterization of biological or artificial (nano)structures. Simultaneously, methods have been established that utilize fluorescence emission for an observation of single particles or (bio-)molecules, i.e. single-molecule fluorescence spectroscopy (SMFS).[1-3] These techniques recently merged in far-field superresolution approaches that are based on the subsequent localization of single molecules.[4-6] While technical developments are proceeding rapidly, most of the current approaches place additional demands on fluorophore design. Accordingly, modern fluorescence microscopy techniques require bright (high extinction coefficient at the excitation wavelength, high fluorescence quantum yield),

* Parts of this chapter have been published in *J.Am.Chem.Soc*. *2010*, 132(7):2404-2409.

photostable, water-soluble, chemically compatible, non-perturbing, or even (photo-) switchable labels.[7]

Hitherto, predominantly fluorophores from the classes of (carbo)rhodamines, oxazines, cyanines, and 2-dicyanomethylene-3-cyano-2,5-dihydrofuran (DCDHF) fluorophores[8] have been employed in biomolecular single-molecule studies or superresolution microscopy. On the other hand, rylene derivatives have been used for single-molecule spectroscopy from the early days.[9] Dyes such as perylene, perylene (di-)imide and others have proven to be bright and photostable fluorophores, well suited for a multitude of important single-molecule studies.[10-12] In recent years, also water soluble and monofunctional derivatives of perylene and terrylene dyes have been developed[13-17] and were applied in first biomolecular single-molecule studies.[18, 19] Their photophysical characterization, however, lags behind and single-molecule studies have generally been carried out in polymer matrices instead of physiologically relevant buffer conditions.[20, 21] In other cases fluorescence correlation spectroscopy was used that has a limited time range due to diffusion and does not reveal heterogeneity.[14]

7.2 Time-resolved single-molecule spectroscopy of perylene diimide (PDI) in aqueous buffer

In this investigation, spectrally- and time-resolved single-molecule spectroscopy[22] were used to study the photophysics of water-soluble perylene diimide (PDI) dye. The investigated PDI derivative is water-soluble due to the presence of four aryl substituents bearing a sulfonic acid group. The fluorophore was coupled to a 38-mer single stranded DNA (Figure 7.1).

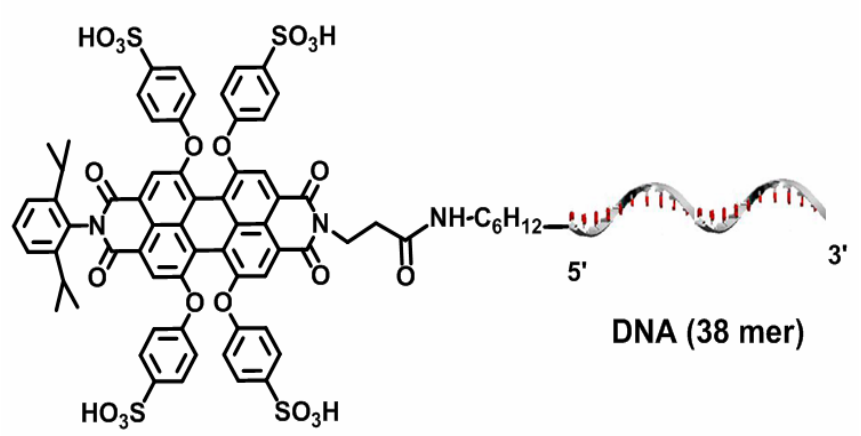

Figure 7.1 Chemical structure of the DNA-PDI conjugate used in this chapter.

The attachment of the chromophore to the nucleic acid moiety was achieved by coupling the activated ester of the dye to the 5'-amino-modified DNA still bound to the solid support employing the so called "syringe synthesis technique".[29] This technique allows the conjugation of synthetic oligonucleotides with fluorophores, taking advantage of the solid-phase chemistry that obviates the more laborious methods of solution phase labeling and purification. In principle, the synthesis take place in a column prepacked with a solid support onto an amino-modified oligonucleotide is attached. The solution with the carboxyl-functionalized flurophore is placed in syringes and the synthesis is carried out by successively drawing and expelling them from the syringe.[30] Then the column is washed, eliminating that way the excess of non reacted dye. Finally the product is cleaved from the solid support by a treatment with ammonia. This method can be applied to any molecule with a reactive carboxylic acid group. Some flurophores, such as rhodamine, are not sufficiently stable to allow preparation of phosphoramidites and to be use on the automated DNA synthesizer,[29] but employing the syringe technique permits the attachment of such kind of dyes to oligonucleotides in a simple way and in a good yield. The ssDNA-PDI conjugate was purified by PAGE and characterized by MALDI-TOF MS. The MALDI-TOF spectrum shows well resolved signals, suggesting that the method is appropriate for the

characterization of such kind of modified oligonucleotides (see experimental section 7.6.1).

Single fluorophores can be investigated in solution and on the surface using a confocal microscope. However, solution based measurements are limited to short acquisition times, due to the short transient time through the diffraction limited observation volume of diffusing molecules.[23] Therefore single molecules have to be immobilized on the surface in a way, that the influence of the surface upon the photophysics is minimal. The conjugation of the PDI to the DNA facilitated the immobilization on glass surfaces via hybridization to the complementary strand that was bound to cover slides via BSA/biotin/streptavidin (Figure 7.2).[31] This immobilization strategy ensures that the fluorophores largely show the same properties as in free solution while they can be studied for extended time compared to measurements of freely diffusing molecules.[32]

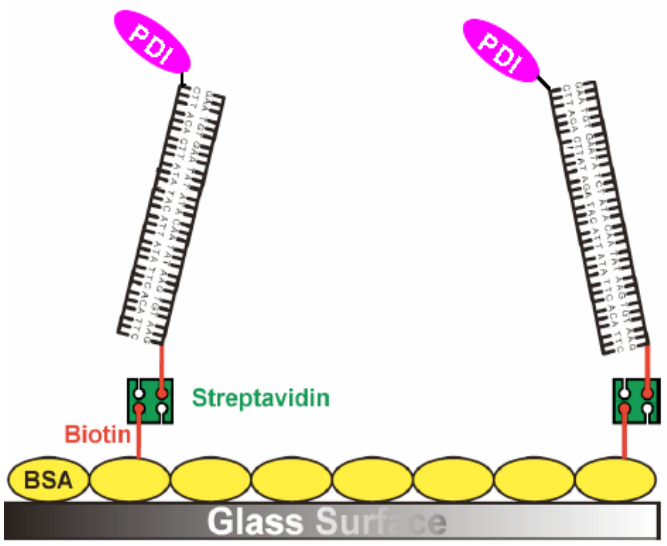

Figure 7.2 Schematic representation of the DNA-PDI conjugate immobilization by using biotin/streptavidin coupling.

For the first time, single PDI dyes were studied in aqueous buffer by attaching the fluorophore to DNA. In water, the PDI exhibits a structured absorption with

distinct bands in the visible and near ultraviolet (Figure 7.3). The lowest energy transition shows a maximum at 560 nm while another transition is observed at ~425 nm. Fluorescence emission is red-shifted by 60 nm with a maximum at 620 nm.

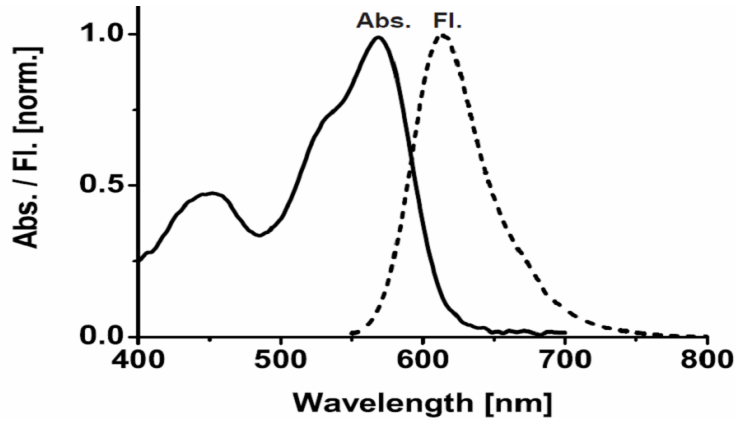

Figure 7.3 Normalized absorption and emission spectra of the investigated PDI-dye attached to ssDNA in aqueous solution (Excitation wavelength was 560 nm).

Largely homogeneous photophysical properties of the PDIs with similar photostability as for other single-molecule compatible fluorophores excitable at around 550 nm were found. Further, it was demonstrated that the fluorescence properties of PDIs are largely dominated by their redox potentials in different buffer-environments, i.e. aqueous and organic media. Due to the low energy of the reduced state blinking is easily induced and controllable in accordance with a concept involving a reducing and oxidizing system (ROXS).[23-26] Since the redox-potentials of perylene derivatives can be controlled through suitable substituents at the chromophore,[27] these results pave the way for tailored photophysical properties that show the required emission for the specific application: Stable fluorescence or blinking could be adjusted at will for applications such as superresolution Blink-Microscopy.[24, 28]

In the following sections a general description will be given how water soluble perylene derivates attached to DNA can be employed as fluorescent labels for

biological objects with resolutions lower than the diffraction limit. Details of the photophysical measurements are described in the corresponding article.[33]
The photophysical measurements described in this chapter were performed by *Dr. Thorben Cordes* in the group of *Prof. Dr. Tinnefeld* (Ludwig Maximilian University *of* Munich*).*

For the single-molecule measurements of the DNA-PDI conjugate a confocal microscope was used. Laser excitation at 560 nm resulted in images such as depicted in Figure 7.4A that shows the sum fluorescence of the two detectors. The diffraction limited spots represented single immobilized PDI molecules in aqueous phosphate buffered saline (PBS) at pH 7.4. Figure 7.4B shows the fluorescence of the conjugate as function of time, recorded under the same experimental conditions with no observable amplitude in the autocorrelation function.

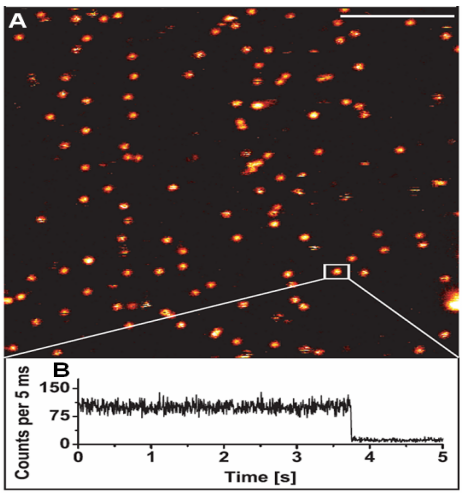

Figure 7.4 (A) Confocal fluorescence image of immobilized dsDNA-PDI conjugate in aqueous PBS-buffer at pH = 7.4. The shown area (20×20 µm) was scanned by excitation at 560 nm with an average intensity of 3.8 kW/cm^2. Scale bar in the upper right is 5 µm. **(B)** Fluorescence transient recorded under the same experimental conditions. The image and the transient show the sum of both spectrally separated detection channels.

The fluorescence transient of the DNA-PDI conjugate in PBS buffer (Figure 7.4B) showed stable emission with rare and brief OFF-states. To quantify the

photostability of the PDI under physiologically relevant condition, total internal reflection (TIR) microscopy was used.[23] TIR microscopy is a technique used to observe the interface between two media with different diffractive indexes such glass and water.[34] With this technique was possible to determine the average photon number (44000 ± 15000 photons per molecule) by considering the mean intensity of a single fluorophore per frame. Accordingly, PDI in aqueous buffer features good photostability and performance for single-molecule experiments better than other commonly used fluorophores in this spectral range.[23] For example ATTO565, a fluorophore with comparable spectral properties, emits < 10000 photons under similar conditions.

7.3 Study of the photophysics of the water soluble DNA-PDI conjugate using a reducing and oxidizing system (ROXS)

The photophysics of the DNA-PDI conjugate using a reducing and oxidizing system (ROXS) was also studied.[24] Previous investigations have shown that redox blinking could be induced or suppressed by controlling the lifetime of radical ions formed via the triplet state with the aid of reducing and oxidizing agents (see Figure 7.5).[23, 35]

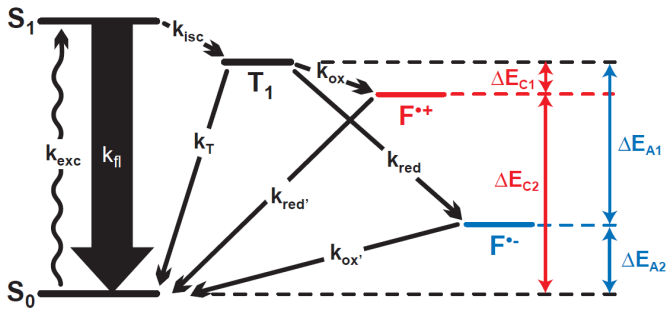

Figure 7.5. Jablonski-diagram according to the ROXS concept: electronic ground- and first excited single-state S_0/S_1, triplet state T_1, reduced ($F^{\bullet-}$) and oxidized ($F^{\bullet+}$) state, excitation rate k_{exc}, emission rate k_{fl}, rate of intersystem crossing k_{isc}, rate of triplet depletion k_T, and k_{ox} and k_{red}, oxidation and reduction rates.

It has been shown that some fluorophores with high electron affinity could even be switched between a bright and a dark state by inducing a photoinduced electron transfer with a reductant, yielding a metastable radical anion that could be recovered by the complementary redox reaction using an oxidant.[24] Interestingly, PDI exhibits redox potentials that are in between those of recently studied dyes with E_{ox} ~ 1.4 V and E_{red} ~ -0.6 V versus SCE (Figure 7.5).[36] So the electron affinity of PDI is higher than that of e.g., ATTO647N, whose fluorescence is stabilized by common redox agents and lower than that of ATTO655.[23, 24]

In the following the influence of ROXS on the DNA-PDI conjugate was investigated. The fluorescence transients were used to compare the behavior of the dye under different concentrations of the reductant (ascorbic acid, AA) and oxidant (N,N-methylviologen, MV) (Figure 7.6).

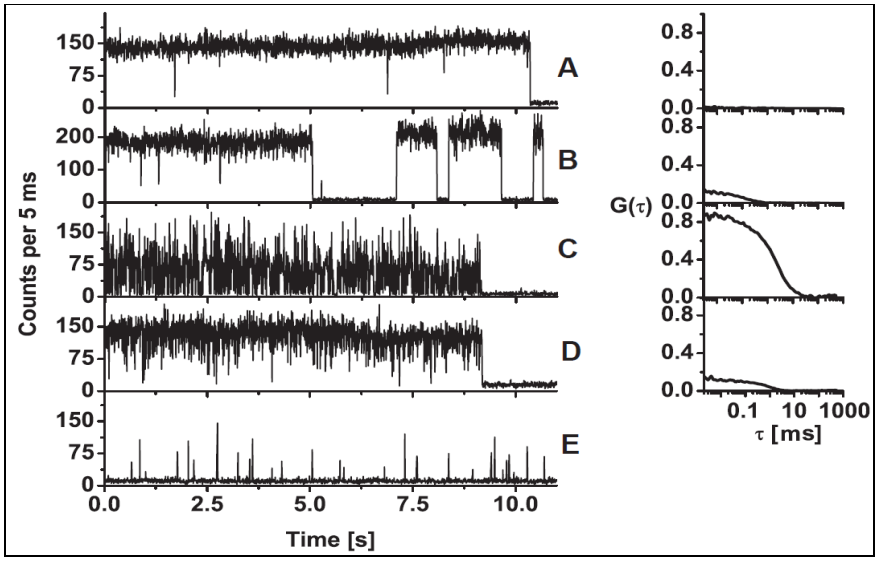

Figure 7.6 (A-D) Fluorescence transients and corresponding autocorrelation functions from single immobilized dsDNA-PDI under different aqueous buffer conditions. Excitation was at 560 nm. **(A)** PBS buffer. (B,C) ROXS-buffer conditions: **(B)** Deaerated PBS-buffer with 100 µM AA and 1 mM MV. **(C)** Deaerated PBS-buffer with 50 µM AA and 10 µM MV. (D,E) Reducing buffer conditions: **(D)** PBS-buffer with 100 µM AA. **(E)** Deaerated PBS-buffer with 100 µM AA. Here OFF-times of 500 ± 380 ms were observed.

Figure 7.6A shows the PDI emission in PBS, where no considerable amplitude is observed in the autocorrelation function. Adding 1 mM MV and 100 µM AA after enzymatically removing oxygen[23] also yields stable fluorescence over several seconds with some long OFF-states (Figure 7.6B). The oxygen must be removed owing to its dye dependent influence on photostability and oxidizing properties. By reducing the amount of AA and MV to 50 µM and 10 µM, respectively, blinking is more pronounced (Figure 7.6C) and the OFF-state assigned to the radical anion becomes significantly longer. This dependence on MV concentration supports previous assignment of this state to the radical anion. This assignment is also in accordance with the lifetime of PDI triplet states determined before,[37] and previous findings of two components in the blinking of dyes at low ROXS concentrations.[24] Figure 7.6D-E shows the fluorescence transients under reducing buffer conditions. The emission of PDI in PBS-buffer with 100 µM AA (Figure 7.6D) shows also a more pronounced blinking than in only PBS. On the other hand, under deaerated PBS-buffer with 100 µM AA longer off-states were observed. These results indicate that the addition or removal of reducing or oxidizing agents switches on/off the fluorescence of the PDI dye between stable fluorescent and non-fluorescent states. This ‘‘switching mode’’ could be of great utility for diverse applications, including bottom-up nanotechnological devices in computers, data storages, (bio-) sensors and displays.[25]

7.4 Photophysics of PDI under non-aqueous conditions

Considering the superior photostability presented by the PDI in hydrophobic media, the ROXS concept was also studied in organic solvent. To test whether the photophysics of PDI could be manipulated similarly in non-aqueous conditions, a PDI was immobilized via a poly(ethylene glycol) (PEG) linker (Figure 7.7) to BSA/BSA-biotin in acetonitrile. The biotin-PDI-PEG conjugate was prepared, employing a new dehydrating condensing agent called 4-(4,6-

dimethoxy-1,3,5-triazin-2-yl)-4-methylmorpholinium chloride) (DMT-MM), that enabled to carry out amidation of carboxylic acid in protic solvents such as water.[38, 39] Again the immobilization of the biotin-PDI-PEG construct on surface was achieved by directly linked in to the BSA/BSA-biotin surface that was treated with streptavidin. Interestingly, the immobilization was even stable under these conditions. In acetonitrile, the PDI molecules were significantly brighter and similar fluorescence count rates were obtained at lower excitation intensities of 0.6 kW/cm^2 (Figure 7.7A). Importantly, redox-blinking was also induced upon the addition of AA to the immobilized molecules in acetonitrile (Figure 7.7B). For 20 molecules, mean OFF-times of (8 ± 4) ms, ON-times of 13 ± 8 ms were measured.

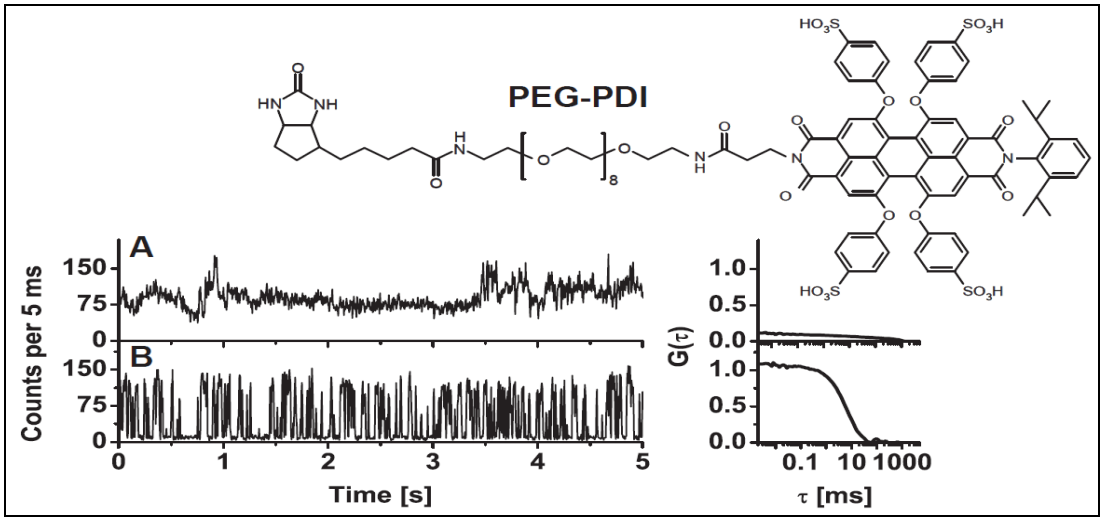

Figure 7.7 Structure of PDI attached to biotin via an oligoethylene glycol linker and fluorescent transients with corresponding autocorrelation analysis from confocal microscopy of the dye immobilized on a surface under the organic solvent acetonitrile. Excitation intensity was 0.6 kW/cm^2 at 560 nm. **(A)** Data in acetonitrile with intensity fluctuations on various timescales but no distinct blinking (see autocorrelation analysis in the right panel). **(B)** Data in acetonitrile with additional 100 µM AA. In the presented trace ON-times of 15 ms with 255 ON-counts and OFF-times of 16 ms were determined by autocorrelation analysis (see right panels). The blinking is attributed to transitions into a reduced non-fluorescent form of the PDI molecule.

7.5 Conclusions

In conclusion, the photophysics of single water soluble PDI, an important member of rapidly emerging rylene dye biolabels, were studied under aqueous conditions for the first time. The results indicate that PDIs are suited for a wide range of applications in single-molecule fluorescence spectroscopy. All results could be explained on the basis of the ROXS concept and with the knowledge of the electronic properties of the PDIs. The high electron affinity easily enabled the induction of redox blinking to metastable radical anion states while no evidence for radical cation states was found. Interestingly the PDIs were most photostable in the presence of oxygen since oxygen is an efficient quencher of the radical anion state (more efficient than MV). Taking into account that oxazine fluorophores, which also exhibit a high electron affinity, are similarly photostable in the presence of oxygen, this seems to become a common feature of “oxygen resistant” fluorophores.[24, 40]

The redox properties are one of the most important characteristics of single-molecule compatible fluorescent dyes. Since the redox potentials of PDIs can be well adapted by chemical substituents, they could be well designed for single-molecule applications requiring stable emission in ROXS by decreasing their electron affinity. This in combination with their tunable solubility properties from organic solvents to aqueous medium and their variable functionalizability strongly points towards their broad applicability in the rapidly growing field of single-molecule fluorescence spectroscopy.

Undoubtedly, further developments in the controlling of fluorescent probes to increase photostability including reducing and oxidizing reagents (ROXS concept) can have significance for diverse applications. In this regard, the study of the effects of different oxidizing and reducing agents in the emission properties of PDI or other organic dyes result of immense value. The reductant ascorbic acid (AA) and the oxidant methylviologen (MV) employed in this investigation and

in further studies[23,24] can help to avoid blinking. However, a less toxic system with better stability and high solubility in aqueous media is desirable, especially for possible biological applications. Previous studies[26] have shown alternatives to non toxic redox systems based on Trolox (TX) and Trolox-Quinone (TQ), demonstrating the potential of this system within the ROXS concept and the quantitative differences between diverse redox agents. However, the success of this strategy not only depends on the redox system but also on the fluorescent dye used.[23] In this context, a step forward and a possible improvement of flurophore emission control employing ROXS system could be the direct covalent attachment of the reductant or oxidant (depending the needs) to the organic dye allowing the control of the ratio between chromophore and reductant/oxidant, increasing this way the efficiency of the system and protecting the dye of photobleaching. The success of this approach could be demonstrated also by labeling the DNA with the fluorophore-reductant/oxidant and immobilizing the structure via streptavidin/biotin on BSA coated coverslides, ensuring that the fluorophore shows the same properties as in free solution and allowing the study of the photophysical properties for extended time at the single molecule level.[29] Such kind of dye-reductant/oxidant system could be of great significance for live-cell imaging and could be used as fluorescent marker, presenting excellent photostability.

7.6 Experimental section

7.6.1 Synthesis of perylene fluorescent probes

7.6.1.1 ssDNA-PDI conjugate

The synthesis of the DNA-PDI conjugate was carried out as described in *Chapter 3* (Experimental Section 3.8). The sequence of the 38mer oligonucleotide that was functionalized with an amino hexyl group at the 5'end was the following one: 5´-NH_2-CCTCGCTCTGCTAATCCTGTTA-3´. The material was purchased from Biomers GmbH, Germany.

The DNA-PDI conjugate was purified by polyacrylamide gel electrophoresis (PAGE) and desalted with a dialysis membrane with molecular weight cut-off (MWCO) of 1000 g/mol yielding 476 μg (0.0351 μmol) of product (73%).
The purified material was characterized by PAGE as well as by MALDI-TOF mass spectrometry (Figures 7.8 and 7.9).

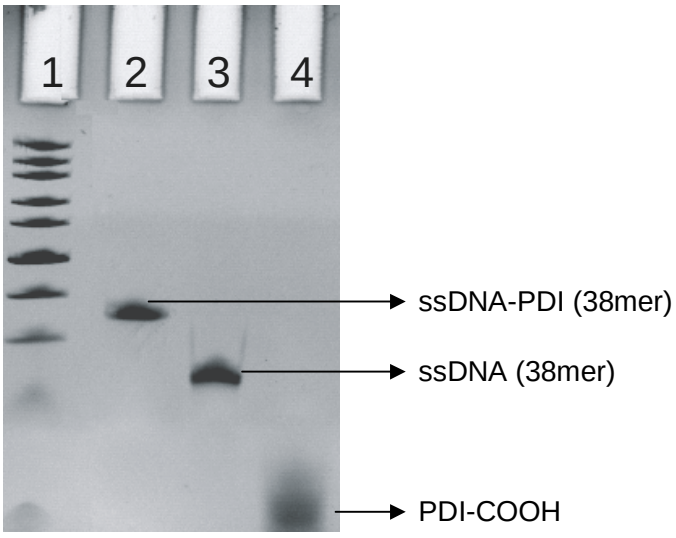

Figure 7.8. PAGE analysis of purified ssDNA-PDI conjugate. *Lane 1*: Ultra low range DNA ladder. Lane 2: ssDNA-PDI conjugate (38mer). Lane 3: ss DNA(38mer). *Lane 4*: Water soluble PDI.

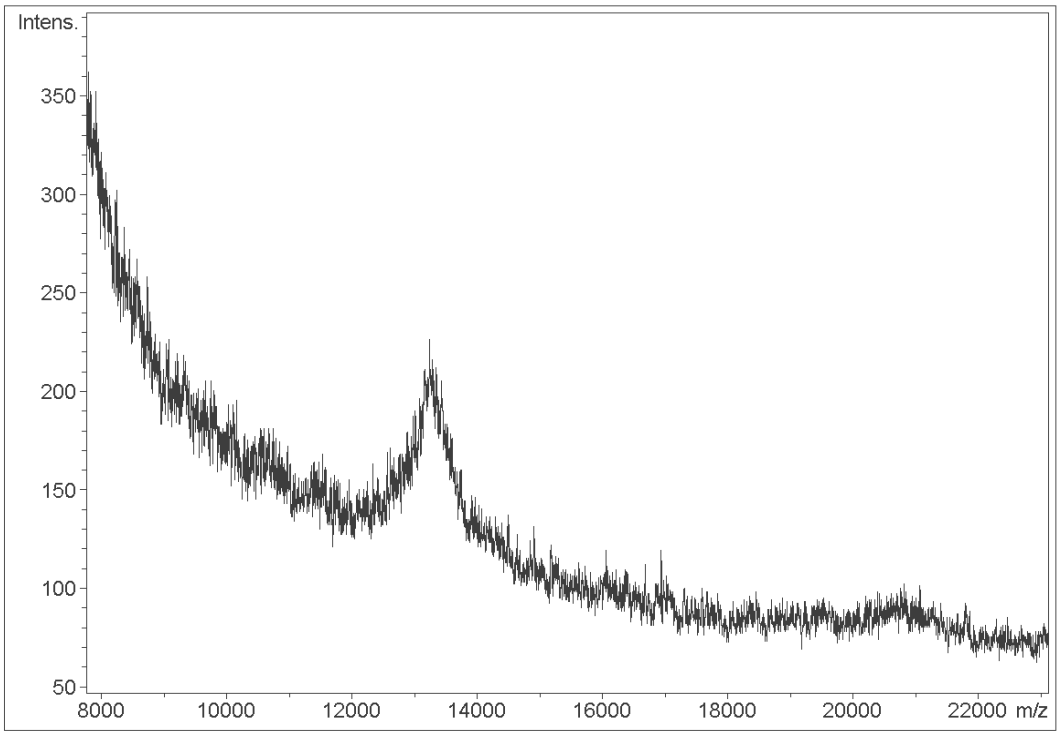

Figure 7.9 MALDI-TOF mass spectrum of ssDNA-PDI conjugate (38mer) (found: 13038 g/mol, calculated: 13034 g/mol).

7.6.1.2 Biotin-PEG-PDI conjugate

For the synthesis of this conjugate the carboxyl-functionalized PDI (0.15 mg, 112 nmol) and a biotin molecule functionalized with a polyethylene glycol (PEG) spacer terminated with an amine group (NH_2-PEG(10)-Biotin) (IRIS Biotech GmbH) (0.4 mg, 560 nmol) were mixed to form an amide bound in the presence of the activating reagent 4-(4,6-dimethoxy-1,3,5-triazin-2-yl)-4-methylmorpholiniumchloride) (DMT-MM) (616 nmol) in water (Figure 7.10).[38, 39] The mixture was allowed to react for 12 hours at room temperature.

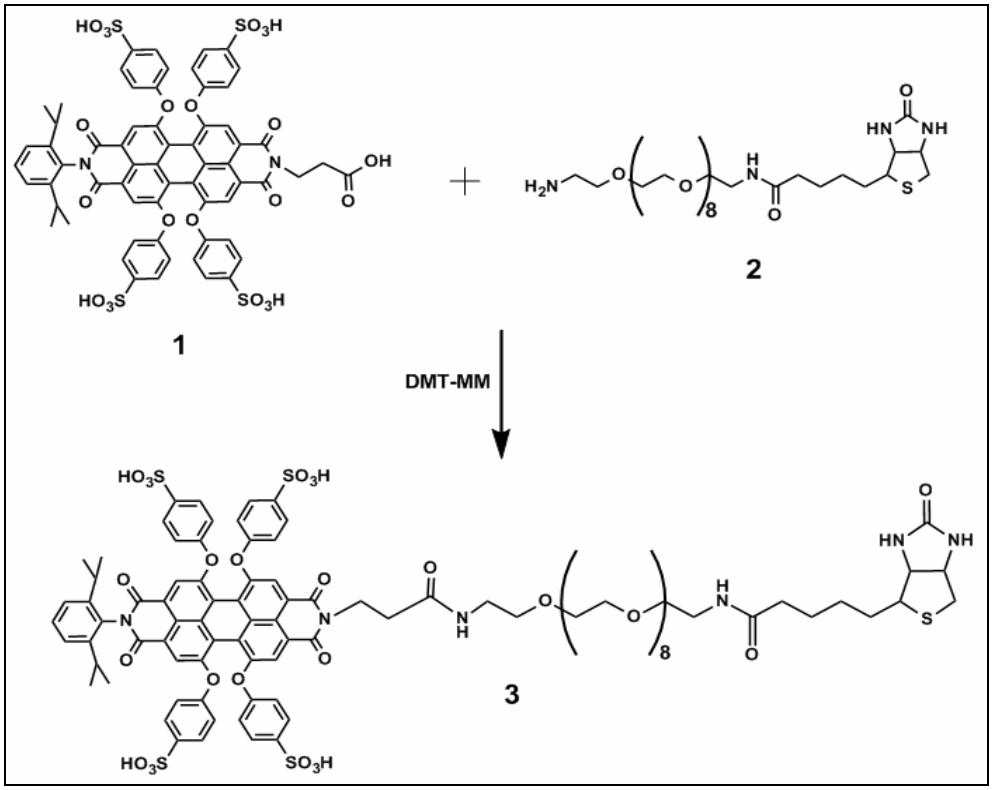

Figure 7.10 Synthesis of the PDI-PEG-Biotin conjugate.

The biotin-PEG-PDI conjugate was purified using 20% denaturing PAGE (Figure 7.11). After excision of the bands, elution and dialysis of the product for 24 h against water the biotin-modified dye was obtained in a yield of 69%.

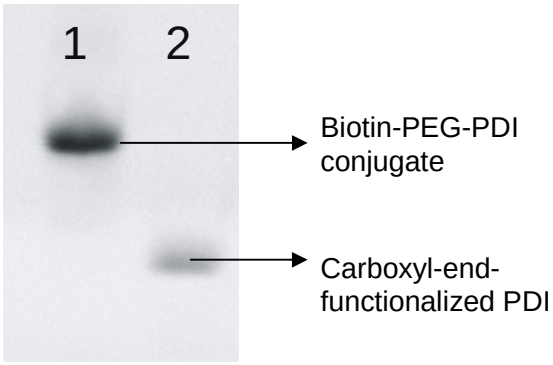

Figure 7.11 20% PAGE without ethidium bromide staining of purified PDI-PEG-Biotin conjugate. Lane 1: PDI-PEG-Biotin conjugate, Lane 2: PDI-COOH.

7.6.2 Immobilization of the PDI-constructs on glass surface

For the investigation of single immobilized dye-molecules LabTek 8-well chambered cover slides (Nunc) with a volume of ~750 µl were treated with 0.1 % HF for 30 seconds and were washed three times with PBS-buffer. Each of the chambers was subsequently incubated with a solution of 5 mg/ml BSA and 1 mg/ml BSA/biotin (as received from Sigma Aldrich) in PBS for at least ten hours at 4 °C. The surface was then washed three times with PBS and was incubated with a ~0.1 mg/ml solution of streptavidin for five minutes and washed again for three times with PBS. For immobilization of single fluorophores a biotinylated 38mer oligonucleotide (5'-biotin-ATG CTA AGC TAA GGA ATG TGA ATA TAA TGT ATC GAT AT-3', as received from IBA, Göttingen) was first incubated on the surface for one minute. Then the DNA-PDI conjugate described above (5'-PDI-ATA TCG ATA CAT TAT ATT CAC ATT CCT TAG CTT AGC AT-3') was hybridized resulting in a dsDNA-fluorophore construct that was permanently linked to the surface. Experiments in acetonitrile were conducted with a different PDI fluorophore-construct (see structure in Figure 7.7) that could be directly linked in to a BSA/BSA-biotin surface that was treated with streptavidin. After the same procedure as described, i.e., linking single-molecules to the coverslide surface, the PBS-buffer was removed from the LabTek chamber. Then the imaging compartment was carefully rinsed with water, rinsed at least five times with acetonitrile and finally refilled with pure acetonitrile.

Single-molecule experiments of the different samples were carried out at room temperature (22 ± 1 °C) under standard phosphate buffered saline (PBS) with a pH of 7.4. If indicated oxygen was removed from the buffer system utilizing an oxygen-scavenging system (PBS, pH = 7.4, containing 10% (wt/vol) glucose and 12.5% (vol/vol) glycerine, 50 µg/ml glucose-oxidase, 100-200 µg/ml catalase, and 0.1 mM Tris(2-carboxyethyl)phosphine hydrochloride (TCEP)). Additionally, different concentrations of oxidant (N,N-methylviologen, MV) or reductant (ascorbic acid, AA) were added to the solvent buffer as indicated in the text.

7.6.3 Ensemble spectroscopy

Absorption spectra of the samples were recorded on a standard absorption spectrometer equipped with a diode-array. Ensemble emission spectra of the samples were recorded on a spectrophotometer (Fluoromax-3, Jobin Yvon Inc, Edison, NJ, USA). The spectra were measured in standard quartz cuvettes with an optical path-length of 0.3 cm using PBS-buffer or water (pH = 7.4). In order to avoid re-absorption effects the concentrations were kept below 1 mM for all experiments.

7.6.4 Single molecule fluorescence spectroscopy and confocal microscopy

A custom built confocal microscope as described in the literature[22] was used to study fluorescence on the level of single molecules. Filtering the laser beam of a pulsed supercontinuum-source (SuperK Extreme, Koheras, Denmark) with an acousto-optical tunable filter (AOTFnc-VIS, AA optoelectronic) allowed selecting 560 nm as excitation light (spectral width of 2 nm). The beam was subsequently coupled into a single-mode fiber, entered an inverse microscope and was coupled into an oil immersion objective (60×, NA 1.35, UPLSAPO 60XO, Olympus) by a dichroic beam splitter (Laser-Beamsplitter z561RDC, AHF Analysentechnik, Germany) for recording fluorescent transients. The average light intensities for these measurements were 3.8 kW/cm^2 at 560 nm unless stated otherwise. The resulting fluorescence was collected by the objective, focused onto a 50-µm pinhole and spectrally separated (640DCXR, AHF Analysentechnik, Germany). The two fluorescence signals were additionally filtered (first channel: Razoredge Long Pass 568; second channel: Brightline HC655/40, both AHF Analysentechnik, Germany) and detected by avalanche

photodiodes (SPCM-AQR-14, PerkinElmer). The detector signal was registered and evaluated using custom made LabVIEW software.

For characterization of the fluorescent properties of PDI the OFF- and ON-times were determined according to established procedures:[24] i) An autocorrelation of the fluorescence transients was generated. ii) The autocorrelation-curve was fitted using an exponential function. iii) The off- times τ_{off} and on-counts N_{on} were derived from the amplitudes and the characteristic time-constant of the autocorrelation after background correction.

7.7 References

[1] S. Weiss, *Science* **1999**, *283*, 1676.

[2] P. Tinnefeld, M. Sauer, *Angew. Chem., Int. Ed.* **2005**, *44*, 2642.

[3] C. Joo, H. Balci, Y. Ishitsuka, C. Buranachai, T. Ha, *Annu. Rev. Biochem.* **2008**, *77*, 51.

[4] E. Betzig, G. H. Patterson, R. Sougrat, O. W. Lindwasser, S. Olenych, J. S. Bonifacino, M. W. Davidson, J. Lippincott-Schwartz, H. F. Hess, *Science* **2006**, *313*, 1642.

[5] M. J. Rust, M. Bates, X. Zhuang, *Nat. Methods* **2006**, *3*, 793.

[6] S. T. Hess, T. P. Girirajan, M. D. Mason, *Biophys. J.* **2006**, *91*, 4258.

[7] S. W. Hell, *Nat. Methods* **2009**, *6*, 24.

[8] S. J. Lord, N. R. Conley, H. L. Lee, S. Y. Nishimura, A. K. Pomerantz, K. A. Willets, Z. Lu, H. Wang, N. Liu, R. Samuel, R. Weber, A. Semyonov, M. He, R. J. Twieg, W. E. Moerner, *ChemPhysChem* **2009**, *10*, 55.

[9] T. Basche, W. E. Moerner, *Nature* **1992**, *355*, 335.

[10] J. Hofkens, M. Maus, T. Gensch, T. Vosch, M. Cotlet, F. Kohn, A. Herrmann, K. Müllen, F. De Schryver, *J. Am. Chem. Soc.* **2000**, *122*, 9278.

[11] J. Hofkens, M. Cotlet, T. Vosch, P. Tinnefeld, K. D. Weston, C. Ego, A. Grimsdale, K. Müllen, D. Beljonne, J. L. Bredas, S. Jordens, G. Schweitzer, M. Sauer, F. De Schryver, *Proc. Natl. Acad. Sci. USA* **2003**, *100*, 13146.

[12] A. Zurner, J. Kirstein, M. Doblinger, C. Brauchle, T. Bein, *Nature* **2007**, *450*, 705.

[13] S. Icli, S. Demiç, B. Dindar, A. O. Doroshenko, C. Timur, *J. Photochem. Photobiol., A.* **2000**, *136*, 15.

[14] K. Peneva, G. Mihov, A. Herrmann, N. Zarrabi, M. Borsch, T. M. Duncan, K. Müllen, *J. Am. Chem. Soc.* **2008**, *130*, 5398.

[15] T. Weil, M. A. Abdalla, C. Jatzke, J. Hengstler, K. Müllen, *Biomacromolecules* **2005**, *6*, 68.

[16] J. Qu, C. Kohl, M. Pottek, K. Müllen, *Angew. Chem., Int. Ed.* **2004**, *43*, 1528.

[17] K. Peneva, G. Mihov, F. Nolde, S. Rocha, J. Hotta, K. Braeckmans, J. Hofkens, H. Uji-I, A. Herrmann, K. Müllen, *Angew. Chem., Int. Ed.* **2008**, *47*, 3372.

[18] S. Rocha, J. A. Hutchison, K. Peneva, A. Herrmann, K. Müllen, M. Skjot, C. I. Jorgensen, A. Svendsen, F. C. De Schryver, J. Hofkens, H. Uji-i, *ChemPhysChem* **2009**, *10*, 151.

[19] R. Samudrala, X. Zhang, R. M. Wadkins, D. L. Mattern, *Bioorg. Med. Chem.* **2007**, *15*, 186.

[20] A. Margineanu, J. Hofkens, M. Cotlet, S. Habuchi, A. Stefan, J. Qu, C. Kohl, K. Müllen, J. Vercammen, Y. Engelborghs, T. Gensch, F. C. De Schryver, *J. Phys. Chem. B* **2004**, *108*, 12242.

[21] C. Jung, N. Ruthardt, R. Lewis, J. Michaelis, B. Sodeik, F. Nolde, K. Peneva, K. Müllen, C. Brauchle, *ChemPhysChem* **2009**, *10*, 180.

[22] P. Tinnefeld, D. P. Herten, M. Sauer, *J. Phys. Chem. A* **2001**, *105*, 7989.

[23] J. Vogelsang, R. Kasper, C. Steinhauer, B. Person, M. Heilemann, M. Sauer, P. Tinnefeld, *Angew. Chem., Int. Ed.* **2008**, *47*, 5465.

[24] J. Vogelsang, T. Cordes, C. Forthmann, C. Steinhauer, P. Tinnefeld, *Proc. Natl. Acad. Sci. USA* **2009**, *106*, 8107.

[25] T. Cordes, J. Vogelsang, P. Tinnefeld, *J. Am. Chem. Soc.* **2009**, *131*, 5018.

[26] T. Cordes, I. Stein, H., C. Forthmann, C. Steinhauer, M. Walz, W. Summerer, B. Person, J. Vogelsang, P. Tinnefeld*, Proc. SPIE-Int. Soc. Opt. Eng.*, **2009**, p. 73671D.

[27] B. A. Jones, A. Facchetti, M. R. Wasielewski, T. J. Marks, *J. Am. Chem. Soc.* **2007**, *129*, 15259.

[28] C. Steinhauer, C. Forthmann, J. Vogelsang, P. Tinnefeld, *J. Am. Chem. Soc.* **2008**, *130*, 16840.

[29] R. Vinayak, H. Tang, *Nucleic Acids Symp. Ser.* **2000**, *44*, 257.

[30] T. Tanaka, R. L. Letsinger, *Nucleic Acids Res.* **1982**, *10*, 3249.

[31] N. Dontha, W. B. Nowall, W. G. Kuhr, *Anal. Chem.* **1997**, *69*, 2619.

[32] B. Okumus, T. J. Wilson, D. M. J. Lilley, T. Ha, *Biophys. J.* **2004**, *87*, 2798.

[33] T. Cordes, J. Vogelsang, M. Anaya, C. Spagnuolo, A. Gietl, W. Summerer, A. Herrmann, K. Müllen, P. Tinnefeld, *J. Am. Chem. Soc.* **2010**, *132*, 2404.

[34] D. Axelrod, T. P. Burghardt, N. L. Thompson, *Ann. Rev. Biophys. Bioeng.* **1984**, *13*, 247.

[35] J. Vogelsang, T. Cordes, P. Tinnefeld, *Photochem. Photobiol. Sci.* **2009**, *8*, 486.

[36] W. Chengyun, T. Wei, Z. Hanbin, Z. Xuechao, S. Yongjia, *J. Heterocycl. Chem.* **2009**, *46*, 881.

[37] T. D. M. Bell, S. Habuchi, S. Masuo, I. Oesterling, K. Müllen, P. Tinnefeld, M. Sauer, M. van der Auweraer, J. Hofkens, F. C. De Schryver, *Aust. J. Chem.* **2004**, *57*, 1169.

[38] M. Kunishima, C. Kawachi, J. Monta, K. Terao, F. Iwasaki, S. Tani, *Tetrahedron* **1999**, *55*, 13159.

[39] M. Kunishima, C. Kawachi, F. Iwasaki, K. Terao, S. Tani, *Tetrahedron Lett.* **1999**, *40*, 5327.

[40] B. A. Jones, A. Facchetti, M. R. Wasielewski, T. J. Marks, *J. Am. Chem. Soc.* **2007**, *129*, 15259.

[41] M. Bossi, J. Folling, V. N. Belov, V. P. Boyarskiy, R. Medda, A. Egner, C. Eggeling, A. Schonle, S. W. Hell, *Nano Lett.* **2008**.

[42] R. E. Thompson, D. R. Larson, W. W. Webb, *Biophys. J.* **2002**, *82*, 2775.

[43] J. Enderlein, E. Toprak, P. R. Selvin, *Opt. Express* **2006**, *14*, 8111.

Chapter 8

SUMMARY

In the last two decades the utilization of DNA has expanded from biology into other various scientific disciplines. The programmable assembly capability of DNA, in which the selective affinity of base pairs along the strands is exploited, has allowed this “molecule of life” to be employed as building block in new areas of research. The facile preparation of DNA via automated solid phase synthesis combined with molecular biology and organic chemistry techniques proved to be a powerful tool for the development of novel hybrid materials consisting of oligodeoxynucleotides (ODNs) and organic compounds.

The goal of this thesis was to increase the functionality of pristine DNA scaffolds by functionalizing them with fluorescent dyes and hydrophobic moieties. Two important steps were necessary to realize this aim successfully. First, nucleic acids needed to be synthesized making use of multidisciplinary toolbox for the generation and manipulation of polynucleic acids. The most important techniques were the solid phase synthesis involving the incorporation of standard and modified phosphoramidite building blocks as well as molecular biology procedures like the polymerase chain reaction, the bacterial amplification of plasmids and the enzymatic digestion of circular vectors. Second, and evenly important, was the characterization of the novel bioorganic hybrid structures by a multitude of techniques, especially optical measurements. For studying DNA-dye conjugates methods like UV/Vis and photoluminescence spectroscopy as well as

time resolved luminescence spectroscopy were utilized. While these measurements characterized the bulk behavior of an ensemble of DNA-dye hybrids it was necessary for a complete understanding of the systems to look at single structures. This was done by single-molecule fluorescence spectroscopy and fluorescence correlation spectroscopy. For complete analysis the optical experiments were complemented by direct visualization techniques, i.e. high resolution transmission electron microscopy and scanning force microscopy.

In the following a detailed summary will be given, how the individual DNA hybrid materials were generated and how they were characterized in the multidisciplinary approach described above entailing methods from chemistry, biology and nanoscience.

The self-assembly and dimerization of DNA nanostructures induced by π-π interactions of a perylenediimide dye were introduced in the first part of this thesis (*Chapter 3*). The Watson-Crick base-paring of DNA was used to precisely position perylene dyes on a DNA scaffold; the π-π stacking of the dyes was exploited to arrange different DNA strands into structures of higher complexity resulting in parallel aligned double helices on surfaces.
To achieve such ordered DNA-dye arrangement, the water soluble PDI was coupled to single stranded (ss) DNA (22mer) to form the ssDNA-PDI conjugate. The attachment of the chromophore to the nucleic acid moiety was successfully achieved by coupling the activated ester of the dye to 5'-amino-modified DNA still bound to the solid support by employing the so-called "syringe synthesis technique". The DNA-PDI conjugate was characterized by Polyacrilamide Gel (PAGE) and MALDI-TOF MS. MALDI analysis of DNA is not straightforward, however with the use of novel matrices combined with ammonium acetate was possible to improve the resolution. The spectra of the DNA-PDI conjugates showed broader distribution of the signals compared to that of DNA-conjugates of lower molecular weight. This observation makes sense considering that MALDI imparts large kinetic energies to ions of high mass/charge ratio *(m/z).* However,

the method was appropriate for the molecular weight determination of such kind of DNA-hybrids. The short labeled nucleic acid segments were hybridized with long DNA templates of 88 nucleotides, forming double helices where four PDI units were separated on a double helix by 22 base pairs. The self-assembly of these structures into dimers was analyzed employing Atomic Force Microscopy (AFM) and Polyacrylamide Gel (PAGE) and in solution via Fluorescence correlation spectroscopy (FCS), photoluminescence (PL) and UV/vis spectroscopy. The control of the aggregation of the dyes and the spatial organization of the chromophores is significant for numerous technological applications. In the future, DNA might be used as a scaffold to position optically active molecules in electrooptical devices.

In the second part of the thesis (*Chapter 4*), the dynamic behavior of linear labeled DNA was studied at different concentrations of a confining surrounding matrix consisting of linear unlabelled DNA. The PCR (Polymerase Chain Reaction) technique was used to amplify DNA of 7 kbp and to incorporate the donor and acceptor dyes at the end of the extremely long double helix. The unlabeled DNA was generated by transformation of *E.coli* cells. The cells were transformed with a pET44a+ plasmid and afterwards the amplified plasmid was linearized using a restriction enzyme. This allowed obtaining unlabeled DNA in milligram quantities. Single–molecule FRET and wide-field fluorescence microscopy measurements were employed to obtain information about the dynamic behavior of the DNA. Initially, the fluorescence lifetime of the donor in presence of the acceptor at different concentrations of unlabeled DNA were measured on a confocal microscope set-up. The decays of the fluorescence were almost independent of the unlabeled DNA concentration. In case of increasing DNA concentration a larger number and longer duration of end-to-end contacts, expressed in shorter lifetimes of the donor is expected because of FRET. However such a behavior was not revealed by the measurements, possibly due to the low concentration of the unlabeled DNA. For that reason higher concentrations of the non-labeled DNA and another detection strategy were

employed. The simultaneous motions of individual molecules were directly observed using wide-field fluorescence microscopy. Despite the higher concentration of the unlabeled DNA used in this second part of the experiment (~7.5 times above the theoretical critical overlap concentration) the wide-field fluorescence microscopy measurements revealed a very rapid and pure diffusive motion of the labeled DNA. These results indicated first, that the repulsion forces between the individual DNA chains might be one cause of the entanglement suppression. The model for estimating C* does not take into account these forces, implying that the regime of entangled polymer is achieved for DNA at higher concentration C* to that predicted by the model. Second, the entanglement of DNA in solution depends not only on DNA concentration, but also on its length. In previous studies the reptation of a 45 kbp DNA was determined, suggesting that the length of the 7 kbp DNA might to be too short to induce any entanglements, which would lead to reptation motion.

The third part of the document (*Chapter 5*) focuses on the fundamental role that hydrophobic moieties play in the aggregation behavior of DNA-micellar systems. Three lipid-DNA molecules were designed, containing either two or four dodec-1-ynyluracil units at different positions in the sequence, and all formed micelles at room temperature. The synthesis of an alkyl-modified nucleobase and its precise incorporation into short ODN sequences was achieved using automated chemical DNA synthesis. The lipid-DNA structures were studied with AFM, DLS and PAGE. The Critical Micelle Concentration (CMC) of the three systems was also determined as evaluation parameter of the micelle stability. The results revealed that the size and stability of the micelles primarily depend on the degree of hydrophobicity, with the greater number of alkyl chains resulting in smaller, thermodynamically more stable micelles. In contrast, the position of the hydrophobic chains in the sequence has at most weak influence on morphology and size of the self-assembled aggregates.

The primary utility of DNA based micellar systems is the potential for functionalization through DNA hybridization. For this reason, complementary

DNA was hybridized onto the corona of lipid-DNA micelles to study the effects of this process on their physical characteristics. Successful hybridization was confirmed using SYBR Green I fluorescence analysis and electrophoresis, corroborating that the alkyl chains do not interfere with DNA hybridization. The more significant outcome of this alkyl-modified base method, though, is the ability to systematically introduce well-defined hydrophobic nucleotides into DNA amphiphiles and thereby alter their supramolecular properties. This study represents the first investigation of the fundamental role of hydrophobics in determining aggregation behavior in DNA micellar systems. Furthermore, these DNA-micelles exhibit reproducible aggregation behavior and can be easily obtained in large scales, resulting of immense value in various drug and gene delivery processes.

After establishing the physical characteristics of the lipid-DNA micelles, one possible application of that kind of amphiphiles was studied. The aim of this investigation was to find a strategy for the facile self-assembly and loading of virus using the negatively charged polymer aggregates. The DNA-amphiphiles template the formation of an intact virus coat and enable their loading. In view of the fact that hydrophobic drugs are known to accumulate within the hydrophobic core of the micelles, this behavior was successfully exploited for introducing the fluorescent aromatic compounds pyrene and DiI into the micelles that act as a template for the capsid formation. It needs to be pointed that the dyes served as model compounds for small hydrophobic molecules like drugs. Additionally, the lipid-DNA micelles were labeled by hybridization with the hydrophilic dye 6-carboxylic-X-rhodamine (ROX). Fast protein liquid chromatography (FPLC), TEM images and gel electrophoresis analysis confirmed successful envelopment of the functionalized micelles by the viral coat protein.

This novel loading strategy marks a significant step towards virus-based targeted therapeutics, facilitating the incorporation of hydrophobic drugs, which are difficult

to couple chemically to water-soluble capsid proteins due to solvent incompatibilities and avoiding the need of altering environmental conditions.

While dye-labeled DNA allowed to calculate conveniently the number of oligonucleotides present within the virus capsids, there is still a high demand to further improve fluorescent labels, especially in regard to solving biological questions. This holds true for ultrasensitive and superresolution fluorescence microscopy, which call for fluorescence markers with increased photostability and new functionalities. In the last chapter of this thesis (*Chapter 7*), single-molecule spectroscopy was used to study water-soluble perylene dicarboximide fluorophores (PDI), by attachment of the fluorophore to DNA and immobilization via streptavidin/biotin on bovine serum albumin (BSA) coated cover slides. This immobilization strategy ensured that the fluorophores largely show the same properties as in free solution while they can be studied for an extended time compared to measurements of freely diffusing molecules. Under these conditions bright fluorescence, comparable to that of single-molecule compatible organic fluorophores, was observed with homogeneous spectral and fluorescence decay time distributions. Additionally, it was shown how the fluorescence of the PDI can be controlled through photoinduced electron-transfer reactions by using different concentrations of reductants and oxidants, yielding either blinking or stable emission. These properties were explained by the redox potentials of PDI and the ROXS (reducing and oxidizing system) concept.
The results of this investigation indicate that the fluorescence properties of PDI make it a suitable and an interesting candidate for a wide range of applications in single-molecule fluorescence spectroscopy. In this regard, rylene dyes could develop into universal labels for many microscopy techniques and applications in biology as well as material science in the future.